DETECTOR-BASED REFERENCE CALIBRATIONS FOR ELECTRO-OPTICAL INSTRUMENTS

George P. Eppeldauer

Detector-Based Reference Calibrations for Electro-Optical Instruments

Detector-Based Reference Calibrations for Electro-Optical Instruments

By

George P. Eppeldauer

Cambridge
Scholars
Publishing

Detector-Based Reference Calibrations for Electro-Optical Instruments

By George P. Eppeldauer

This book first published 2021

Cambridge Scholars Publishing

Lady Stephenson Library, Newcastle upon Tyne, NE6 2PA, UK

British Library Cataloguing in Publication Data
A catalogue record for this book is available from the British Library

Copyright © 2021 by George P. Eppeldauer

TABLE OF CONTENTS

PREFACE

Improved detector technology in the past two decades opened a new era in the field of optical radiation measurements. An increased number of calibration and measurement facilities and procedures could be developed with lower measurement uncertainties using the newly developed detector/radiometer standards instead of traditionally applied source standards (blackbodies and lamps). Shrinking of the traditional source-based calibrations and the large increase of optical detector-based calibrations motivated the writing of this book series.

The book series is a comprehensive description of optical detector based radiometric practices. Instead of giving the traditional lexical-type tutorial information, a research-based material is systematically organized and described. The large number of examples cover modern detector applications in the field of radiometry, photometry, colorimetry, and radiation temperature measurements. All the discussed devices and applications have been implemented, realized, tested, verified, and evaluated. These applications are described to obtain uniform results with low measurement uncertainties. They are described with enough details to successfully repeat them by the readers/users. The applications and evaluations follow the recommendations of international standardization. The described subjects are detailed and distributed in five volumes.

Properties of radiometric quality detectors, their use and selection for optical radiometers, design considerations of radiometers and detector-based standards, description of spectral and broadband detector-based calibrations and measurements using modern setups based on the new radiometer standards are described for practicing scientists, engineers, and technicians.

The book series includes many hundreds of designs, drawings, measurement schemes, a large number of detector-based measurement and calibration setups, measurement equations and results, calibration-transfer and measurement methods/procedures

all tested in practical applications.

In addition to reference level detector/radiometer calibrations, measurement of radiometric quantities used in practice (secondary laboratory and field applications), are discussed. Such quantities are radiant power, irradiance, and radiance. Measurement of spectral and broadband (integrated) quantities are discussed from 200 nm in the ultraviolet to 30 μm in the infrared.

All discussed calibrations and measurements are traceable to the System International (SI) units through National Measurement Institutes (NMIs) and/or the discussed intrinsic detector standards.

Linear and traceable measurement of detector output signals, including DC and AC photocurrent (sub-scale) and voltage measurements, detector-amplifier gain-calibrations, and gain-linearity tests are discussed in detail.

Uncertainty determination/calculation methods of detector-based measurements are described. It is a general rule for the discussed large number of design and application examples, to keep the calibration/measurement uncertainties low.

The author thanks all the colleagues listed in the references at the end of each volume for their help and contribution to perform the discussed large number of measurements and evaluations.

Dr. George P Eppeldauer, author

1. INTRODUCTION

In order to utilize the significant improvements obtained in detector performances during the past 20 years, user friendly responsivity standards and responsivity measurement techniques were developed. Spectral responsivity is one of the most important detector characteristics widely used to derive device and system calibrations from high level detector standards. The goal is to convert from the traditional source-based optical radiation measurements to the more efficient and higher accuracy detector-based applications and calibrations. In addition to the single element detectors that are discussed in this book, radiometers with multiple-reflection input geometries (trap, wedge, and sphere), filters, windows, diffusers, and apertures are used. Also, small field-of-view and/or narrow band-pass are frequently used in modern radiometers. In addition to radiant power (flux) responsivity calibrations, irradiance and radiance responsivity measurements are needed in many applications, especially in field measurements.

This book describes how to perform spectral radiant power, irradiance, and radiance responsivity measurements. Measurement methods are described for detectors, radiometers and photometers to determine the relative spatial, angular, and spectral variations of their responsivities. Determination of absolute responsivities are also discussed in detail. The book describes measurement geometry, measurement setups, typical types and properties of different detectors, radiometers, and photometers, and measurement methods. The measurement methods include procedures to obtain traceability to National Metrological Institutes (NMI) and guidance on selecting standards. Responsivity scale realizations and extensions are described from reference Si standards for the ultraviolet (UV) to infrared (IR) ranges. Directional errors when using the detector and radiometer standards are also discussed. The spectral responsivity calibrations are discussed for photometers and tristimulus colorimeters and also for electronic imaging devices. Evaluation of measurement uncertainty and state of the art measurement uncertainty values are discussed. Responsivity uncertainties are derived from principal measurement equations. Common problems

in all of the above measurements, such as spectral issues, DC and AC measuring methods and instruments are also discussed. An extended list of references are given to find more details for the above discussed subjects.

The book is to guide the optical radiation measurement community, researchers, manufacturers, calibration laboratories, students, and practicing engineers to switch from the old and limited use measurement methods to the higher performance and wider use detector-based measurements.

Details of the primary standards and related procedures for the realization of the SI units (the tasks of NMIs) are not discussed in this book. More discussions about multi-element devices can be found in Technical Reports (TR) of the International Commission on Illumination (CIE) such as the TC2-51 TR.

2. Spectral responsivity based calibrations

The responsivity s of an optical radiation detector (radiometer or photometer) is the ratio of its output electrical signal Y to its input radiometric quantity Q. In general, responsivity is the ratio of two integrals:

$$s = \frac{Y}{Q} = \frac{\int_\lambda R(\lambda) S_\lambda \, d\lambda}{\int_\lambda S_\lambda \, d\lambda}$$

(1)

where $R(\lambda)$ is the absolute spectral responsivity and S_λ is the spectral power distribution to be measured. The spectral responsivity $R(\lambda)$ is the responsivity at a specific wavelength λ. The spectral power distribution (e.g. spectral flux in radiant power measurement) is the input signal (density) at a wavelength λ.

The responsivity of a detector is determined during a measurement (calibration) transfer. After calibration, the detector can be taken as a standard and can measure the same kind of radiometric quantity it was calibrated for. The magnitude of the radiometric quantity to be measured will be equal to the measured electrical signal of the device divided by the responsivity. The three basic radiometric quantities can be determined from three different measurement equations. The radiant power is

$$\phi = \frac{Y}{s_\phi} ,$$

(2)

Where s_ϕ is the radiant power responsivity;

The irradiance (radiant power per area) is

$$E = \frac{Y}{s_E} ,$$
(3)

where s_E is the irradiance responsivity;

The radiance (radiant power per solid angle per projected area) is

$$L = \frac{Y}{s_L} ,$$
(4)

where s_L is the radiance responsivity.

For all three cases, Y is the result of an integration as shown above.

For a perfect radiometer that can measure radiant power, irradiance, and radiance, the responsivities may be interrelated:

$$s_P = \frac{s_E}{A} = \frac{s_L}{A\Omega}$$
(5)

where A is the detector active area and Ω is the viewing solid angle of the radiometer.

A test device can be calibrated against the detector standard if it can be substituted for the detector standard. The responsivity of the test device will be the ratio of its electrical output signal (current or voltage) to the magnitude of the measured radiometric quantity determined by the detector standard.

Responsivity measurements can be made broadband or spectrally (versus wavelength). This document is mainly focused on spectral responsivity measurements. In order to make uniform measurements, the bandwidth of the detector (radiometer) has to be designed according to the bandwidth of the source to be measured. E.g., a broad-band source can be measured with a broad-band detector only if the spectral responsivity of the detector is known. The relative standard measurement uncertainty of the test device will be always larger than that of the standard device because of the increased number of the calibration steps (during the measurement transfer).

Responsivity related calibrations are:

- Relative spectral responsivity (in power, irradiance, and radiance modes)
- Absolute spectral responsivity (in power, irradiance, and radiance modes)
  - Uniformity:
    - relative variation within spatial responsivity (versus wavelength)
    - relative variation within angular responsivity (versus wavelength)
  - Aperture effective area measurement
  - Linearity versus wavelength
  - Temporal characteristics
  - Temperature coefficient of detector responsivity

Responsivity measurements can be utilized in the field of:

- Optical radiometry
- Photometry
- Colorimetry
- Temperature measurements of blackbody radiators
- Optical pyrometry
- Solar photovoltaic quantum efficiency measurements

The optical radiation related quantities and units are defined in Section 845-01 and the radiometric, photometric, and colorimetric measurements, including physical detectors, are defined in Section 845-05 of the International Lighting Vocabulary (ILV) [1] . More definitions are given in the International Vocabulary of Basic and General Terms in Metrology (IVM) [2]. These definitions will be used in this work where applicable.

2.1 Calibration methods

The purpose of spectral responsivity calibrations is to transfer the spectral responsivity function from the selected reference standard to different test devices.

If low uncertainties are needed, a reference trap-detector can be used between 405 nm and 920 nm. The trap detector field-of-view has to be larger than the convergence angle of the beam to be measured.

If the spectral range of the Si trap detector is in not large enough for a given application, a spectrally flat transfer device can be used for extension of the wavelength range. In this case, the relative spectral responsivity of the wavelength extending transfer device can be determined first. As an example, the wavelength extending transfer standard can be a pyroelectric detector [3]. Its transmission for the incident beam is negligible. The front surface of the detector can be measured for spectral total reflectance to determine the spectral absorption (one minus reflectance). The spectral absorption is proportional to the relative spectral responsivity. As a second step, the absolute (tie) points can be determined against a reference standard detector, using the substitution method. E.g., the reference standard is a silicon tunnel-trap radiometer. The transfer standard pyroelectric detector is substituted for the reference standard and both are underfilled by the same laser beam [4]. In this example a 442 nm stabilized laser beam was used.

A secondary calibration laboratory can be prepared for spectral responsivity calibrations. Test detectors are always substituted for the standard detector of the calibration laboratory to further derive the spectral responsivity function.

2.1.1 Detector substitution method.

The substitution method transfers the radiant power responsivity of a standard detector to a test detector that has similar properties as the standard detector. When the standard detector measures the input (incident) beam, its output signal (e.g. photocurrent) is:

$$I_S = s_S \cdot \Phi$$

(6)

where s_S is the known responsivity of the standard detector and Φ is the constant (stabilized) incident radiant power that underfills the detector. In the following step, the test detector is substituted for the standard detector and measures the same power in the same arrangement:

$$I_T = s_T \cdot \Phi$$

(7)

where I_T is the output signal of the test detector and s_T is the unknown radiant power responsivity of the test detector that can be calculated from Eqs.(6) and (7):

$$s_T = s_S \frac{I_T}{I_S}$$

$\hspace{11cm}$ (8)

This is the principle measurement equation for the detector substitution method. Here it is assumed that any background contributions are negligible or have been corrected for.

When detectors are substituted for each other in power measurement mode the distance of the detectors relative to the origin of the source is not critical.

A monitor detector can be used to continuously measure the time dependent changes of the incident beam. Simultaneous ratio of the detector signal (both standard and test) to the monitor signal will reduce contributions to the combined uncertainty of the responsivity due to power fluctuations in the incident beam [5], provided the monitor detector and its preamplifier have characteristics similar to the test detector as well as to the standard detector and their preamplifiers.

2.1.2 Measurement transfer to test devices

The calibration transfer starts with the spectral responsivity measurement of the transfer standard against the realized spectral responsivity function at an NMI and ends in a secondary or field calibration laboratory where the responsivity of test detectors is measured. Low uncertainty of the responsivity value of a realization always needs sophisticated measurement setups and selected and well characterized detector standards. In applications where the relative measurement uncertainty requirement is 1 % or larger, the substitution method gives satisfactory results to transfer the spectral responsivity. The substitution can be made at all wavelengths where the detector responsivities overlap. Often, chopping or stability corrections with a monitor radiometer are not needed and lower power throughput is sufficient for the spectral instrument and the related optics. In this case, the simplified version of the measurement

setup (as shown below in Fig. 2) can be used.

When signal modulation (chopping) is needed, such as in case of pyroelectric detectors or other infrared measurements (where separation of the useful signal from the DC background signal is needed), the responsivity transfer can be more complicated. In this case, during calibration, the responsivity versus frequency function should be measured (using the chopper and lock-in amplifier of the calibration laboratory) and the equivalent (or virtual) DC responsivity should be determined by fitting a curve to the measured data points. Frequently, this DC responsivity is reported by calibration laboratories even if the calibrated detector can be used only in AC measurement mode. When the calibrated detector is used in an application where different instruments (chopper, lock-in amplifier etc) are applied, the DC responsivity (reported by the calibration laboratory) can be derived (extended) to any other frequencies if the responsivity versus frequency curve is measured again with the different instruments of a given application. This method is very convenient and can result in very small increase in the measurement uncertainty during a calibration transfer.

Photometers used for luminous intensity lamp calibrations, usually have an aperture and a filter combination in front of the Si photodiode. Sometimes, the filters are temperature controlled. If the separation between the aperture and the detector is large, the photometer FOV can be small. Care should be taken that the FOV is large enough for the detectors when they measure the total beam power during a calibration procedure. Similarly, the beam convergence angle of the monochromator in the calibration setup should be made small enough to reach the detectors even in applications where the detector FOV is small. This way, beam clipping can be avoided.

Photometers usually measure illuminance or luminance. In field applications, diffusers or cosine corrections are used between the aperture and the filter combination to achieve compliance with the cosine law of illuminance measurement. In these applications, the cosine response is important because the radiation reaches the photometer (illuminance meter) from the hemisphere above the aperture. The side effect of a diffuser (cosine corrector) application can be poor uniformity in the spatial responsivity.

Illuminance meters can be calibrated in radiant power measurement

mode. The photopic filter inside the photometer modifies the spectral power responsivity of the photodiode such that it will be similar to the standard photometric observer (the CIE V(λ) function) [6]. As a result, the radiant power will be converted into luminous flux, the photometric equivalent of radiant power. Both the filter package and the detector can have significant spatial non-uniformity. In order to decrease uncertainty contributions, the radiant power responsivity of an illuminance meter has to be mapped out and the average power responsivity should be used. Averaging the spatial non-uniformities of the photometer is important to make the measurement geometry at calibration equal to that at applications. The calibration geometry should be similar to that of a luminous intensity lamp measurement, where the lamp produces a uniform field of radiation in the aperture plane and the filter and detector spatial non-uniformities are averaged out. In radiant power mode calibrations, the calibration and measurement geometry will not be equal because the beam shapes at calibration (converging beam from the monochromator) and application (collimated within the aperture) will be different resulting in different reflection patterns for the two cases.

Radiometers with filters and/or apertures can be calibrated similarly to photometers. The important requirement for keeping the measurement uncertainty low is to use equal calibration and application beam-geometry to obtain the same reflection pattern inside the test radiometer for both cases. The similar rule applies for a detector standard used in a substitution type calibration unless the standard is invariant for the changes in the beam geometry between its own calibration and the application.

The equal calibration and application geometry requirement for illuminance meters can be achieved perfectly in irradiance calibration mode using a spectral irradiance responsivity standard where the uniform monochromatic radiation overfills the apertures of both the test photometer and the irradiance responsivity standard.

2.1.3 Pyroelectric spectral-reflectance based responsivities

Pyroelectric detectors have a renaissance for use in radiometric standardization. Their noise-equivalent power (NEP) has been improved [7] by orders of magnitude in the last several years. The improved NEP pyroelectric detectors can exhibit excellent radiometric characteristics as well [8]. The NEP is low enough to

obtain high signal-to-noise ratios at the output of monochromators which was impossible or difficult before the NEP improvement. Fast, monochromator-based measurement of the spectral reflectance of their black coating with couple of percent uncertainty, made it possible to determine the spectral responsivity of these pyroelectric detectors from UV to IR with close to 0.1 % (k=2) uncertainty [9]. This is a significant improvement in calibration time and measurement simplicity compared to tunable laser applied detector-substitution type responsivity calibrations.

In a few previously discussed examples, the spectral response of the pyroelectric detector was not "flat". It changed several percent in the VIS-IR. The flat response from a reference pyroelectric detector for spectral (responsivity) calibrations is not needed. The obtained uncertainties when the above described traditional spectral-responsivity calibration methods were applied (the test detector was substituted for the standard detector of known spectral responsivity and the responsivity from the standard detector was transferred to the test detector while measuring the output signal from both detectors for the same incident radiation) were in the percent level.

The monochromator applied spectral reflectance measurements of the black-coatings can produce the frequently required close to 0.1 % (k=2) uncertainty in the relative spectral responsivity of the herein discussed pyroelectric hybrid detectors even if the uncertainty of the spectral reflectance measurements is a few or several percent. Utilizing the relative spectral response of a pyroelectric hybrid detector determined from its spectral reflectance measurements, reference responsivity scales can be realized from the UV to the IR even at high-accuracy (e.g. tunable laser applied) detector calibration facilities. The conversion of the relative response into absolute can also be performed with low responsivity uncertainty, by substituting the pyroelectric detector against a transfer standard detector (e.g. Si trap detector) traceable to a primary standard cryogenic radiometer. This monochromator-used pyroelectric-based responsivity scale realization can be much faster and less expensive than calibrations performed at tunable-laser applied responsivity calibration facilities.

The spectral reflectance characteristics and measurements of selected pyroelectric detectors were discussed in Section 5 of Volume 1: The Properties of Optical Radiation Detectors and

Radiometers. The design issues of pyroelectric transfer standard radiometers were discussed in Section 3.2.1 of Volume 3: Optical Detector and Radiometer Standards.

Typically, the spectral responsivity calibration problems are different in the UV and IR ranges compared to the VIS and near-IR ranges.

Usually, power- and irradiance-responsivity scales are traceable to power measuring primary-standard cryogenic radiometers. Most frequently, Si trap-detector transfer standards are used for the VIS and silicon wavelength ranges [10], and sphere-input InGaAs [11] and sphere-input extended-InGaAs [12] detectors are used for the near-IR and short-wave IR ranges. Usually, these transfer standards are not used to hold the scales because of instability (response degradation) problems. Si trap detectors may exhibit UV-damage-caused responsivity degradation for wavelengths shorter than 450 nm. In spite of this degradation problem, sometimes they are calibrated down to 365 nm. In this case, the responsivity degradation can be avoided if an input shutter is used to minimize the UV exposure-time for the trap-detector. Also, the power-level of the incident radiation within the UV range should be low to avoid the response damage. The Spectralon [13] coated sphere, mounted at the input of the InGaAs or extended-InGaAs transfer standard detector, is exposed to the ambient and the degradation of the coating may cause long-term stability problems for these detector standards. Accordingly, these transfer standards should be used only for short-term responsivity transfer. Both the trap detectors and the input spheres have precision apertures (of known area) at their (front) inputs and they can be used as power-to-irradiance responsivity converters.

Typically, the responsivity scales are held by sealed single-element detectors. For radiant power measurement, large-area single-element detectors with small spatial nonuniformity of response are selected. These detectors are not used for power-to-irradiance responsivity conversion, primarily because their spatial uniformity is not good enough (it is close to 1 % peak-to-peak response variation) and their active area is not known. An added front-aperture may cause inter-reflections increasing the irradiance responsivity uncertainty. The detectors that hold the irradiance responsivity scale, might have significant spatial response non-uniformities if the measured (incident) radiation is spatially uniform.

Based on the above considerations, pyroelectric UV and IR responsivity scales have been developed at NIST [8]. The applied organic-black coated pyroelectric hybrid detectors with low NEP are excellent candidates to realize accurate and stable UV and IR responsivity scales with low uncertainties when they are calibrated based on spectral reflectance measurement of their black coating.

In early NIST performed scale realizations, sphere-input extended-InGaAs transfer standards gave the SI traceability of the responsivity function to the cryogenic radiometer. They produced the absolute responsivity tie points for conversion of the reflectance-based relative response function of the pyroelectric detector into an absolute function. Later, Si trap detectors were used to produce the tie points with significantly lower responsivity uncertainty. Using this method, the wavelength coverage of the NIST IR-SCF was extended from 0.6 μm to 24 μm in radiant power measurement mode and from 0.6 μm to 12.5 μm for irradiance responsivity calibrations. The responsivity uncertainties in both modes were between 2 % and 3 % (k=2) [14].

Both the monochromator used and the tunable laser applied calibration facilities require UV responsivity scales with low responsivity uncertainty. For the 200 nm to 600 nm range, UV trap detectors were used at NIST as transfer and working standards. These trap detectors were built using UV damage-resistant Si photodiodes. These are nitride-passivated or thin oxide nitrided-Si photodiodes with 1 cm^2 active areas [15]. These UV trap detectors can be calibrated against the cryogenic radiometer in power measurement mode. Since they are equipped with a front aperture, they can be used as irradiance responsivity standards as well. The organic-black coated pyroelectric detectors with the low-NEP were first-time used as reference irradiance measuring detectors at high accuracy UV and IR responsivity calibration facilities.

2.2 Calibration/measurement setups

2.2.1 Monochromator based setups

Most commonly, monochromator based measurement setups are used for spectral responsivity measurements. The complexity of a spectral responsivity measurement setup depends on the measurement uncertainty level and the wavelength range needed for

the test detector. For instance, if the spectral responsivity function has to be extended from a high accuracy Si trap detector to a pyroelectric detector (where the noise floor is high), the setup has to be more versatile than for similar type test and working standard detectors especially when both have high sensitivity.

2.2.1.1   Filter monochromator.

One or more (narrow) bandpass filters can be used in place of a monochromator for spectral responsivity determinations at one or several wavelengths or when the budget is severely constrained. For successful results, the filters chosen must be of high quality and meet demanding specifications. Typically bandpass filters are used with a continuous source such as a tungsten-halogen incandescent lamp. Sometimes satisfactory results may be obtained by using a filter to isolate a single line from a source that contains many lines (e.g., Hg) or to reduce the background from wavelengths other than those from a selected source (e.g., a laser). The following definitions and discussion is limited to bandpass interference filters, the only ones suitable for passbands between 5 and 20 nm.

- Center Wavelength - the wavelength of peak transmission for a symmetrical filter, or the wavelength midway between the 50 % points for an asymmetrical filter.
- Percent Transmission - The transmission at the peak wavelength.
- Bandpass - Conventionally, the wavelength difference between the 50 % transmission points. The moments normalization method generally gives somewhat wider effective passbands.
- Bandpass Shape - Typically like a Gaussian or Lorentzian curve. Because many filters have several stacks in series (like 4th order), the Gaussian or Lorentzian may be raised to an arbitrary power for optimal curve fit.
- Out-of-Band Rejection - The transmission at wavelengths beyond the limits of the bandpass. Usually given as 10^{-4}, for example.
- Clear area and uniformity over clear area - The clear area is the area where the filter action takes place. For a 25mm diameter circular filter, it is typically 21mm diameter. The margin should be masked to prevent light from traversing that portion of the filter.
- Variation of Characteristics with Incident Angle - All of the

following filter characteristics change with incidence angle

    a. The peak transmission decreases.

    b. The center wavelength shifts to shorter wavelengths.

    c. The bandwidth increases.

    d. The transmission characteristics become different for s and p polarization.

    e. The transmission characteristics become far more complex in a converging beam as many incidence angles are simultaneously present.

- Environmental Considerations - Filters are subject to reversible change of transmission with temperature, and irreversible degradation with exposure to humid atmospheres. In addition, the transmission changes slightly with atmospheric pressure.

- Stability over time with frequent exposure to source - Intense sources, particularly UV, may cause permanent degradation in the filter transmission. They should be characterized regularly to establish the time over which they can be reliably used.

- Fluorescence in filters - Some materials of construction may have fluorescence, emitting visible radiation when excited with ultraviolet. All filters should be inspected before use.

- Cleaning Method - Manufacturers specify the way a filter should be cleaned. Keeping the instrument closed when not in use is recommended. Avoid getting liquids on the edges to prevent seepage and subsequent filter delamination.

As for determination of the wavelength setting of a monochromator, the wavelength should be determined as the centroid of the radiation passed by the combination of the source and filter.

In spectral radiant power responsivity measurements, where broadband-sources are used with either narrow-band filters or monochromators, the incident beam is usually convergent onto the detectors. Figure 1 shows a typical arrangement for this type of measurement using a lamp-source and a series of interference filters. The field stop restricts the viewing area of the source to obtain a uniform source image. The radiation emerging from the field stop is collimated by a plano-convex lens with the flat side facing the source. The interference filters are mounted in a filter wheel and each of them converts the broadband parallel radiation into a quasi-monochromatic beam. This beam is then re-focused on the detectors.

The optimal position of the lenses depends on the wavelength. The detectors are single element detectors and the beam spot on the detector has to be smaller than the sensitive area of the detector. Test detectors can be calibrated against a standard detector of known spectral power responsivity. When filters are used, their temperature should be controlled. They can be recalibrated to minimize ageing effects, using the same geometry. Usually, the effective bandpass and centre wavelength of the individual filters are different, depending in part on the spectral responsivities of the test and standard detectors.
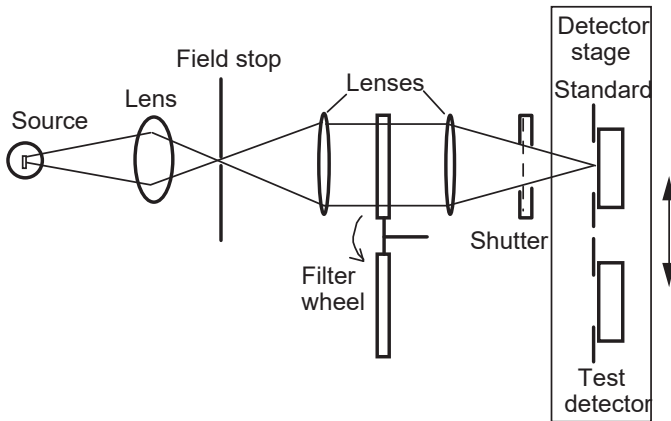
Fig. 1. Converging beam geometry for spectral radiant power responsivity measurement using a broadband-source with interference filters.

2.2.1.2 Monochromators

A typical monochromator-based responsivity measurement setup is shown in Fig. 2. A broadband lamp is imaged onto the input slit of the monochromator using lens or mirror imaging systems. Mirrors have no internal reflections, unlike lenses and are preferable for wide spectral range applications because they show no chromatic aberrations. Spherical mirrors are most commonly used for imaging, operated at near-normal angles of incidence to reduce off-axis aberrations. Spherical aberration is usually negligible for slow (i.e., F/8 or greater) mirrors. Double monochromators are used in high accuracy applications where high stray light rejection is needed. Single monochromators have higher throughput but lower performance in terms of spectral stray light.
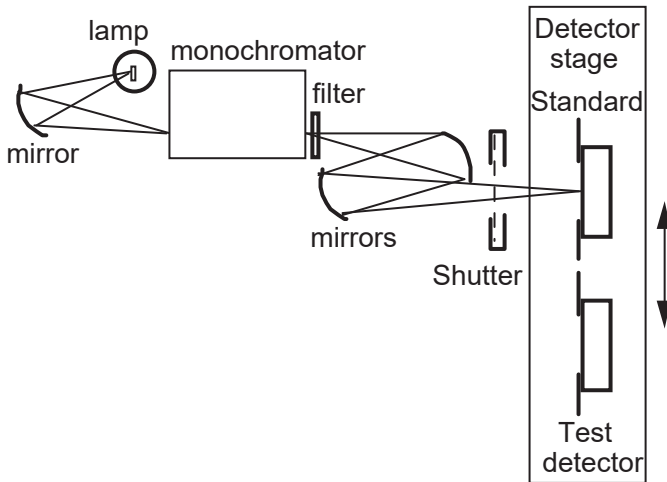
Fig. 2. Spectral responsivity measurement setup using a monochromator.

The dispersing elements are either prisms or gratings. The dispersion of prisms is highly non-linear. Therefore, when constant spectral bandpass is needed, elaborate cams have to be used for both the wavelength and the slit-width drives. It is difficult to find prism materials that have high enough transmission and dispersion in a wide wavelength range. Prism monochromators are more complex, hence, more expensive than grating versions. Gratings have anomalies that render their spectral efficiency highly irregular and they need order sorting (cut-on) filters. The output slit is imaged at the surface of the detectors. A light shutter can be used to subtract both the background radiation and the output offset voltage of the detector-amplifier from the output signal.

A versatile monochromator-based measurement setup is shown in Fig. 3. This setup has a computer controlled detector stage where test detectors can be calibrated against the standard detector. All detectors are operated in underfilled mode and measure the same total power of the monochromatic beam leaving the output imaging optics of the monochromator. Different broad-band sources can be imaged to the input slit of the monochromator through the input imaging optics. The power level and the spectral purity of the monochromatic beam (imaged on a detector) depend on the

properties of the monochromator, the related optical system, and the type of the illuminating source. Usually, a combination of tungsten halogen lamps, Xenon lamps, and/or Argon arc sources is used to cover a wavelength range from 200 nm to 2.5 µm. The detector stage is optically shielded from the source related components of the setup using a baffle inside the light-tight box. The baffle can minimize the stray radiation seen by the detectors. A shutter can also reduce the contribution to the combined measurement uncertainty of the spectral radiant power responsivity by further decreasing stray and background radiation.
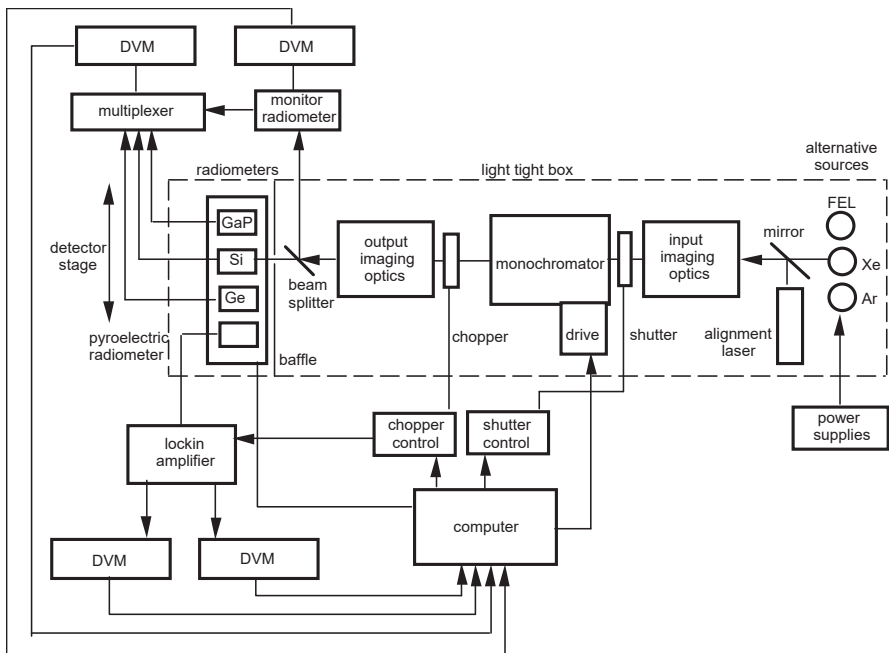
Fig. 3. A versatile monochromator setup to measure spectral responsivity.

In order to subtract the same dark signal as the one superimposed on the signal (for the shutter off and on), the shutter should be positioned far from the detectors. If a monitor detector measures a (constant) part of the monochromatic beam simultaneously with the signal of the measured detector, the ratio of the two output signals (signal to monitor) can decrease the source fluctuations in the measured data. The ratio method will be efficient only if both the

spatial and the temporal changes are equal (or very similar) in both channels. All detectors, the monitor, the test, and the standard detector need short-circuit current-to-voltage converters to obtain linear operation. The output voltages of the converters are measured by digital voltmeters (DVMs), usually under computer control as is the data acquisition.

2.2.1.3 Monochromator characteristics

A monochromator is an optical instrument which is capable of isolating a narrow range of wavelengths. It is a tunable optical bandpass filter where both the wavelength and the width of the passband may be varied. Monochromators are the key spectral component in spectroradiometers, spectrophotometers, and spectroreflectometers, and are also used as tunable sources or detectors. For this document, a monochromator is combined with a source of optical radiant energy to form a narrow-band source for use in a spectral responsivity measuring setup (spectral comparator). (Characteristics of monochromators are briefly discussed in CIE Publication 63 [16]).

In order to perform this task, a monochromator must meet certain minimum requirements regarding the following characteristics:

- Spectral range
- Resolution, passband (slit function)
- Throughput (speed, F/#)
- Spectral purity (stray light)
- Wavelength uncertainty (calibration and reproducability)

Optical schematic diagrams of basic monochromators are shown in Figures 4 and 5.
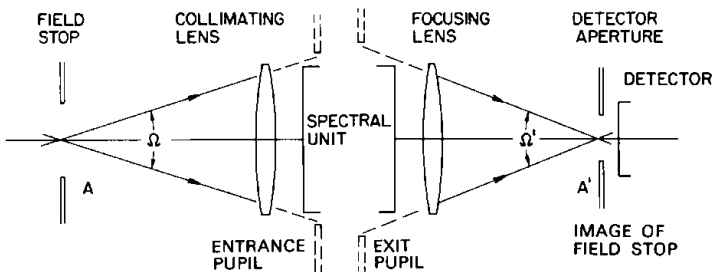
Fig. 4. Basic monochromator schematic of Goodman [17].
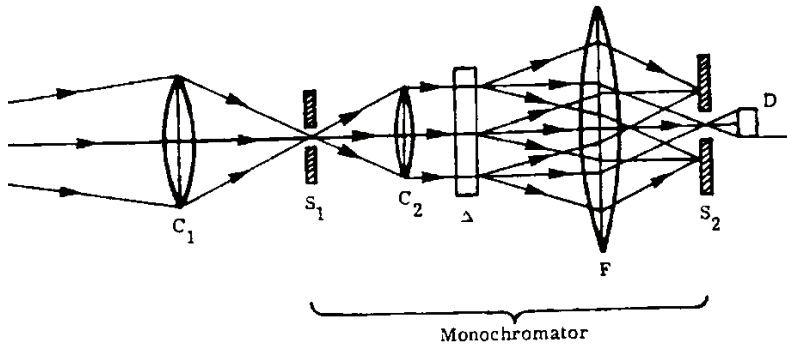
Fig. 5. Basic monochromator schematic of Zissis [18]. C_1 and C_2 are collimating lenses, S_1 is the input slit, S_2 is the output slit, Δ is the disperser, F is the focusing lens, and D is the detector.

2.2.1.3.1. Basic operation

Optical radiation entering the entrance aperture (circular or slit), is collected and collimated by the collimator lens or mirror. In Figs. 4 and 5, lenses are shown for clarity, but mirrors are normally used as they are achromatic. Collimated radiation is presented to the disperser that can be prism or grating. The disperser angularly separates the radiation as a function of wavelength. The focusing optic, which can be lens or mirror, collects the dispersed radiation and forms a series of overlapping images of the entrance aperture. The linear dispersion at the exit aperture is the angular dispersion multiplied by the focusing optic focal length. In most instances, unit magnification is used (collimator focal length equals focal length of focusing optic). The exit aperture, that can be circular or slit, selects a narrow range of wavelengths to transmit.

The spectral range is governed by the disperser. In prisms, it corresponds with the wavelength range over which the material is transmissive. In gratings it is related to grating line spacing, grating efficiency and provisions for order-blocking filters.

The resolution depends on the aperture width and the disperser resolving power.

The throughput (etendue) of a monochromator is the product of the aperture area A_{ap} and the solid angle subtended by the collimator.

$$T = \frac{\pi A_{ap}}{4 \left(F / \# \right)^2} \quad \left(\mathrm{m^{-2} sr^{-1}} \right)$$

(9)

where ($F/\#$) is the focal ratio of the collimator. (It is assumed that the entrance aperture and the collimator are the limiting components.) The $F/\#$ is one of the important parameters for a monochromator.

The spectral purity is defined by the transmission of the monochromator outside the passband.

The wavelength uncertainty relates to the mechanical construction and to the procedure used to calibrate the wavelength scale.

2.2.1.3.2. Spectral purity

Typical stray light specification for single monochromators is 10^{-4}, the effective transmission for wavelengths outside the passband. This relatively high stray light specification causes trouble particularly at shorter wavelengths where both the source and the detector response may be low.

A single monochromator is unsatisfactory as a low-uncertainty spectral comparator. Placing two monochromators in series can improve the stray light specification to 10^{-8}, which is more than sufficient. Most double monochromators consist of two identical Czerny-Turner grating monochromators arranged such that the exit slit of the first monochromator also functions as the entrance slit of the second monochromator. The two are mounted on a common base-plate and the wavelength drives may be coupled via a timing belt. More sophisticated designs may employ the first monochromator mounted over the second monochromator such that both gratings (matched) are driven by a common shaft.

A double monochromator may be constructed on one of two ways. For additive dispersion, the gratings are arranged such that the dispersions are in the same direction, increasing the dispersion over a single monochromator. The resolution is primarily determined by the exit slit. For subtractive dispersion, as shown in Fig. 6, the mounting of the second grating reverses the dispersion of the first, and the output at the exit slit is homogenous, having all wavelengths uniformly mixed across the slit. The dispersion is that solely of the first monochromator, and the intermediate slit governs the resolution.
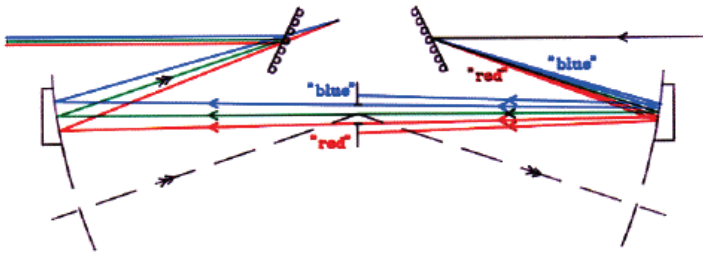
Fig. 6. Subtractive dispersion in a double-grating monochromator.

A satisfactory arrangement uses a low-dispersion prism monochromator to function as a pre-disperser (order-sorter) for a high-resolution grating monochromator. Among the most popular is the venerable Cary 14. This instrument uses a 30 degree fused silica prism and a single 600 line-per-mm echelette grating to cover the wavelength range from 185 nm to 2750 nm with few grating anomalies. The focal length of the prism monochromator is 300mm and the focal length of the grating monochromator is 400mm. The dispersion (in nm, FWHM per mm of slit width) is fairly constant at 3.5±0.2 nm/mm from 400 nm to 1700 nm, dropping to 2 nm/mm at 260 nm and at 2750nm. The arrangement of the Cary 14 prism-grating monochromator is shown in Fig. 7.
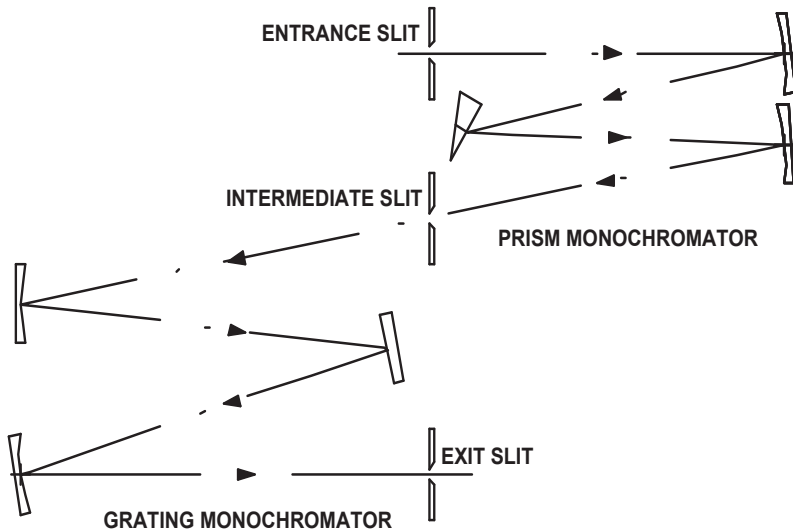
Figure 7. Scheme of the Cary 14 prism-grating double monochromator.

2.2.1.3.3. Stray light

Spectrographs are spectroradiometers with multi-element array detectors that can acquire an entire spectral image, over some finite spectral region, simultaneously. Spectrographs commonly consist of an entrance port, a dispersing element (such as a grating) to spatially resolve the spectral components of the incident radiation, and mirrors to image the entrance port (often a slit) onto a reference plane where the array detector is located. Because of the dispersing element, the spatial image of the entrance port falls on different regions of the detector array, depending on its wavelength; broadband sources form an image across the entire array. The spectral coverage of a spectrograph is determined by the size of its detector array, the dispersion properties of its grating, and its optical layout. Compared with conventional, scanned grating systems, source spectral distributions can be acquired in a matter of seconds, as opposed to minutes. The ability to rapidly acquire a spectrum has led to the use of array-based systems in a variety of radiometric, photometric and colorimetric applications where acquisition speed is an issue, for instance on a product line, or in cases where the source being measured is not be stable over extended periods of time.

The measurement uncertainties of spectrographs are still generally larger than conventional scanning spectrometers. Spectrographs are single grating instruments and there are intrinsic limitations in the background signal originating from radiation scattered from imperfections in the grating and other optical elements. This unwanted background radiation, called stray light, while small — on the order of 100 ppm or less of the incident spectral radiance in a single grating spectrograph — can give rise to unforeseen errors, often much larger than anticipated, when the spectral distribution of a source being measured differs significantly from the spectral distribution of the calibration source. In comparison, a conventional scanning spectrometer is usually constructed as a double-monochromator instrument (double-grating or prism-grating) that has a stray light level lower than 1 ppm.

In many applications, the spectral distributions of the test source and the calibration source differ significantly. Spectrometers are typically calibrated against standard incandescent lamps with correlated color temperatures (CCTs) ranging from 2800 K to 3100 K. Most of the emission from these sources lies in the red and near infrared regions.

Measurement errors, often significant, arising from stray light are inevitable when instruments calibrated against standard lamps subsequently measure light sources that have dissimilar spectral distributions such as LEDs, displays, discharge lamps, and fluorescent lamps. In these situations, stray light is often the dominant source of spectrograph measurement error.

Algorithms have been developed to correct the output of a spectrograph for stray light based on the spectral imaging properties of the instrument. The tunable lasers available on SIRCUS are used to characterize a spectrograph's response for stray light. Figure 8 is a semi-log plot of images acquired from a spectrograph with excitation wavelengths ranging from 254 nm to 700 nm. Each spectrum is a single image normalized by the peak value. The strong central line in the figure corresponds to the image of the entrance slit formed on the detector array. The broad shoulder and finite baseline are signals from radiation that is not properly imaged onto the detector, *i.e.* from stray light within the spectrograph. By measuring the system response at a number of wavelengths, the evolution of the image as the excitation wavelength moves across the array can be determined. Based on these measurements, a stray light correction algorithm can be implemented that reduces the errors arising from stray light an order of magnitude or more [19, 20].

2.2.1.3.4. Source considerations for monochromators

Since the throughput of a monochromator is quite small, we must maximize the available power emanating from its exit aperture by employing three strategies:

(a) Collect as much radiation from the source as possible
(b) Image the source onto the entrance aperture such that the size of the source image matches the size of the aperture.
(c) Select the source optics such that the angular spread of the beam converging on the entrance aperture matches the acceptance angle of the collimator.

Certain sources are extended to a degree that they may be placed directly in front of the entrance aperture. The source position should be carefully chosen such that its cross-section exactly matches the acceptance angles of the monochromator. It may be necessary to mask the source, as a match in both orthogonal angles is unlikely.

A fiber of the proper numerical aperture (NA) can also be used to transport energy from a source to the entrance aperture. The NA of the fiber should be no larger than that required to fill the collimator. The input end of the fiber can then be placed immediately adjacent to the source, or auxiliary optics can be used to maximize the power into the fiber. There are fiber bundles available which have one end in a circular configuration and the other end in the form of a slit. If the NA is appropriate, the rectangular end can be used in lieu of a slit.
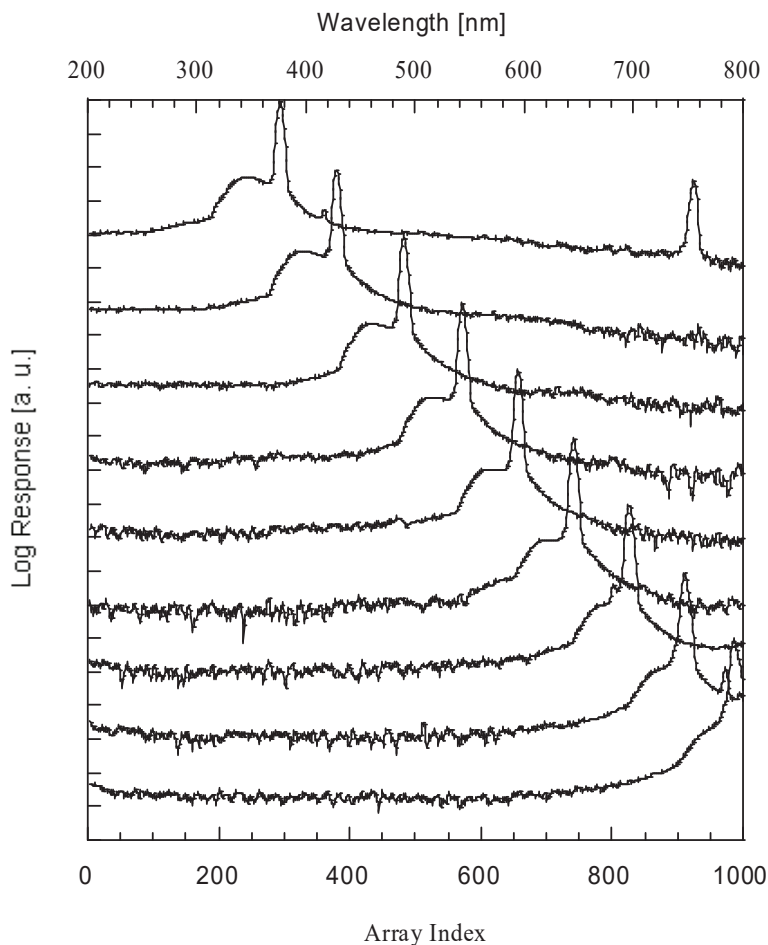
Fig. 8. Spectrograph images.

2.2.1.3.5. Slits and slit functions

The slit function (often called instrument function) is the spectral signature obtained when scanning a single narrow spectral line. It represents the relative spectral transmission of the monochromator, exclusive of transmission and reflection losses. The slit function, as shown in Fig. 9, is the convolution of the entrance and exit slits. If the slits are of equal width, the slit function is triangular. In the general case, as shown in Fig. 10, it is trapezoidal as a function of wavelength. The slit functions for matched and unequal slit widths are illustrated in Fig. 11. The width of the entrance slit is directly related to the optical power into the monochromator. The width of the exit slit determines the amount of the dispersed spectrum that is selected, which is related to resolution. The slit function is the product of the slit width and the linear dispersion. It is nominally constant for a grating instrument and is non-linear for a prism instrument.

The amount of optical power transmitted through a monochromator is related to the slit widths. For a single narrow monochromatic line, the entrance slit governs the input, and the exit slit is unimportant. The transmitted power varies directly as the slit width. For a continuous source, the entrance slit again governs the input, and the exit slit selects which wavelengths to pass. The transmitted power varies as the square of the slit width. There is always a trade-off between power and resolution. Wider slits allow more power at the sacrifice of spectral resolution. The slits should be set at equal width for most applications.

The typical slit function is the convolution of two rectangle functions and is a triangle. Diffraction can round the function for narrow slits. The peak is normalized to 100 %. The bandwidth is usually considered to be the full width at the 50 % transmission points, or full width at half-maximum (FWHM). In fact, the instrument is sensitive in some degree to greater than this width [21]. For the triangle function with equal slits, the instrument responds to twice the FWHM, and energy outside the FWHM is discounted.
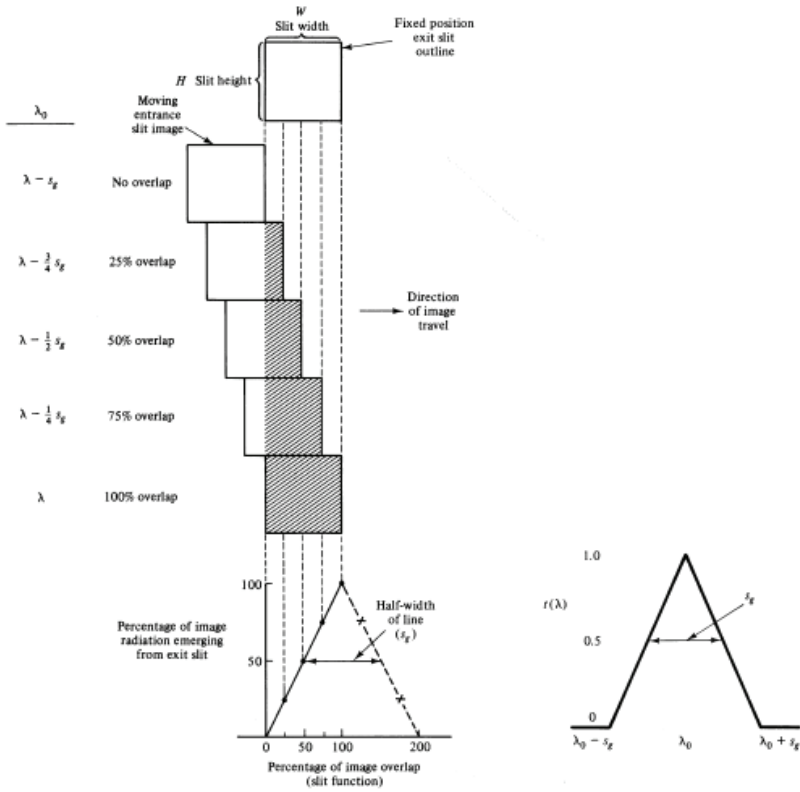
Fig. 9. Triangular slit function

SLIT IMAGE AND   INSTRUMENT
DETECTOR APERTURE   FUNCTION
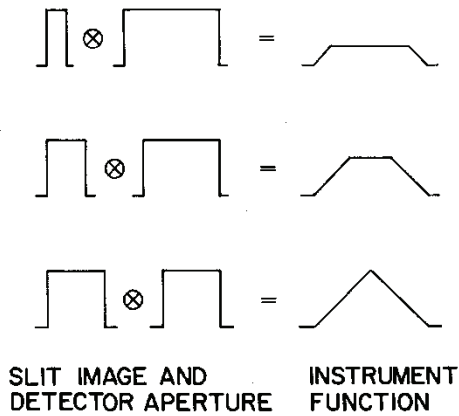
Fig. 10. Convolution of entrance and exit slits.
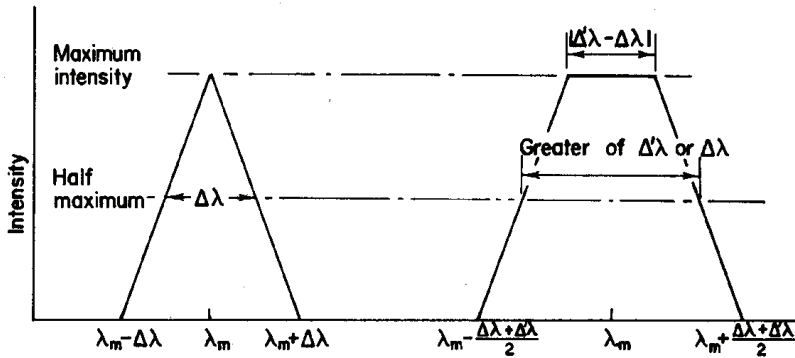
Fig. 11. Slit function for matched and unequal slit widths.

2.2.1.3.6. Exit optics

Optical radiation of the selected wavelength and passband is emanating from the exit aperture, and must be presented to the detector under test (DUT). The divergence angle of this radiation is the same as the F/# of the monochromator. Several choices are available.

If the test detector has a large active area, it can be inserted directly into the diverging beam with no auxiliary optics. This procedure, while

simple, is valid only if the exiting beam and the detector are both spatially uniform.

A lens or mirror system may be used to re-image the exit aperture onto the test detector. The chromatic aberration of the lens is not particularly important here, as long the test and reference detectors are treated equally. The image of the exit aperture should underfill the test detector, and it may require anamorphic optics (like a cylindrical lens or a toroidal mirror) to modify the aspect ratio of the image. Note that if the reference detector is of the light-trapping type, the convergence angle into the trap must be smaller than the acceptance angle of the trap else the trap performance will be compromised.

An optical fiber can also be used to gather optical radiation from the exit aperture and transport it to the test detector. The NA of the fiber should be large enough to include all of the angular spread from the exit aperture. The output end of the fiber can then be placed immediately adjacent to the test detector. There are incoherent (i.e., scrambled) fiber bundles available which have one end in a circular configuration and the other end in the form of a slit.

2.2.1.3.7. Order sorting

Inspection of the grating equation [22] shows that at any given grating angle, several harmonically related wavelengths are present. For example, if the monochromator is operated in first order (m=1) at 800nm, radiation at 400 nm (m=2), 267nm (m=3), etc. will also be present at the exit slit. The radiance associated with these wavelengths may be comparable to the m=1 radiance, depending on the blaze characteristics of the grating. It is imperative that long-wavelength pass (LWP) filters be inserted in the beam to block the higher orders. The filters should preferable be inserted between the source and the entrance slit to help minimize spectral stray radiation. For a monochromator operated over a wide wavelength range, the LWP filters can be mounted on a motorized filter wheel and controlled via the system computer.

2.2.1.3.8. Wavelength calibration

For a prism monochromator, the wavelength calibration typically reflects the dispersion of the prism. It is quite non-linear, and special procedures must be employed to ensure acceptable results. One of

the best methods, outlined by Ho [23], assumes a sine bar wavelength drive is used and that the refractive index of the prism is known over a significant portion of the wavelength range. It plots data taken from a number of line sources to a straight line transformation and does a linear least-squares fit to that line. The method can easily be modified to accommodate direct wavelength drives.

The presence of higher orders in a grating monochromator can simplify the wavelength calibration. The use of line sources is the same as for prism monochromators, with the advantage that a given line also shows up at longer wavelengths. For example, the 435 nm Hg line also appears (still as blue) when the monochromator wavelength drive is set at 870 nm. Since most grating monochromators have a sine bar wavelength drive, the dial should be quite accurate, and deviations are largely due to poor sine bar adjustment. In addition, the presence of the zero order functions as another calibration point at $\lambda=0$. Where the slit function is asymmetric, it is important to determine wavelengths at the centroid values. Wavelength settings depend on the uniformity of illumination across the grating, and may be different for narrow and wide slit settings. Narrow slit settings are best to determine the scanning accuracy. The most accurate calibration of the wavelength setting for wider slit settings is obtained by fitting the slit function to isolated calibration lines [24].

Many modern grating monochromators use direct rotation of the grating by a fine-stepped motor and a worm drive. Positions of the calibrated wavelengths are then fitted directly to the grating equation, as a sine function.

As an example, the wavelength of the infrared monochromator at the infrared spectral calibration facility of NIST (IR-SCF) [25] was calibrated using a He-Ne laser when the order sorting filters (at the monochromator input) were removed. Due to the nature of reflections from the diffraction grating during its rotation, the detector output has a periodic structure with a period of 0.6328 μm. Even with the weak radiation of a He-Ne laser, well detectable peaks can be created for very high orders of the diffraction grating. Thus, by assigning any peak to its absolute value

$$\lambda_n = 0.6328 \, n \; (\mu m) \tag{10}$$

where n is a grating diffraction order used to create a set of spectral calibration points. Note, that the accurate valu of n and therefore λ_n, may be obtained using a spectral reference such as the transmission edge of a filter. An example for the calibration spectrum is shown in the inset of Fig.12.
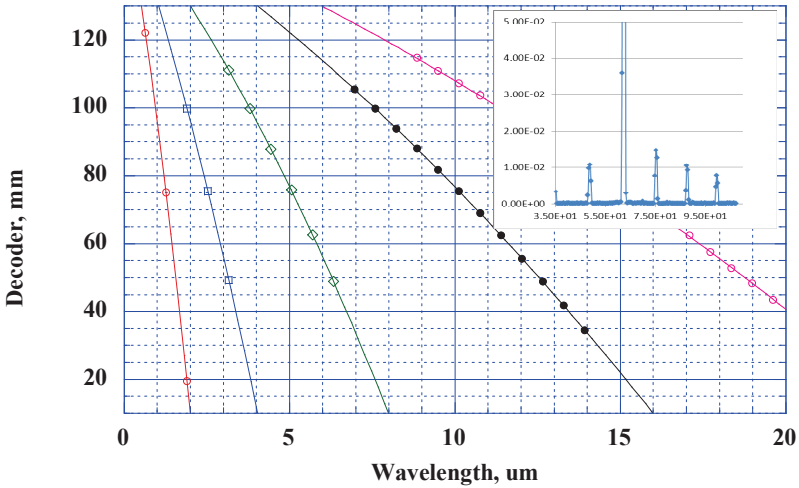
Fig. 12. Inset: detector output corresponding to different diffraction orders of grating illuminated by He-Ne laser. The five curves represent the calibration of decoder position against the wavelength for the different gratings.

Here, the X-scale is expressed in the units of the absolute encoder, D (mm), which is coupled with the position of the grating. The five peaks correspond to a range of n equal to 6 through 10. Using the relation between $\lambda_n(n)$ and $D(\lambda_n)$, the whole calibration curve $D(\lambda)$ may be obtained from the multipoint fitting. The calibration curve is then used in the program that controls the wavelength of the monochrometer. A 2nd order polynomial fitting was used in Fig. 12.

The wavelength related error in the detector responsivity $R_t(\lambda)$ is estimated as

$$\Delta R/R = [(\Delta U_t/U_t)^2 + (\Delta U_s/U_s)^2]Fi^{0.5} \tag{11}$$

where

$$\Delta U_t = \partial U_t / \partial \lambda \cdot \Delta \lambda \text{ and } \Delta U_s = \partial U_s / \partial \lambda \cdot \Delta \lambda. \tag{12}$$

The $\Delta\lambda$ which represents the wavelength reproducibility was found experimentally as standard deviation of the wavelengths from multiple records of the same $\lambda_n(n)$. The partial derivatives were taken from the slope of the related output spectral distributions.The derivative value is not a constant in the entire spectral range. For the worst case scenario, the maximum values were selected for the estimates. The calculated $\Delta R/R$ errors and the basic monochromator parameters are shown in Table 1. In the chosen optical configuration of the IR-SCF calibration facility, the $\Delta R/R$ values had a smaller affect than the other uncertainty components in the responsivity calibration. Accordingly, the wavelength related errors do not affect the total uncertainty.

Table 1. Summary of the monochromator parameters and wavelength related relative uncertainties.

Grating	Range, µm	Resolution, µm	$\Delta R/R$ wavelength related error, %	Number of calibration Points
A	0.8 –1.4	0.013	0.14	3
B	1.4 – 3.5	0.025	0.085	5
C	3.5 – 6.5	0.05	0.093	6
D	6.5 – 11	0.09	0.05	11
E	11 – 20	0.16	0.12	16

2.2.1.3.9. Bandwidth effects

The measured spectral responsivity values represent an average value over the bandwidth of the monochromator. The spectral distribution of the light source, the slit function of the monochromator itself and the reference and test detector responsivities all influence the measured values of the device under test [26]. These effects are all strongest where these quantities are changing rapidly with wavelength.

Ideally the test and reference detectors used in a measurement should be the same type as this cancels bandwidth effects. However, this is not practical and the next best choice is to use a trap detector as the reference, because its spectral response is linear with wavelength over a wide wavelength range. Using a lamp with a

smooth spectral distribution also reduces bandwidth errors.

In a measurement, the wavelength of the test is taken to be that of the setting of the monochromator, determined as the centroid of the slit function. The slit function is determined by scanning the spectrometer over a monochromatic line, or series of monochromatic lines (such as the Mercury 546 nm emission line). For symmetric distributions typically encountered, the peak and centroid wavelengths coincide. For non-symmetric slit functions, such as may be found with fibre-coupled spectrometers, the centroid and peak wavelengths may not coincide. Similarly, where the lamp spectrum, grating efficiency or detector responsivity are varying within the monochromator bandwidth, the effective slit function becomes the convolution of all these influences and may be non-symmetric and hence lead to the spectral values reported at the wavelength of the monochromator setting being in error.

One method of dealing with the error is to report the values not at the monochromator wavelength setting, but at an effective wavelength shifted slightly depending on the measured responsivity values, the slit function and the source distribution [27]. Another method is to apply a correction filter of the type originally described by Stearns and Stearns [28]. This assumes that the original data can be represented as a quadratic function of wavelength across the bandwidth of the measurement, and refines the measured values to those that would apply for zero bandwidth. Stearns and Stearns assumed a symmetric slit function and data spacing related to the bandwidth; the method has recently been extended to arbitrary slit functions and data spacings [29], [24].

In this method, moments of the slit function

$$I_n = \int \lambda^n s(\lambda, \lambda_0) d\lambda \tag{13}$$

are calculated for $n=0,1,2$. These are used in turn to calculate three filter coefficients

$$a_{-1} = \frac{1}{2}\left(\frac{I_2}{\delta^2} - \frac{I_1}{\delta}\right)$$

$$a_0 = \left(I_0 - \frac{I_2}{\delta^2}\right)$$

(14)

$$a_1 = \frac{1}{2}\left(\frac{I_2}{\delta^2} + \frac{I_1}{\delta}\right)$$

where δ is the wavelength spacing between data points, within the bandwidth. Data points are typically recorded at a spacing equal to the full-width-half-maximum bandwidth. Where data are significantly oversampled, as is typical for array spectrometers, points at a spacing approximately equal to the bandwidth are used.

Data corrected for bandwidth errors are calculated by replacing each measured point M_0 by a convolution of the surrounding points,

$$S_0 = \frac{a_{-1}{}^2 M_{-2} - a_{-1}M_{-1} + a_0 M_0 - a_1 M_1 + a_1{}^2 M_2}{a_0{}^2 - 2a_{-1}a_1}$$

(15)

2.2.1.3.10. Monochromator recommendations

If a prism-grating monochromator is unavailable, a double grating monochromator is recommended. Operate it in a subtractive dispersion mode to ensure uniformity and homogeneity at the exit slit. Set the center slit slightly wider than the entrance and exit slits. Use a tungsten-halogen lamp with a filament structure whose image can be matched to the entrance slit. Alternatively, use a spatially-stabilized xenon arc with smaller apertures. Temperature and current stabilized (and maybe battery-operated) LED sources in the UV produce higher signal and lower noise than tungsten halogen lamps.

2.2.2. Uniform sources for responsivity calibrations

Because of the low flux in a lamp-monochromator system, instruments may not be calibrated for irradiance or radiance responsivity. The low flux associated with lamp-monochromator excitation sources (~ 1 μW) limits the effective dynamic range of responsivity measurements. The out-of-band response of filter

radiometers can only be measured to approximately 0.001 % of the peak response. Also, the beam profile of lamp-monochromator sources is highly non-uniform (spatially). Instead of traditionally used lamp-monochromator sources tunable laser sources coupled to an integrating sphere are more frequently used to realize monochromatic and uniform radiance and irradiance sources that are suitable for both irradiance and radiance responsivity transfer.

2.2.2.1. Tunable lasers, collimators, and integrating spheres

With the development of tunable dye lasers in the 1970s, high-power, monochromatic, tunable sources became available for scientific use. Replacing the lamp-monochromator source with a tunable laser source has a number of advantages for radiometric applications, in particular the high-power, very narrow spectral bandwidth, and extremely low wavelength uncertainty of the laser-based source. The high-power, tunable lasers can be introduced into an integrating sphere producing uniform, quasi-Lambertian, high radiant flux sources. High spatial uniformity can be achieved not only inside the sphere exit port, but also in a plane (or planes) where the reference and test detectors are mounted. Reference irradiance detectors, calibrated directly against national primary standards for spectral power responsivity, can be used to determine the irradiance at a reference plane. Knowing the measurement geometry, the source radiance can be readily determined as well. Instruments can be calibrated directly in irradiance or radiance mode with uncertainties approaching those available for spectral power responsivity calibrations.

The spectral coverage of the tunable lasers defines the spectral range of a laser-based responsivity calibration while the quality of the reference detectors and their calibration uncertainties determine the uncertainty of that measurement.

In a practical arrangement, the output of a high power, tunable laser is first directed through an intensity stabilizer that can control the relative optical power in the beam to within 0.01 % of the set point. A portion of the laser beam can be sent into a wavelength meter, such as a Michelson interferometer, that can measure the radiation to within 0.001 nm. Another portion of the laser beam can be sent into a Fabry-Perot interferometer to measure the bandwidth and mode stability of the laser. The laser radiation is typically introduced into an

integrating sphere, often using an optical fiber. Different size spheres can be used, depending on the application. Collimators also can be coupled to the sphere and used as calibration sources. Speckle in the image from the source, originating from the coherent nature of the laser radiation, can be effectively removed by either rastering the beam inside the sphere with a galvanometer-driven mirror or by placing a short length of optical fiber in an ultrasonic bath. Note that the speckle is still present, but is altered on a much shorter time constant than the observing radiometers, effectively averaging out the distribution. A monitor photodiode can be located on the sphere to correct for any radiant flux changes in the sphere output between measurements with the reference detector and the device under test. The sources can be located inside a light-tight box. Typically, two baffles are needed between the source and the detectors to minimize effects of stray radiation on the measurement.

Calibrations can be performed by direct substitution against reference irradiance meters. For both irradiance and radiance responsivity calibrations, the distance between the source aperture and the defining aperture on the reference detector should be known.

Continuous tunability can be provided by dye lasers and Ti:Sapphire lasers that are pumped by either an Argon ion laser or a frequency-doubled Nd:Vanadate laser. A number of discrete wavelengths can be provided by the pump lasers themselves. Ti:Sapphire lasers cover the spectral range from 680 nm to 1050 nm. Frequency doubling of Ti:Sapphire lasers enables tuning from 350 nm to 500 nm. Over 300 mW of optical power can be obtained from dye lasers and Ti:Sapphire lasers (with optical powers of 1 W or greater over much of the spectral range). The power available from the cw, frequency-doubled radiation is typically in the range from 100 mW to 200 mW. Quasi-cw, mode-locked laser systems have been shown in the past to be equivalent to cw systems for radiometric calibrations of silicon radiometers, with no additional uncertainties in the calibration arising from the quasi-cw nature of the radiation [30]. Non-linear optical systems take advantage of the pulsed nature of the radiation: it is significantly easier to generate sum and difference frequency radiation using a mode-locked laser rather than a true cw laser because of the high peak power of the mode-locked source. One useful feature of the quasi-cw system is that the bandwidth of the radiation is considerable broader than radiation from the cw systems. This may help to alleviate some of the problems associated with

interference fringes.

Computer-controlled actuators can be used to rotate the angle of the birefringent tuner in dye and Ti:sapphire lasers. The minimum step size is determined by the free spectral range of the etalon in the lasers. For a 1 mm etalon, the minimum wavelength step using the birefringent tuner is 0.16 nm at 600 nm. For finer spectral resolution, the etalon angle can be changed as well.

For the infrared wavelength range, periodically poled Lithium Niobate (PPLN) OPO pumped by a Nd:YAG laser, mode-locked PPLN OPO pumped by a ND:Vanadate laser, and mode-locked LBO OPO pumped by the 2nd harmonic of a Nd:Vanadate laser can be used up to 5 μm [31]. The power level is in the 100 mW to 1 W range.

Different integrating spheres can be used for different radiometric calibrations. Small diameter integrating spheres – typically diameters of 2.5 cm to 5 cm – equipped with precision apertures with diameters ranging from 3 mm to 8 mm can be used for irradiance responsivity calibrations. Larger diameter spheres – 30 cm to 40 cm diameter – with 5 cm to 10 cm diameter exit ports can be used for radiance measurements. Coatings with high diffuse reflectance should be used. Sintered polytetrafluoroethylene-based coating can be used from about 250 nm to 2.5 μm. Typical irradiance levels at 1 m using a 2.5 cm diameter integrating sphere with a 5 mm diameter aperture range from about 1 μW/cm^2 to 10 μW/cm^2. Radiance levels between 1 mW/cm^2/sr and 5 mW/cm^2/sr are typical for a 30 cm diameter sphere with a 7.5 cm diameter output port. Gold coated spheres are used for the infrared range. The area of the exit apertures is to be measured [32].

When a radiometer or photometer is designed to measure sources that are collimated, the calibration source should also be collimated to obtain low measurement uncertainties. Collimated sources made from spheres with lenses are frequently used to calibrate filter radiometers and transmission of lenses [33]. Also, off-axis parabolic mirrors can be used to prepare the quasi-collimated source. Mirrors have the advantage over lenses of achromaticity from the UV to the IR. The irradiance can be orders of magnitude greater than with the integrating sphere alone [34]. However, angular divergence which determines the degree of collimation, spatial uniformity which is greatly effected by the spatial uniformity of the mirror, and the degree

of the Lambertian output of the source should be assessed to obtain the lowest uncertainty in the calibrations.

Collimators are frequently used for irradiance responsivity calibrations using the substitution method.

2.2.2.2. Stray light and fluorescence

Spectral responsivity of detectors is normally measured by using a tunable monochromatic source and a reference detector (eg. a Si photodiode). Measurement errors may be significant due to the spectral impurity of the monochromatic source, especially in the case of measuring filter radiometers such as tri-stimulus colorimeters, photometers, etc, which have very dissimilar spectral responsivities compared to those of typical reference detectors.

A filter radiometer typically has low spectral responsivity near the edges of the defined bandpass region. When a monochromatic source is tuned to the spectral region near the edge of the bandpass of a filter radiometer, the result of the spectral responsivity measurement becomes very sensitive to the small spectral radiant flux components from the light source of the monochromator at the center region of the bandpass interval, where the responsivity of the filter radiometer is high.

The spectral impurities of a monochromatic source arise from the scattered light or so-called stray light inside a monochromator, from fluorescence of optical elements in the measurement system, and from the out-of-band leakage of a bandpass filter, etc.

2.2.2.2.1. Stray light in monochromators

Monochromators are commonly used for measurement of spectral responsivities of detectors. A double monochromator has a level of stray light of 10^{-6} to 10^{-9}, depending on the quality of the double monochromator, and the measurement errors from stray light are normally insignificant. Kostkowski estimated that the stray light error is less than 0.1 % at 250 nm with a high quality double monochromator [22]. However, since a double monochromator is a two-dispersion-element system, its throughput is typically very low (on the level of a few percent). Therefore, single monochromators are often used for measurement of detectors with low responsivities such as pyrometers. Single monochromators are also being used for

measurement of material optical properties such as bidirectional reflectance distribution function (BRDF). A high quality single monochromator has a stray light level of 10^{-4} to 10^{-5}, and the measurement error from stray light reaches 30 % at 300 nm and 90 % at 250 nm [22]. Figure 13 shows the problems (the unwanted signal components) of a monochromator system. In addition to the desired spectral output (the real signal), stray light, fluorescence, and second order diffraction are included in the output signal of the monochromator.
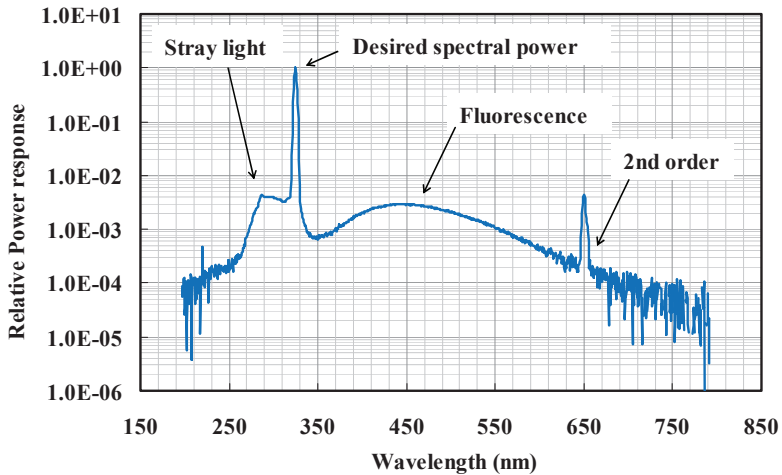
Fig. 13. Monochromator output signal with the desired spectral output, stray light, fluorescence, and 2nd order diffraction.

2.2.2.2.2. Fluorescence of optical elements

Optical elements such as integrating spheres, and colored glass optical filters, etc., often have fluorescence for source excitance in the deep-blue and UV regions. Fluorescence of an optical element is associated with the optical material, with the fabrication process, and more commonly associated with the contamination by ducts, oil, and gas, etc. Figure 14 shows the fluorescence of a V(λ) filter in the blue. Because of the fluorescence, an error is measured in the spectral responsivity between 380 nm and 460 nm.

Tunable lasers with an integrating sphere are increasingly used as a uniform Lambertian monochromatic source for measurement of spectral radiance and irradiance responsivities of detectors, because the tunable laser sources have high spectral radiant power and extremely narrow bandwidths and potentially can achieve lowest measurement uncertainties. However, fluorescence of the integrating sphere in the UV region can be an serious issue and may become the dominant uncertainty in the measurement of spectral responsivity of detectors [35] [36].

A simple matrix method has been developed for correction of stray light inside spectrometers, based on the characterization of a spectrometer for spectral line spread functions [20, 37, 38]. This method can be used to correct measurement errors from both stray light and fluorescence for measurement of spectral responsivities of detectors.
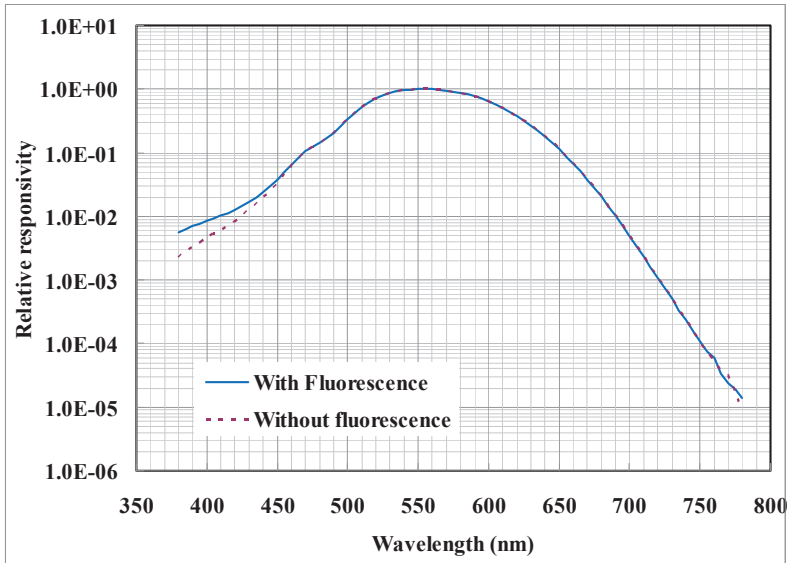
Fig. 14. Fluorescence caused spectral responsivity increase in a V(λ) filter.

2.2.2.3. Tunable laser-used responsivity calibration facility

In the calibration facility of the National Institute of Standards and Technology (NIST), emission from high-power, tunable lasers is

introduced into an integrating sphere producing uniform, quasi-lambertian, high radiant flux sources. Reference standard irradiance detectors, calibrated directly against national primary standards for spectral power responsivity, are used to determine the irradiance at a reference plane. Knowing the measurement geometry, the source radiance can be readily determined as well. Instruments are calibrated directly in irradiance or radiance mode with uncertainties approaching or exceeding those available for spectral power responsivity calibrations.

There are three components to the Spectral Irradiance and Radiance Responsivity Calibrations using Uniform Sources (SIRCUS) facility: an ultraviolet, visible and near infrared (UV-Vis-NIR) SIRCUS, an infrared (IR) SIRCUS, and a high accuracy electrical substitution cryogenic radiometer system. A cryogenic radiometer is a primary standard for the measurement of optical power. The UV-Vis-NIR facility operates over the spectral region from 210 nm to 960 nm; extensions to the short-wave infrared, out to 2.5 μm, has also been made. The IR SIRCUS facility has a spectral coverage from 700 nm to 5.3 μm using tunable Optical Parametric Oscillator (OPO) systems, and coverage to 11 μm using discrete laser sources. Lasers from both SIRCUS facilities can be introduced into the POWR radiometer for detector responsivity measurements. Typically, reference instruments used on SIRCUS are calibrated against absolute cryogenic radiometers (ACR). A small, L1 ACR [1], is frequently used for reference calibrations. It has a short cavity response time and is located on a portable table and can be readily moved between facilities. Intercomparisons using transfer standard detectors establish the equivalence between the existing cryogenic radiometers.

The spectral coverage available with the tunable lasers ultimately defines the spectral range of the SIRCUS facility while the quality of the reference standard detectors and their radiometric uncertainties ultimately determines the uncertainty achievable on SIRCUS. As an example, the UV-Vis-NIR facility is discussed below and the spectral range, covered by the tunable lasers shown in Fig. 15, is limited from

---

[1] Identification of commercial equipment is for information purposes. It does not imply recommendation or endorsement by the author, nor does it imply that the equipment identified is necessarily the best available for the purpose.

210 nm to 960 nm where silicon reference detectors are available.

2.2.2.3.1. Setup

The scheme of the SIRCUS facility is shown in Figure 16. The output of a high power, tunable laser is first directed through an intensity stabilizer that controls the relative optical power in the beam to within 0.1 % of the set point. A portion of the laser beam is sent into a traveling Michelson interferometer that measures the wavelength of the radiation to within 0.001 nm. Another portion of the laser beam is introduced into a Fabry-Perot interferometer to measure the bandwidth and mode stability of the laser.
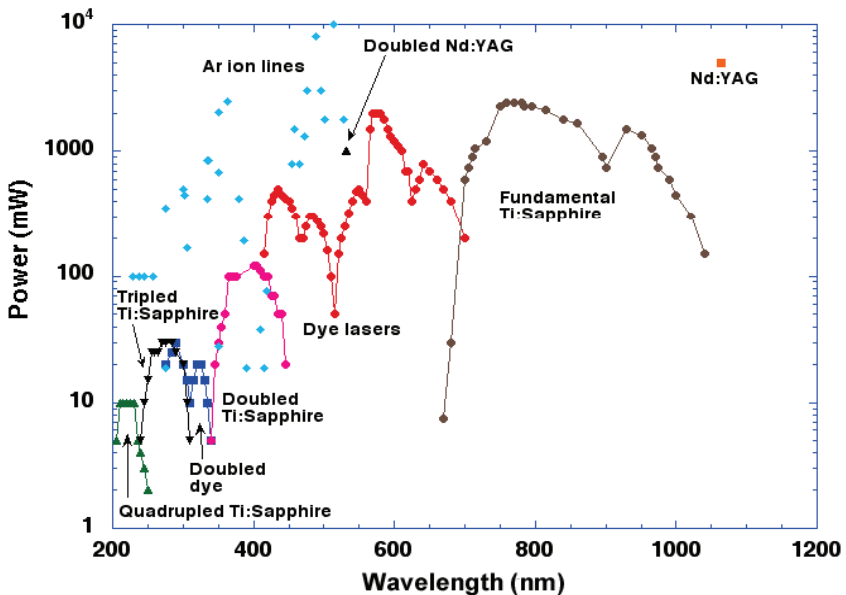
Fig. 15. Lasers, output power and spectral coverage of the UV-Vis-IR SIRCUS facility of NIST.

The laser radiation is typically introduced into an integrating sphere, often using an optical fiber. Different size spheres are used, depending on the application. Occasionally, a collimator coupled to the sphere is used as a calibration source. Speckle in the image from the source, originating from interference due to the coherent nature of the laser radiation, is effectively removed by either rastering the

beam inside the sphere with a galvanometer-driven mirror, or by placing a short length of optical fiber in an ultrasonic bath. Note that the speckle is still present, but is altered on a much shorter time constant than the observing radiometers, effectively averaging out the distribution. A monitor photodiode is located on the sphere to correct for any radiant flux changes in the sphere output between measurements with the reference instrument and the device under test. The sources and detectors are located inside a light-tight box (1.4m wide, 1.2m tall, 3.2m long) that has been covered on the inside with a material of excellent light-absorbing properties: the measured reflectance is on the order of 0.1 % –0.3 % from 300 nm to 2.5 μm. Two baffles are typically installed between the source and the detectors to minimize effects of stray radiation on the measurement.

2.2.2.3.2. Calibrations

Calibrations are performed by direct substitution against primary standard reference irradiance meters. For both irradiance and radiance responsivity calibrations, the distance between the source aperture and the defining aperture on the reference standard detector is required. An electronic ruler with a resolution of 5 μm measures the distance between the source and the detectors.

A calibration relates the measured quantity from a radiometer, usually current or voltage, to the radiometric quantity being measured, e.g. radiance or irradiance, through the instrument's responsivity. Determination of an instrument's responsivity and an evaluation of the associated uncertainties are required in a calibration. The substitution method is used for calibrations in SIRCUS. NIST reference standard irradiance meters determine the irradiance at a reference plane. From the irradiance at the reference plane, which is usually the plane of the detector aperture, the radiance of a source can be determined knowing the distance between the detector and source apertures, as well as the area of the source aperture. The instrument being calibrated, or Device Under Test (DUT), is then placed in front of the source and its signal recorded. The laser is blocked and the dark signal recorded prior to each measurement. The responsivity (at the excitation wavelength) is the instrument's net output signal (with the dark signal subtracted from the light signal) divided by the radiometric quantity to be measured.

The detector substitution method is typically used for calibrations with uniform laser-sphere sources. Reference irradiance meters determine the irradiance at a reference plane. From the irradiance at a reference plane, the radiance of the source can be determined knowing the distance between the detector and source apertures, as well as the area of the source aperture. The instrument being calibrated, or Device Under Test (DUT), is then placed in front of the source and its signal recorded. The responsivity (at the excitation wavelength) is the instrument signal divided by the radiometric quantity.

A measurement equation is a mathematical expression describing the relationship between the measured quantity, the source radiometric quantity, and the instrument responsivity. The simplified measurement for irradiance responsivity, using a trap reference detector, is:

$$s_E\left(\frac{A}{W/cm^2}\right)_{DUT} = \frac{i(A)_{DUT}}{i(A)_{trap}} \cdot s_E\left(\frac{A}{W/cm^2}\right)_{trap} = \frac{i(A)_{DUT}}{i(A)_{trap}} \cdot s_P(A/W)_{trap} \cdot A(cm^2)$$

$$(16)$$

where s_{EDUT} is the irradiance responsivity of the device under test, s_{Etrap} is the irradiance responsivity of the trap, $s_P(A/W)_{trap}$ is the power spectral responsivity of the trap, A is the area of the aperture on the trap, and i is the photocurrent in amps. The photocurrent is converted to voltage in a transimpedance amplifier and then measured with a multimeter.

Eq. (16) assumes that the DUT and trap are in the same plane (defining apertures are located the same distance from the point source). In many cases they are located in different planes. For a point-source geometry, the scale derivations are discussed below.

Figure 17 illustrates the calibration of irradiance (Test 1), radiance (Test 2), and radiant power (Test 3) meters against a transfer standard power/irradiance meter. All four radiometers are mounted on a X-Y moving stage. In this example, the radiant intensity I of the sphere-applied "point" source is determined from the irradiance E_1 measured by the irradiance mode transfer standard. The radiant intensity is equal to the product of the irradiance and the distance-square if the separation between the sphere-port and the detector is

large enough. From measuring the distances D_1 and D_2 and utilizing the equivalence of the radiant intensity in the irradiance responsivity transfer, the irradiance on the Test 1 irradiance meter can be calculated. The irradiance responsivity will be the ratio of its measured output signal (photocurrent) divided by the incident irradiance (calculated for its reference plane). In the next step, the test radiance meter will be moved into the optical axis of the sphere source. The target spot of the meter should be smaller than the size of the exit port and it should be positioned in the center of the port. The radiance of the exit port is equal to the ratio of the radiant intensity (of the sphere point-source) to the area of the exit-port. The radiance responsivity will be obtained by dividing the measured output signal of the Test 2 radiance meter with the measured (and previously calculated) exit-port radiance. In power mode, the Test 3 power meter will measure the known total power in the incident laser radiation. The power responsivity of Test 3 will be equal to the measured output signal divided by the incident radiant power. The scheme of the SIRCUS scale derivation is detailed in Fig. 18.

The monitor detector can hold the spectral radiant-intensity scale of SIRCUS.
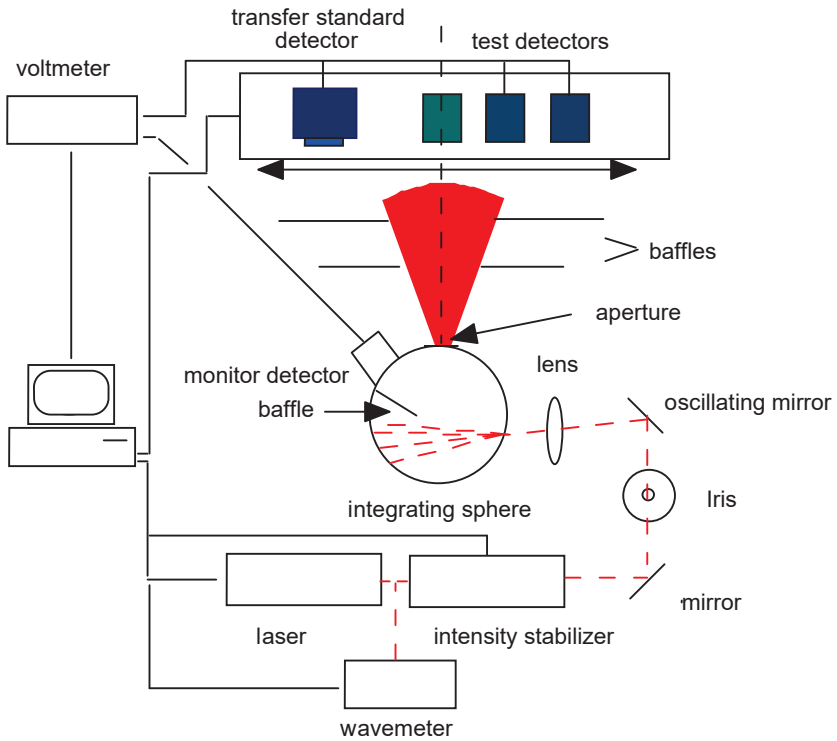
Fig. 16. Scheme of the SIRCUS facility.
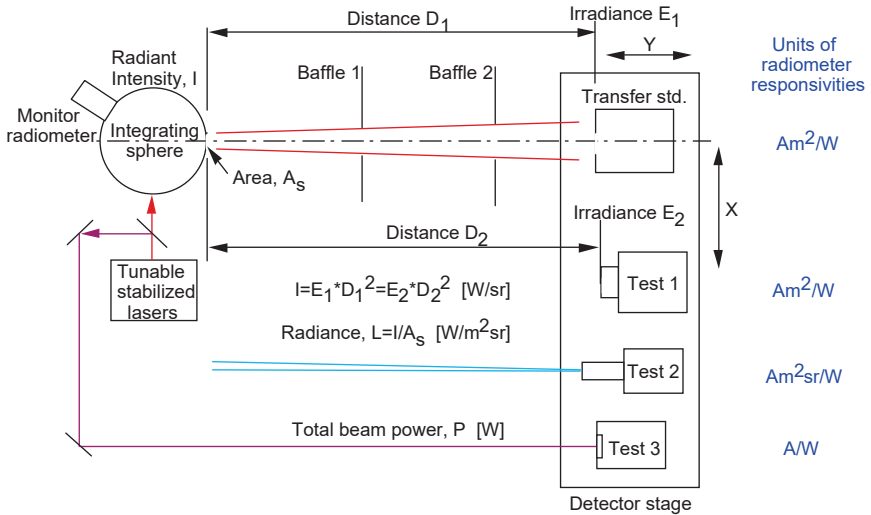
Fig. 17. Calibration of test radiometers at the SIRCUS facility.

Characterization of an instrument and an understanding and evaluation of all meaningful sources of uncertainty are crucial for a proper calibration. A calibration without an associated uncertainty table is of limited use. The evaluation and expression of uncertainty is generally difficult and time-consuming; it is not unusual to have incomplete or inaccurate information in an uncertainty table. Determining how best to express a particular uncertainty component can be confusing. There are a variety of useful references that provide definitions and recommendations for describing and establishing the uncertainties encountered when calibrating a radiometer [39, 40].
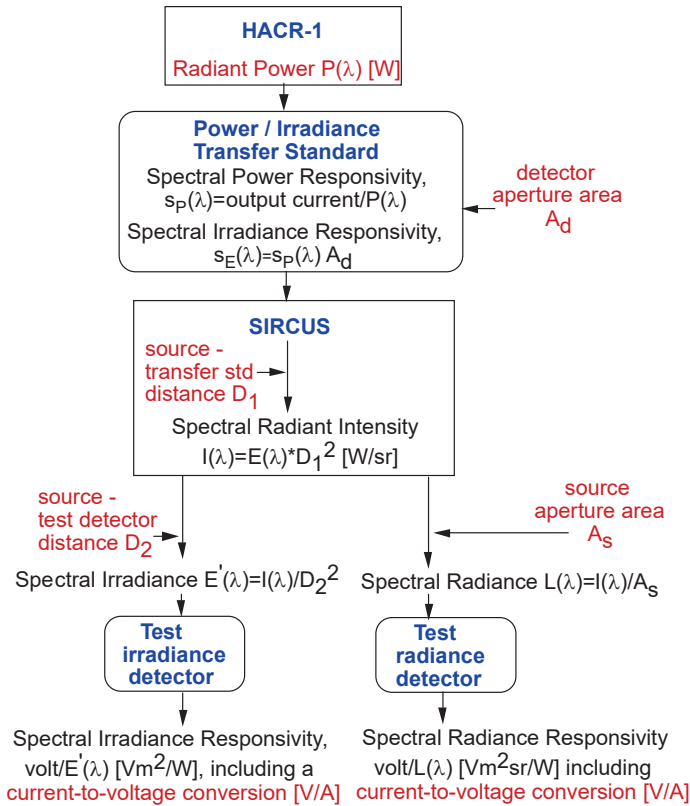
Fig. 18. Scheme of the SIRCUS scale derivation.

In many cases, the reference plane of the DUT is not known and must be determined radiometrically. This can be done by making measurements with the DUT at many distances from the source using a ruler. Using the inverse square law in a curve fit to the measured data [41], the source offset can be obtained. The source and irradiance-DUT separation will be equal to the difference of the DUT position (ruler reading) and the source-offset.

Equation 16 assumes that the reference planes of the DUT and trap are in the same plane, *i.e.* that the defining apertures are located the same distance from the point source. In many cases, they are located in different planes. As shown in Fig. 17, for a point-source geometry,

$$I(\lambda) = E_1(\lambda)D_1^2 = E_2(\lambda)D_2^2 \, , \tag{17}$$

where $I(\lambda)$ is the radiant intensity of the source, E_1 is the irradiance at reference plane 1, located a distance D_1 from the source; and E_2 is the irradiance at reference plane 2, located a distance D_2 from the source. In many cases, the reference plane of the DUT is not known and must be determined radiometrically.

The distance between the source and trap detector apertures (reference planes) is measured optically and mechanically. For a point-source geometry, the irradiance should follow an inverse square law; *i.e.*, the irradiance should be a function of $1/D^2$, where D is the distance between the two reference planes. The relative distance between the source and the detector is measured with an electronic ruler that has a quoted resolution of 5 μm [42]. The 3-axis detector translation stage is moved in the horizontal direction and the detector and monitor signals are acquired as a function of relative distance. The ratio of the trap signal to the monitor signal is then plotted as a function of distance and fit with a non-linear least squares algorithm [43]. Figure 19 illustrates an optical distance measurement, with the solid circles being measured trap to monitor ratios and the solid line the fit to the data. The data were fit to the expression,

$$y = m_1 / (m_0 - m_2)^2 \, , \tag{18}$$

where the radiant intensity is given by m_1, the zero-offset of the fixed source is m_2, and m_0 is the position of the stage measured by the electronic ruler. The uncertainty in the fit to m_2 is 28.7 μm. Since we know the zero-offset from this fit, we also know the absolute separation at any value of the electronic ruler with an uncertainty of 28.7 μm. To validate the radiometric measurements, the aperture separation was also measured using a calibrated ruler [44]. The two separate techniques used to measure the distance between the source and detector reference planes agree, usually within 50 μm. Given a 50-μm uncertainty in the trap reference plane, the uncertainty in the irradiance at a given reference plane for distances of 1 m or greater is less than 0.01%.

For radiometers with a known reference plane, a micrometer is used to make sure that the DUTs and the reference trap aperture lie in the same plane. Using a micrometer, the reference planes can be aligned to within approximately 10 μm. Consequently, this approach significantly reduces the uncertainty in the irradiance at the DUT reference plane. In the case that the DUT reference plane is not known, it is optically determined. For a non-point-source geometry, the full equation including the spatial extent of the source and detector is required [45]; the uncertainties remain the same.

y = m1/(m2-m0)^ 2		
	Value	Error
m1	271875	28.6767
m2	1939.24	0.0287639
Chisq	1.99482e-08	NA
R	1	NA
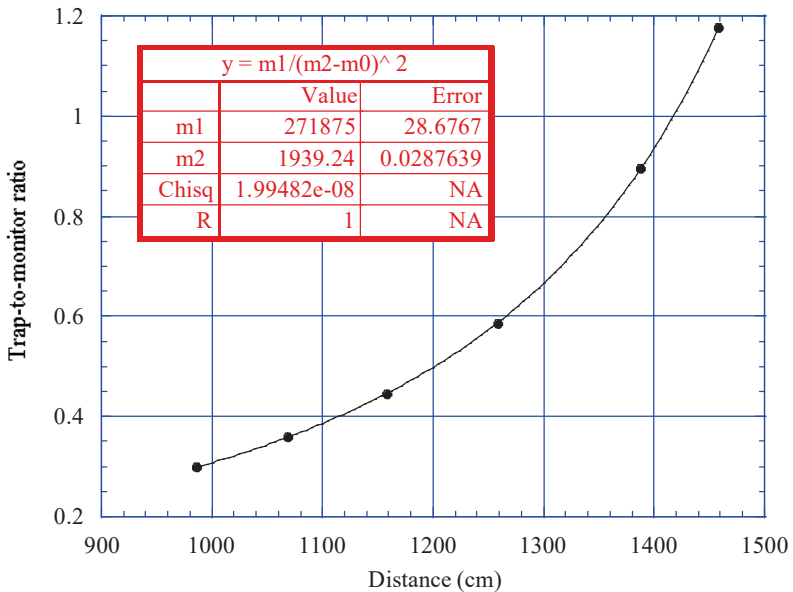
Fig. 19. 1 / r squared radiometric determination of the distance between two aperture planes.

2.2.2.3.3. Uncertainty considerations

There are two types of uncertainty components, designated Type A and Type B. Type A uncertainties are evaluated using statistical methods while Type B uncertainties are evaluated using models or other external information. The term "standard uncertainty" refers to an estimated standard deviation. Assuming each uncertainty component is independent from the others (the components are un-correlated), the combined standard uncertainty is the root sum

square of the individual uncertainty components. Often, the different variables are not completely independent from one another, and correlations between these variables need to be taken into account [46, 47].

The expanded uncertainty is the product of the combined standard uncertainty and a coverage factor k, where the value of k is chosen based on the desired level of confidence. Typically the expanded uncertainty is reported with $k = 2$, corresponding to a confidence level of 95 %. A confidence level of 95 % means that there is a 1 in 20 chance that a measurement will fall outside the interval. A coverage factor $k = 3$ corresponds to a confidence level of 99 %, meaning there is a 1 % chance that a measurement will fall outside the stated interval. In reporting the uncertainty for a measurement, the components of standard uncertainty are listed and their designation stated (A or B).

The dominant uncertainties of the spectral irradiance responsivity scale originate from systematic errors in the absolute scale transfer from the cryogenic radiometer. Temperature variations within the facility, while small, may also contribute to the overall uncertainty in certain spectral regions. The radiometric stability of the source (and monitor detector) and the irradiance uniformity at a reference plane contribute to the overall uncertainty in the measurement. Additional uncertainties from the radiometric characteristics of the DUT need to be quantified to establish the uncertainty in the calibration (and subsequent measurements of a source). Typically, the instrument's response linearity, temperature dependence, polarization dependence, and out-of-FOV blocking are measured. The current-to-voltage converter and the multi-meter used to measure the signal need to be characterized and their contribution to the overall uncertainty established. Finally, both short-term stability (repeatability) and long-term stability (to monitor degradation in time) should be considered.

The radiant power and wavelength stability are two of the primary uncertainty components. A laser intensity stabilizer keeps the laser power level constant to within 0.1 %. The lasers used as excitation sources are equipped with etalons to reduce the wavelength uncertainty from mode hopping. The wavelength uncertainty is on the order of 10^{-3} nm with a typical bandwidth on the order of 10^{-3} nm. The wavelength uncertainty is dominated by the dependence of the index of refraction of air on temperature, humidity and pressure. The wavemeter corrects for the temperature and pressure dependence,

and can be programmed to correct for the humidity.

The sequence for measurements of a DUT is to first measure the trap and monitor signal, then move the stage so that the DUT versus monitor signal is measured, then move back to the trap measurement. If any change is observed in the trap-to-monitor ratio greater than ~0.01%, additional measurements are made and the data are averaged. Typically from 9 to 16 samples are averaged for each data point. Occasionally additional samples are taken, for example when measuring the out-of-band response of a filter radiometer under test.

The irradiance at a reference plane should be spatially uniform to limit the magnitude of corrections for different size entrance pupils. The irradiance is uniform to within 0.1 % over the central $+/-$ 2 cm in both the horizontal and vertical directions. The entrance apertures of most irradiance meters calibrated on SIRCUS have diameters significantly smaller than 4 cm, and no correction for irradiance non-uniformity at the reference plane is applied.

To achieve the lowest possible uncertainties on SIRCUS, the instrument should be designed with the calibration in mind. The uncertainty in the transfer to a test instrument is listed in Table 2 as 0.03 %. This is for a well-designed, well-characterized, stable radiometer. Non-ideal instrument characteristics such as stability, temperature dependence, long-term drift, out-of-field response, etc. all contribute to increased overall uncertainty in a calibration.

Interference fringes from multiple reflections of incident radiation at optical surfaces have been observed in the calibration of instruments with windows and other optical elements if they are not wedged or anti-reflection coated. For example, the absolute spectral responsivity of a pyrometer calibrated on SIRCUS is shown in Fig. 20(a). Interference fringes (the sinusoidal oscillations in the responsivity) are emphasized in the expanded view (Fig. 20(b)). The presence of interference fringes increases the difficulty in the calibration if they need to be measured during the calibration or increases the uncertainty in the calibration.

As an aside, we have found that interference fringes are ubiquitous, caused mainly by the window on the photodiode or parallel-surface windows in the device, or filters [48]. A complete mapping of the

fringes is possible on SIRCUS because of the narrow spectral bandwidth and wavelength stability of the lasers, as well as the fact that the laser wavelength can be tuned automatically. In certain calibration approaches, for example using lamp-monochromator systems, the fringes are not observed. Note however that the fringes are present in the responsivity irrespective of the technique used in the calibration. If they are not observed, the fine structure in the spectral responsivity caused by interference fringes is averaged over the finite source bandwidth. However, the averaging may not be complete, and artifacts caused by incomplete cancellation of the fringes can lead to erroneous results. Also, errors can arise in the determination of an instrument's effective aperture area using the scanning method if fringes are present [48]. In this case, the instrument should be calibrated directly in irradiance mode to obtain the lowest achievable uncertainties.

The spatial uniformity of the radiance of the sphere exit port is shown in Fig. 21 with 0.1 % contours.

Table 2. SIRCUS uncertainty for an irradiance responsivity calibration.

Uncertainty Component	Relative standard uncertainty [%]	
	Type A	Type B
Reference detector responsivity		
400 nm to 920 nm		0.05
Aperture Area		0.004
Response uniformity	0.005	
Cosine dependence		0.01
Polarization		0.00
Linearity	0.00	
Temperature		0.003
Source characteristics		
Radiant Power	0.005	
Wavelength (<0.01 nm)		0.005
Irradiance uniformity	0.005	
Determination of the reference plane	0.01	
I-V Gain		0.01
Voltmeter Reading		0.005
Irradiance	0.054	
Transfer to device under test	0.030	
Combined standard uncertainty ($k = 1$)	0.062	
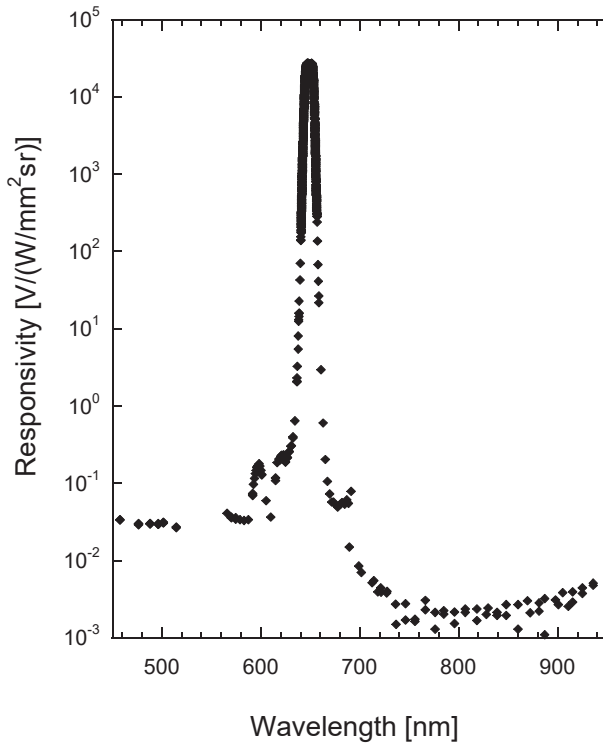
(a)
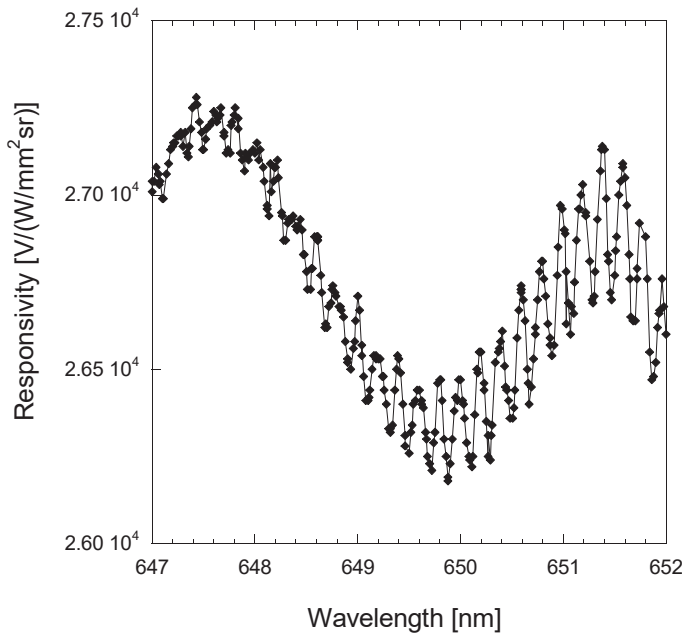
(b)

Fig. 20. (a) Absolute spectral responsivity of a filter radiometer showing
large oscillations in the responsivity arising from multiple interference within
the instrument. (b) Expanded view of the oscillations.
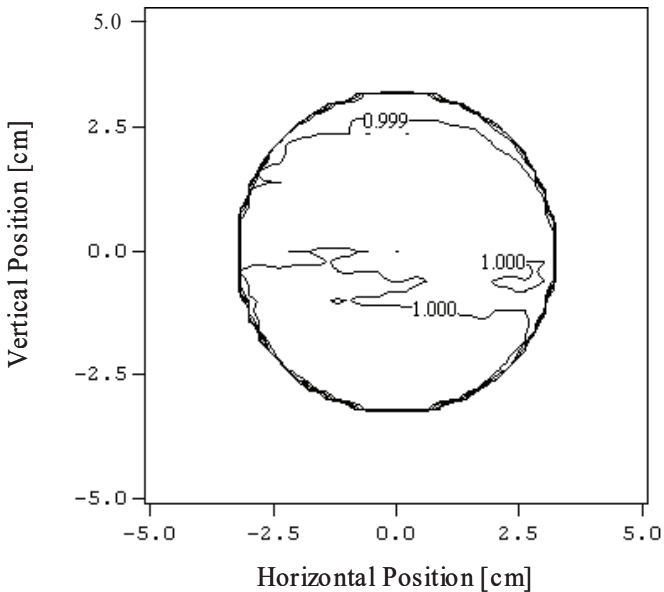
Fig. 21. Spatial radiance uniformity of a shphere exit port.

2.2.2.3.4. Calibration procedure

Before an instrument can be calibrated, it must be aligned with respect to the integrating sphere, as does the reference standard detector. To align the system, a laser is used to define an optical axis. Both the integrating sphere and the detectors are then aligned to the optical axis. The optical axis is typically set to be parallel to the direction of motion of a linear translation stage that moves perpendicular to the sphere exit port (the Z-axis of the detector stage). The Z-axis translation stage sits on a pair of rails and is manually translated. A linear encoder records the stage position along the rails [42].

As illustrated in Fig. 22, to define the optical axis, a laser beam is incident on a pellicle beamsplitter that is mounted on the z-axis rail system. A mirror is positioned behind the pellicle to retro-reflect the light directly back into the laser. The pellicle is in a mirror mount and is adjusted to reflect light that is then aligned to be parallel to the translation stage. This is done by first mounting an iris near the pellicle beamsplitter on the translation stage and aligning it such that

the laser light is centered on the iris aperture. Then, the iris is moved using the translation stage to lie some distance away from the pellicle. The angle of the pellicle beamsplitter is adjusted to have the light reflected from it go through the iris aperture. These two steps are repeated until the beam is centered on the iris at the two translation stage positions. At this point, the optical beam is parallel to the translation stage and the optical axis is defined.

To align the detectors, the motorized x-y translation stage is positioned such that the laser is centered on each detector (one at a time), and the reflection from a flat reference plane on the detector is parallel with the incident beam. For each detector, a computer registers and stores the alignment position. The retro-reflected beam (from the mirror behind the pellicle) is automatically aligned parallel to the rail. The sphere exit port is then centered on this beam (and the angle adjusted to co-align the reflected laser beam with the incident beam).
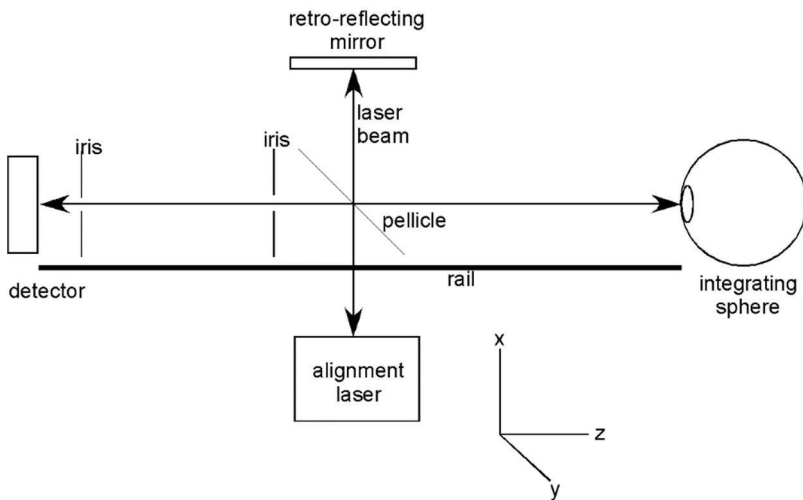
Fig. 22. Schematic of the alignment method for SIRCUS.

The alignment between the detectors and the integrating sphere is radiometrically validated by translating the detectors in the X and Y directions and recording the signals as a function of stage position. The stage position giving the maximum signal from each instrument is compared with the stage position derived from the optical

alignment procedure. The two positions typically agree to within 1 mm, well within the desired alignment uncertainty.

2.2.2.3.5. Comparison of tunable laser and monochromator used calibrations.

The high optical power available with laser-based calibration systems enables radiometers to be calibrated directly for either radiance or irradiance responsivity. The low wavelength uncertainty of the laser is instrumental in reducing the calibration uncertainty for filtered instruments. The source uniformity also enables rapid characterization and calibration of digital imaging systems. Some of the advantages of the laser-based calibration approach are illustrated by the calibration of a Photo-Electric Pyrometer (PEP), an instrument used to radiometrically determine the temperature of a blackbody [49]. The instrument is equipped with a narrow bandpass filter (~ 1 nm) for spectral selectivity.

For accurate radiance temperature determinations, the instrument's spectral out-of-band responsivity needs to be measured as well as its in-band responsivity. Figure 23 shows the relative spectral responsivity of the PEP determined on SIRCUS compared with the relative spectral responsivity determined using a conventional lamp-monochromator system in the SCF. As shown in Fig. 23(a), the spectral responsivity measured with the lamp-monochromator system is dominated by the spectral bandwidth of the source and deconvolution of the spectrum using the source slit scatter function is required. In contrast, the fine detail in the spectral responsivity is easily measured on SIRCUS because of the monochromatic nature of the source. Note that there are several overlying data points at each wavelength along both the rising and falling edges, demonstrating the extreme wavelength stability of the SIRCUS facility. Because of the low flux, the out-of-band responsivity is limited to approximately 10^{-6} with the lamp-monochromator system (Fig. 23(b)). In contrast, the out-of-band responsivity can be measured to the 10^{-9} level in the SIRCUS facility.

In SIRCUS, instruments are calibrated in their operational state: at the system level, with entrance pupils over-filled. This approach avoids unforeseen errors that can occur using other calibration approaches. For example, consider measurements of the relative spectral responsivity of a single channel filter radiometer known as a

Standard Lamp Monitor (SLM) [50]. The SLMs can be operated in irradiance or radiance mode, depending on the fore-optics. The irradiance mode configuration has a Teflon™ diffuser, a window, an interference filter, and a silicon photodiode. The instrument's relative spectral responsivities (RSRs) are used to band-integrate the response to an illumination source. The RSRs of the SLMs were determined using the lamp-monochromator system. During these measurements, the flux from the monochromator exit slit was imaged onto the center of the diffuser. In this case, the irradiance collector was under-filled by the incident radiant flux. The SLMs were also calibrated in irradiance mode for absolute spectral responsivity on SIRCUS. In this case, the irradiance collector was overfilled by the flux from the laser-illuminated integrating sphere. Comparing the two results using peak-normalized data, it was noted that the relative spectral responses did not agree (Fig. 24). There was no dependence on the f/# of the incoming flux. However, spatial maps of the relative response at multiple fixed wavelengths within the in-band region showed that the irradiance responsivity is not spatially uniform (due to the diffuser), leading to the observed differences. These measured differences can cause errors in the band-averaged measurements of spectral irradiance when the spectrum of the source being measured differs from that of the calibration source.
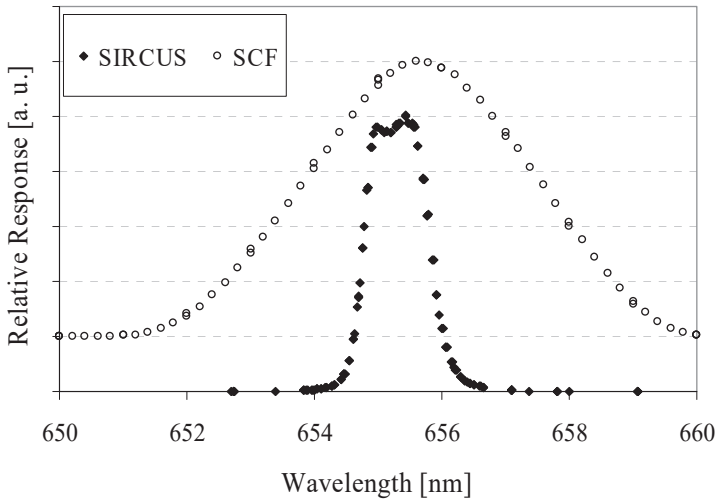
(a)
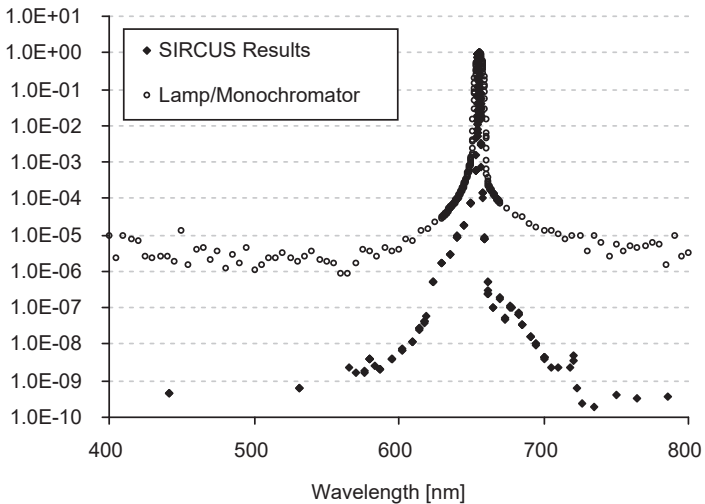
(b)

Fig. 23. The relative spectral responsivity of the PEP measured on SIRCUS
and on the SCF: (a) linear scale; (b) log scale.
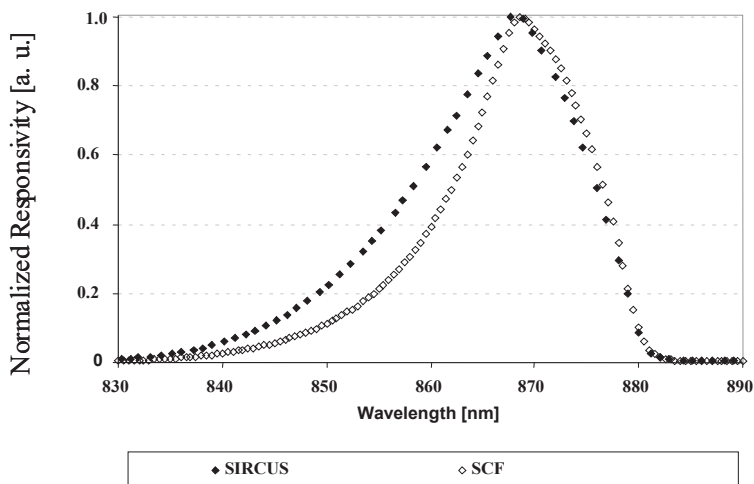
Fig. 24. Relative spectral responsivity of the SLM measured in under-filled mode (SCF) and in overfilled mode (SIRCUS).

2.2.3. FT-based measurement setup

For infrared spectral radiant power responsivity measurements, one could consider replacing the monochromator with a Fourier-transform infrared (FTIR) spectrometer, as shown in Fig. 25. FTIR spectrometers in principle have several advantages over dispersive systems in the infrared spectral region. First, the interferometer in an FTIR spectrometer modulates the entire spectral band defined by the source, beamsplitter, and other optical components simultaneously. If the signal-to-noise ratio (SNR) of the power responsivity data is limited by detector or amplifier noise, rather than by photon or source noise, then for a given observation time the FTIR can improve the SNR by a factor equal to the spectral bandwidth divided by the resolution. This advantage may apply for pyroelectric detectors, but not for Si or InGaAs detectors at shorter wavelengths. Second, the aperture of an FTIR spectrometer is naturally circular instead of slit-shaped, and thus the beam has a larger étendue than a monochromator for a given spectral resolution. This produces an optical throughput advantage. Third, an FTIR spectrometer typically uses a stabilized single-mode laser to measure the optical path difference in the interferometer. This yields excellent wavelength

accuracy and stability; it is not difficult to achieve a relative wavelength uncertainty of 10^{-6}.
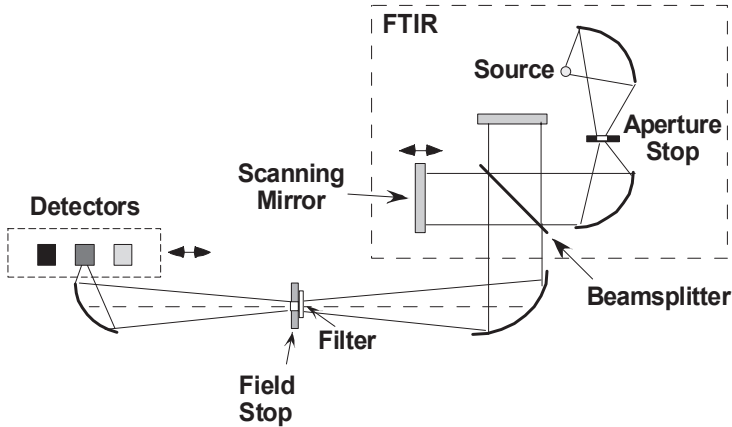
Fig. 25. Spectral responsivity measurement setup using an FTIR spectrometer.

However, these theoretical advantages may not necessarily lead to improved spectral radiant power responsivity measurements. The most troublesome issue for detector calibration with FTIR spectrometers is linearity. The power output of a typical FTIR spectrometer configured for near-infrared spectroscopy with a 3000 K tungsten-halogen source and quartz beamsplitter can be $\approx$ 200 mW for an f/3, 3 mm focal spot. This is enough power to cause changes in responsivity of several percent in many pyroelectric detectors, and completely saturate high-sensitivity InSb detectors. Nonlinearity in the measured interferogram is transformed into harmonic distortion over the entire spectrum. For the most accurate measurements, the power output must be attenuated e. g. with filters or stops, and much of the multiplexing and throughput advantages mentioned above are lost. Also, it is not possible to assess linearity using the dual shutter method that works well with monochromator light. The amplitude and phase of the modulated FTIR output beam vary spatially in such a way as to make this scheme impractical. It is possible to use an integrating sphere and vary the input beam power using a set of apertures, such that the uniformity of modulated irradiance at the detector plane is negligibly affected. The integrating sphere attenuation (typically 100x or more) also can bring the power

level down to the linear regime for cooled photoconductive detectors.

Another possible complication in making FTIR-based power responsivity measurements is the frequency response of the detector. Most FTIR spectrometers operate in a continuously-scanning mode in which the modulation frequency for a given spectral component is given by twice the scanning mirror velocity divided by the wavelength. For typical spectrometers this is in the audio frequency range. If the detector under test and standard reference detector have different frequency responses, the measurement will be more difficult to analyze. Even without this complication, the results of the responsivity measurement would need to be reported at a different frequency for each wavelength in the spectrum. Some FTIR spectrometers can be used in a step-scan mode, and the output beam sent through an optical chopper so that the frequency is fixed for each wavelength. However, this mode is often less stable than the continuously-scanning mode.

The FTIR output beam also contains an unmodulated DC power level that can be larger than the modulated ac component. This must be accounted for in the measurement, especially if linearity of detector response is important. Unfortunately, its spectral content cannot be easily determined. Further, by its nature a scanning FTIR system modulates a fraction of all of the radiant power present within the optical extent of the instrument, not just the output of the source. This includes ambient background radiation as well as possible emission from the detector itself. These components become more significant at longer wavelengths. It may necessary to perform a background measurement with the source blocked, or to use multiple sources (e. g., variable temperature blackbodies) to properly account for the background signal.

It should be possible to achieve low uncertainty spectral power responsivity measurements of detectors with an FTIR spectrometer, but only with appropriate care taken to address the error sources mentioned above. Also, there are more sophisticated 4-port FTIR designs that can be used to directly compare two detectors at the output ports, without moving them in and out of the beam. This approach can produce faster and more stable data output. In general, FTIR spectrometers should be considered alongside laser, filter, or monochromator-based systems for spectral radiant power responsivity measurements in the infrared spectral region. Where other methods

may produce lower absolute uncertainties at given wavelengths, the FTIR may be very useful for interpolating between these points.

2.3. Spectral radiant power responsivity

Radiant power is the fundamental radiometric quantity measured by primary standard radiometers. The optical power Φ in a beam can be measured if the beam is totally detected by an optical radiation detector. The radiant power responsivity of a power meter is equal to the detector (radiometer) output electrical signal divided by the incident (input) optical power. Spectral radiant power responsivity can be determined when tuned monochromatic radiation is measured by a radiometer with certain wavelength increments. Spectral radiant power responsivities can be used as reference functions to propagate calibrations to radiometric, photometric, colorimetric, and pyrometric measurements.

The measurement geometry was discussed in Section 2.1 of Volume 2. When photodiodes are used very close to light sources, the incident radiation can be oblique to the detector surface or may have angular divergence and the detector responsivity can change**.**

Angular responsivity and polarization dependence of responsivity are discussed in Section 2.1.3 of Volume 1 of this book series.

2.3.1. DC mode calibrations/measurements in the Si and near-IR ranges

The detectors are operated in DC measurement mode when spectral responsivity calibrations or measurements are performed in the UV, VIS, and near-IR wavelength intervals. In this typically 200 nm to 1800 nm range, the ambient (background) radiation will produce only negligibly small signal superimposed to the useful signal to be measured.

The signal measurement modes are discussed in detail in Section 4 of this Volume.

2.3.1.1. IR-enhanced Si

IR-enhanced Si photodiodes have improved radiometric and electronic characteristics as compared to other widely used Si photodiodes and can be used as responsivity standards between 300

nm and 1000 nm. Their low predicted uncertainty for radiant power responsivity measurements can result in improvements in existing monochromator-based Si responsivity scales.

Using the Hamamatsu Model S11499-01 IR-enhanced Si photodiodes in low light level measurements (such as monochromator-based UV responsivity calibrations), smaller measurement uncertainties can be obtained than with Si trap detectors [51]. Their performance is similar to Si trap detectors and exceeds it in the NIR range. They can cover an extended wavelength range compared to the 400 nm to 950 nm range of Si trap detectors. They can be used as irradiance meters when equipped with a precision aperture. They have a wider acceptance angle (FOV), and higher shunt resistance than Si trap detectors. Their temperature coefficient of responsivity is close to zero up to 1000 nm and their spatial non-uniformity of response is smaller than 0.2 % (max-to-min) even at 1000 nm. The IR-enhanced Si detector was designed by the manufacturer for 1064 nm laser measurements as the responsivity is twice as high as that of a 1337 detector. Ge or InGaAs detectors are not needed for this extended IR range. They can be used for the 300 nm to 1000 nm wavelength range of monochromator-based facilities without any temperature control. Because of their 1 GΩ shunt resistance, the noise and drift amplification in the attached trans-impedance amplifier is more than a decade lower than those obtained with Si-trap detectors. The result is increased SNR. The high SNR allows for measurements of low signals with improved reproducibility. In the UV range, this allows for smaller exposures of the detectors to the high energy photons.

The results of detailed radiometric and electronic characterizations of IR enhanced Si detectors was discussed in Section 2.1.1, 2.1.2, and 2.1.4 of Volume 1: The Properties of Optical Radiation Detectors and Radiometers. The spectral power responsivity scales can be improved using a set of the IR enhanced Si photodiodes not only to transfer the calibration from the cryogenic radiometer, but also used as the monochromator-facility working standards. This improvement can reduce the length of the calibration chain and create a 1-step scale transfer between the cryogenic radiometer and a monochromator facility.

At present, typically, the signal-to-noise ratio (SNR) at monochromator outputs is not high enough for wavelengths shorter than 350 nm. Therefore, the spectral power responsivity of the IR-enhanced Si

detector was also measured at the Ultraviolet Spectral Comparator Facility (UVSCF) of NIST between 300 nm and 420 nm. The UVSCF operates from 200 nm to 500 nm, where the SNR is high enough for responsivity measurements. The transfer standard of the UVSCF is a UV-100 silicon photodiode [52]. The monochromator calibrated responsivity curves with their expanded relative uncertainties are shown in Fig. 26.
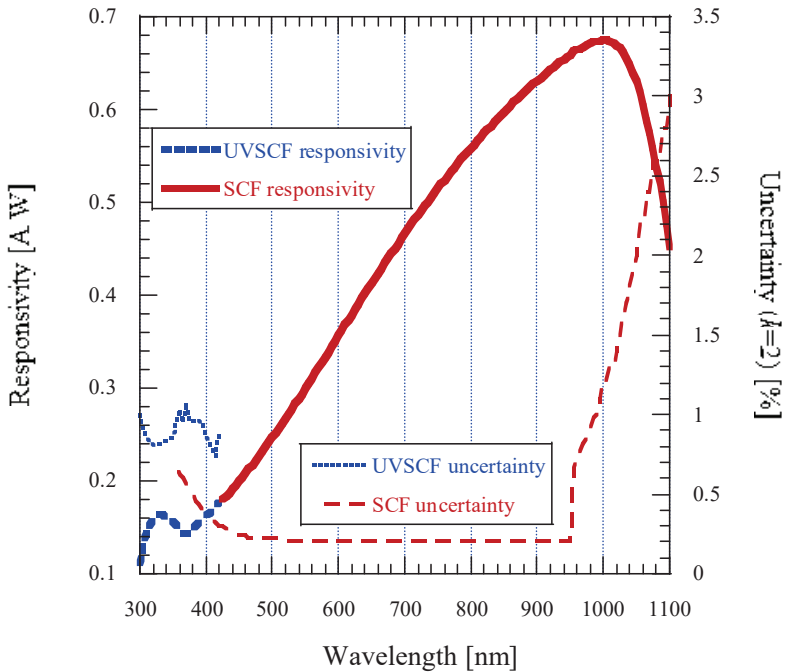
Fig. 26. Spectral power responsivity of the IR enhanced Si photodiode.
The solid thick line was measured at the NIST-SCF and the dashed thick
line at the NIST-UVSCF.
The expanded (k=2) uncertainties are shown with the thin dashed lines.

As illustrated in Fig. 26, the 0.2 % (k=2) responsivity uncertainties (for the IR enhanced Si test detector) increase significantly outside of the 500 nm to 950 nm wavelength range. These increases could be minimized if the IR enhanced Si detector were calibrated directly against a cryogenic radiometer.

The solid curve in Fig. 27 shows the difference of the spectral power responsivities of the IR-enhanced Si detector measured in 2012 and 2014. The responsivity uncertainties of the NIST-SCF calibration facility are shown with dashed lines. The increase in the uncertainties beyond 950 nm is primarily due to the above mentioned limitations of the trap detectors used in the scale transfer.
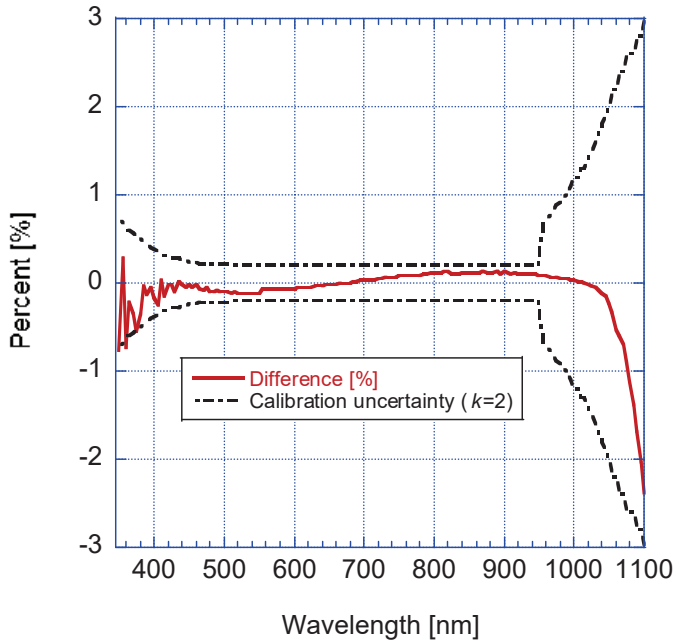
Fig. 27. Difference of two spectral power responsivity curves of an IR-enhanced Si photodiode measured in 2012 and 2014. The responsivity uncertainties of the monochromator-based calibration facility are shown with dashed lines.

For future calibrations at the tunable-laser applied responsivity-calibration facility, the responsivity uncertainties were estimated. Radiometric and electrical characterizations were performed to estimate the different limiting uncertainty factors [51]. The radiometric characterizations included the uncertainty components that can be obtained from the spatial non-uniformity, the temperature dependence, and the long-term stability of the responsivity. The long-

term stability measurement and the electrical characterizations show that the reproducibility, which is now the dominating uncertainty component, can be significantly improved. The improvement over the existing monochromator-based responsivity scale will be significant at the two ends of the wavelength range where the present responsivity scale needs improvement. The relative expanded spectral responsivity uncertainty for test detectors is predicted to be 0.1 % (k=2) from 400 nm to 950 nm and 0.2 % (k=2) outside of this wavelength range between 300 nm and 1000 nm.

More radiometric characterizations are needed between 300 nm and 400 nm to estimate if the UV damage occurs even at decreased signal levels.

2.3.1.2. Extended InGaAs

The primary effort to extend the spectral power responsivity calibrations from the Si wavelength range to 2500 nm is motivated by the measurement needs of the remote sensing and the photovoltaic (PV) communities. The measurement needs arise primarily from the substantial solar spectral irradiance that is still present in the spectral region from 1800 nm to 2500 nm, and the need to calibrate PV cells which can be sensitive in this spectral region. In remote sensing, the calibration requirements at these wavelengths arise from the need to measure the reflected solar radiation in this spectral region.

Extended InGaAs (EIGA) radiometers can be used over the 900 nm to 2500 nm spectral range in both DC and AC measurement modes. It is shown here that regular InGaAs detectors/radiometers will not be needed for responsivity scale realization in the near-infrared wavelength range, and that Si and EIGA detectors can be used as standards (or reference radiometers) to cover the entire wavelength region from 200 nm to 2500 nm.

Instead of cryogenic cooling, 4-stage thermoelectric coolers can be used to stabilize the temperature of the applied 5 mm, 3 mm, and 1 mm diameter detectors at -85 ℃. Cooling is important to increase the detector shunt resistance that would decrease noise and drift amplification for the output of the preamplifier (following the detector). The picture of a 4-stage cooled 5-mm EIGA radiometer standard is shown in Fig. 28. The dissipated heat from the TE coolers can be removed using heat sinks constructed with either air flow or

circulated water cooling. As a result of an additional analog control loop, (including a thermistor which is attached to the detector and an external temperature controller) [53], the temperature of the applied EIGA detectors can be stabilized at temperatures as low as -85 °C. In DC mode, at a bandwidth of 0.3 Hz, a noise-equivalent-current (NEC) of 4 pA could be measured with a 3 mm diameter EIGA detector of 3 MΩ shunt resistance.

For spectral power responsivity calibrations at the NIST IR-SCF facility, 5 mm diameter extended-InGaAs (EIGA) detectors are used. These detectors are large enough to underfill them by the incident f/4 output radiation of the grating monochromator.

Within this section, only the DC measurement mode is discussed. The AC mode measurements, where lower responsivity uncertainties can be achieved, will be discussed in the following sections (below).

Fig. 28. Picture of water-circulated and 4-stage TE cooled 5-mm extended-InGaAs detector/radiometer standard.

2.3.1.2.1. Calibration transfer with sphere-input EIGA

The spectral responsivity calibration of SW-IR radiometers can be derived from an electrical-substitution cryogenic radiometer (ESR). The ESR measures the total radiant power in the incident laser beam with a relative expanded uncertainty of about 0.02 % (k=2). In order to propagate the radiant power responsivity scale with a minimal increase in the uncertainty, transfer standard EIGA radiometers are

needed. These radiometers are expected to measure the total beam power with uncertainties of about 0.1 % (k=2). The spatial non-uniformity of response of EIGA detectors (as measured by the manufacturer) is between 0.5 % and 1 %. This non-uniformity is too high to propagate the responsivity scale with the expected low measurement uncertainty. In order to improve the spatial non-uniformity of response, a few EIGA radiometers (built with 3 mm diameter detectors) were modified. Spectralon [13] coated integrating spheres of 38 mm diameter with 5 mm diameter input apertures were attached to the front of the radiometers. This attachment makes it possible to convert an EIGA radiometer from power measurement mode into irradiance measurement mode. The irradiance responsivity is equal to the product of the power responsivity and the aperture area. The modified EIGA radiometer head is discussed in 3.2.2.2 of Volume 3 where Fig. 46 shows not only the entrance aperture in the sphere, but also the side connector for the temperature controller and the tube-connector on the heat sink for circulating the water-coolant.

The calibrations were performed at discrete wavelengths using the Spectral Irradiance and Radiance Responsivity Calibrations using Uniform Sources (SIRCUS) facility [54]. These measured reference data were interpolated to other wavelengths using the SCF [52] spectral power responsivity scale to 1600 nm, and the spectral responsivity of the low-NEP pyroelectric transfer standard radiometer [55]. Four working-standard EIGA radiometers (with 5 mm diameter detectors) were calibrated against the sphere-input EIGA transfer standard and one of the four radiometers was used here as a reference detector. A 3 mm diameter test EIGA radiometer was calibrated against one of the 5 mm working standard EIGA detectors using the detector substitution method. The calibration was performed in the one-beam measurement mode of the SCF and the output DC voltages of both the test and the reference radiometers were measured, in sequence, during three consecutive spectral scans [12]. The SCF was not modified for this calibration. The radiometers are moved into the output of the monochromator by a motorized detector stage at the end of one wavelength scan (from 700 nm to 2500 nm). The average of the three spectral power responsivities is plotted in Fig. 29. The percent standard deviations calculated from the three spectral power responsivities are also shown. The standard deviations are less than 0.2 % (k=2) between 700 nm and 2500 nm except at three spectral regions. At these three

spectral regions, the standard deviations increased due to the presence of water vapour absorption features near 1400 nm and at 1850 nm and also because of the OH absorption in the prism at 2200 nm. The repeatability of the three spectral power responsivities (from the three scans) compared to their average within the 2 μm to 2.5 μm atmospheric window is shown in Fig. 30. The responsivity differences are within +/- 0.4 % to about 2470 nm. The differences are doubled at the high wavelength-end of the spectral scan because of the decreased signal-to-noise (and drift) ratios.

The uniformity of the sphere-input EIGA transfer standard was tested by scanning a 1 mm diameter beam over the 8 mm diameter sphere entrance port (with the 5 mm aperture removed). The precision aperture was removed during this test. The input sphere improved the spatial non-uniformity of the EIGA radiometer by about a factor of five. This improvement was needed to perform 0.1 % (k=2) responsivity uncertainty in power measurement mode even if different beam positions and different beam diameters were used. Using these optimized transfer standard radiometers, a factor of three uncertainty decrease can be expected compared to the present near-IR detector spectral responsivity calibrations [2]. Also, these radiometers make it possible to extend the NIST spectral responsivity calibrations to 2.5 μm with close to 0.1 % (k=2) responsivity uncertainties in both radiant power and irradiance measurement modes.
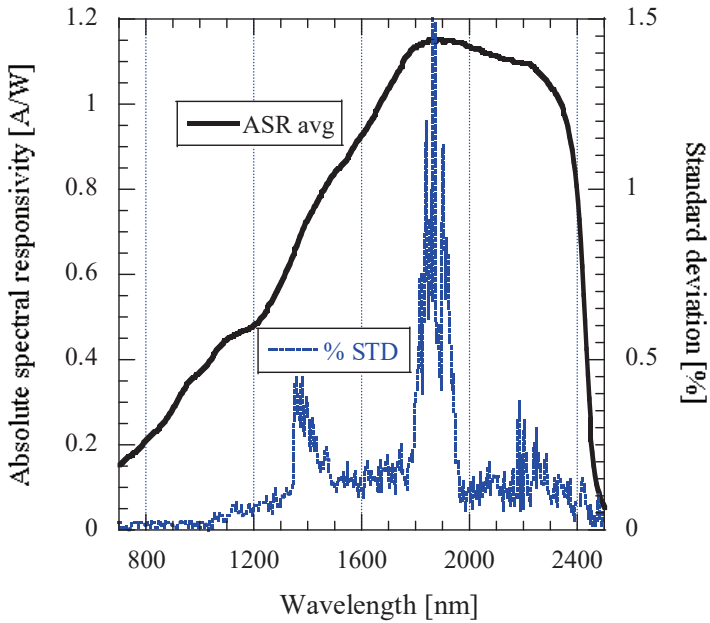
Fig. 29. Average absolute spectral power responsivity (ASR) of an EIGA radiometer from three spectral scans. The standard deviations (on the right-Y axis) are increased because of the absorption bands and the prism contamination (at 2200 nm) of the monochromator.
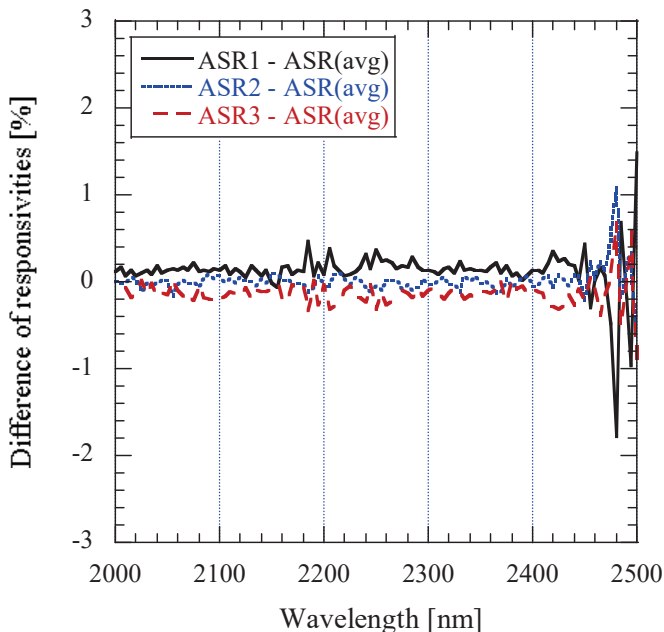
Fig. 30. Difference of the EIGA absolute spectral responsivities measured in three scans within the atmospheric window.

One of the critical tests was checking the ability of the EIGA working standards to measure the DC spectral power output of the NIST SCF with low uncertainties. Typically, the SCF operates in two-beam ratio mode for the Si and near-IR wavelength ranges. In the two-beam ratio mode, a monitor diode is always used so that the ratios of the signals between the working standard detector and the monitor diode detector and the corresponding ratio with the diode under test are used for the calibrations. Any common signal changes in the two channels (such as the lamp intensity changes) can be compensated by the simultaneous (signal/monitor) ratio made by the computer. The simple calibrations described here were performed using a single detector or the one-beam mode so that the noise and the drift components were not measured under optimal conditions.

The effect of the long-term drift for the spectral scans in the one-beam measurement mode was tested. The DC output signal of the reference 5-mm EIGA radiometer (used in the present EIGA

radiometer calibrations at the SCF) was measured in two consecutive spectral scans. The measured signals of the two spectral scans are shown in Fig. 31. The signal differences from the two scans are also plotted. The signal difference fluctuated between 0.2 % and 0.5 % of the signal nominal values. The scan-to-scan signal-change (drift) was 0.3 % with drift and noise fluctuations of about +/- 30 %. The signal differences obtained with another 5-mm EIGA radiometer during four spectral scans were within +/- 0.5 %. These signal changes indicate that the one-beam mode at the Cary-14 based monochromator facility (SCF) is suitable for DC mode calibrations with acceptable measurement uncertainties. It is expected that the long-term signal-drift can be decreased by using the two-beam ratio mode where a monitor EIGA radiometer is used in addition to the test and reference EIGA radiometers. In addition, the water vapour absorption features can be seen near 1400 nm and at 1850 nm. The reduction in the signals observed at 2200 nm is due to the OH absorption in the fused-silica prism in the monochromator. These fluctuations due to the atmospheric absorption can be reduced by purging the path in the monochromator and the detector compartments with dry air.

The uncertainty budget for these DC mode measurements is estimated in Table 3. The dominant uncertainty components of the above EIGA (3 mm) radiometer calibration are the uncertainty of the reference spectral power responsivity scale and the spectral responsivity changes (repeatability) from the three consecutive spectral scans performed in the one beam measurement mode. The spectral responsivity changes are caused by the temperature- and noise-dependent responsivity variations during the spectral scans when the positions of the reference and test detectors were not changed. The uncertainty components caused by monochromator wavelength errors and EIGA-detector non-linearity are negligibly small compared to the discussed dominating components.
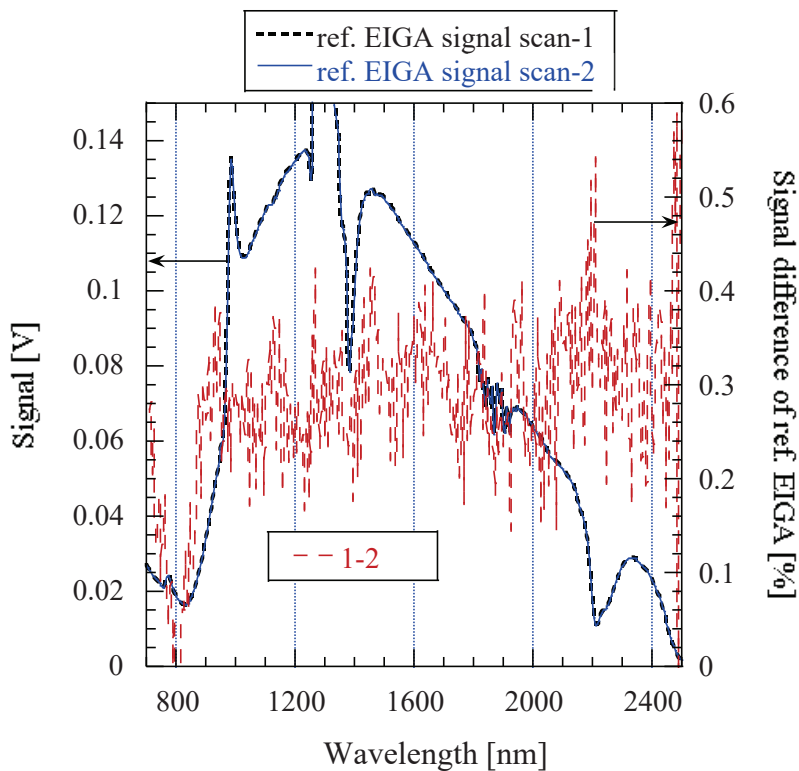
Fig. 31. Measured signals from two consecutive spectral scans (left-Y axis) and the percent signal difference from the two scans (right-Y axis).

Table 3. Uncertainty budget for the spectral power responsivity calibration of an EIGA (3 mm) radiometer for the wavelength interval between 1200 nm and 2300 nm.

Dominant uncertainty components	Type A [%]	Type B [%]	Total [%]
Reference radiant-power responsivity scale	0.5		
Reference-detector position		0.3	
Test-detector position		0.3	
Spectral responsivity differences from 3 scans	0.4		
Relative combined standard uncertainty			**0.8**
Relative expanded uncertainty with _k_=2			**1.6**

The relative expanded uncertainty between 900 nm and 1200 nm and also from 2300 nm to 2400 nm is 2.0 % (k=2) and it increases to 3.0 % (k=2) between 2475 nm and 2500 nm.

Note, that significantly (about a factor of two) lower responsivity uncertainties can be achieved in AC measurement mode where the DC background changes are not measured.

2.3.2. AC calibration/measurement mode for the IR

At wavelength longer than about 2000 nm, a significant DC signal will be produced by the background radiation. This background signal shows up only in infrared detectors that respond to optical radiation longer than 2000 nm. An IR detector cannot be calibrated at a DC measuring setup because the background produced DC signal (photocurrent) is high compared to the useful DC signal (to be measured). Since the high DC background radiation is not stable, the DC (background) signal will drift. Because of the drift, the DC background signal cannot be subtracted from the useful DC signal. Therefore, measurement of IR detectors in DC mode would result in drift dominated signal measurements. In order to avoid drift dominated measurements, IR detectors should be measured in AC mode.

For short-wave IR calibrations either photovoltaic (PV) HgCdTe (MCT) detectors or extended-InGaAs detectors are used. Both can have high detector shunt resistance needed for high sensitivity applications. EIGA detectors with small active area (such as 1 mm^2) and high shunt resistance (about 15 MΩ) have low-NEP. As discussed in 3.2.2.2 of Volume 3 (Optical Detector and Radiometer Standards), in AC mode, an NEC=7 fA was measured with a 1 mm diameter EIGA detector (using a cold FOV limiter) at an electrical bandwidth of 0.16 Hz. This corresponds to an AC-mode NEP = 5.4 fW which is close to the 3 fW typical DC-mode NEP of silicon photodiodes.

As an example, Fig. 32 shows a calibration setup where EIGA 1 and EIGA 2 working standards were calibrated for spectral power responsivity against sphere-input EIGA and pyroelectric transfer standards [56].
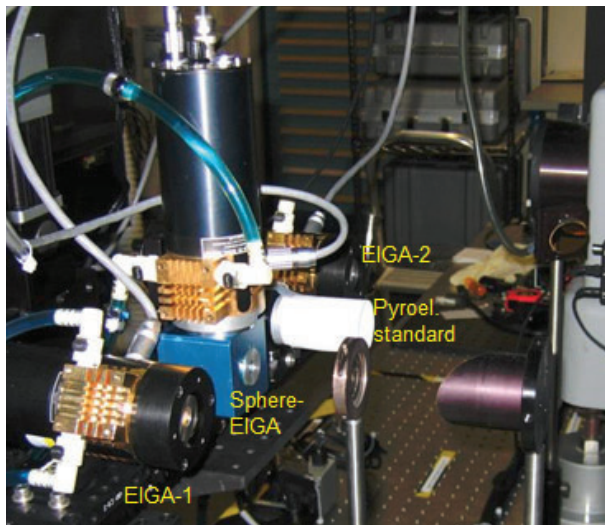
Fig. 32. Calibration of EIGA 1 and 2 working standards against sphere input EIGA and pyroelectric (cylinder-covered) transfer-standards.

The pyroelectric transfer standard detector is used to extend the spectral responsivity measurements to a wider wavelength range. For pyroelectric detector use, the optical radiation must be chopped. Either voltage mode or current mode preamplifiers are used. In the voltage mode preamplifiers, Field Effect Transistors (FETs) are used to amplify the voltage drop on the detector. Here, the total input stray capacitance including detector is typically 10 to 100 times the stray feedback capacitance of a current mode preamplifier circuit. Therefore, the frequency response of the current mode preamplifiers (current-to-voltage converters) is much broader. The output of the preamplifier is measured by a synchronized lock-in amplifier and the filtered (DC) lock-in output signals (X and Y) are converted into digital signals using linear analog-to-digital converters or digital voltmeters (DVMs). When the pyroelectric detector is calibrated against a standard detector, or working standard detectors are calibrated against a pyroelectric detector, all the detectors should be operated in AC (chopped) measurement mode. The responsivity of pyroelectric detectors is low (about six orders of magnitude lower than Si) therefore their noise-equivalent-power (NEP) is high. The NEP is a ratio of the preamplifier's output noise to the responsivity. High NEP needs high beam power from the monochromator. Using traditional pyroelectric detectors with NEP = 40 nW/Hz^1/2, 4 µW or higher beam-power is needed to achieve a relative standard measurement uncertainty of 1 % (that needs a signal-to-noise ratio of 100). Recently, the NEP of pyroelectric detectors has been decreased by an order of magnitude as a result of frequency compensations performed by the organic black paint coating [57] and also by decreasing the $LiTaO_3$ crystal thickness. This means that traditional monochromators can be used with low-NEP pyroelectric detectors for spectral power responsivity measurements in a wide wavelength range. In spectral responsivity measurements where traditional pyroelectric detectors are used, the power of the source, the efficiency of the imaging optics (including flux collection from the source), and the power throughput of the monochromator have to be high. Also, the responsivity of the lock-in amplifier can depend on the shape of the chopped input signal. This can be an issue if the standard detector and the test detector have different response times. Sine-wave measuring lock-in amplifiers that measure the fundamental frequency component of the input signal can be less invariant for the AC signal shape changes than square-wave measuring lock-in amplifiers. AC radiation measurements using

choppers and and lock-in amplifiers are discussed in Sections 4.5 and 4.6 of Volume 2: Optical Detector Applications for Radiometric Measurements. The calibration of the sine-wave measuring lock-in amplifier is discussed in Section 4.7 of Volume 2.

As an example, the scheme of the NIST Infrared Spectral Calibration Facility (IR-SCF) which operates in AC measurement mode, is shown in Fig. 33 [25].

The measurement equation for detector responsivity calibration using the detector substitution method is:

$$s_{\text{Test}} = s_{\text{Std}} \frac{I_{\text{T}}}{I_{\text{S}}}$$

(19)

The output optics of the monochromator can be changed. Off axis paraboloid mirrors are used to calibrate detectors in power (underfilled) measurement mode. In irradince responsivity calibrations, an integrating sphere is moved into the output beam of the monochromator. The sphere will produce a uniform irradiance in the reference planes of the detectors. However, the signal loss can be 2-3 orders of magnitude. The reference detector of the IR-SCF is a low-NEP pyroelectric detector that can cover the visible to infrared spectral range to about 24 μm.

During the calibration process the detectors are aligned on the moving stage so that the incident beam gets into the center of both the standard and the test detectors. An example for the positioning of the standard is shown in Fig 34 [25].

The profile of the incident beam is important to perform a good alignment. The beam is formed by the monochromator aperture and the output parabolic mirrors. The profile must be controlled for both small diameter of the sensitive area and also for the spatial nonuniformity of detector response. The final adjustment of the beam profile can be performed based on an experimental beam scan where a 0.5 mm diameter aperture is moved in the X, Y (and also Z) directions. The beam profile is shown in Fig. 35.
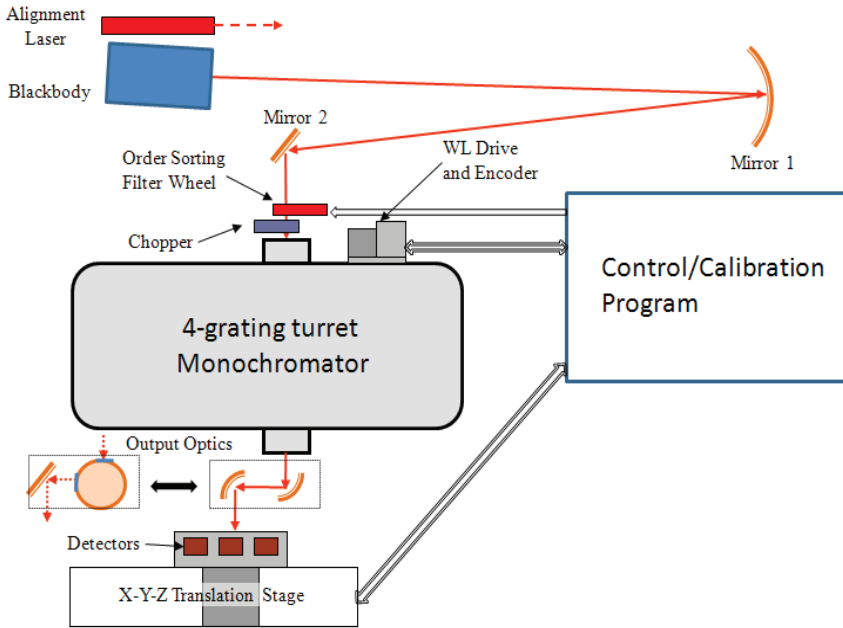
Fig. 33. Scheme of the NIST IR-SCF.
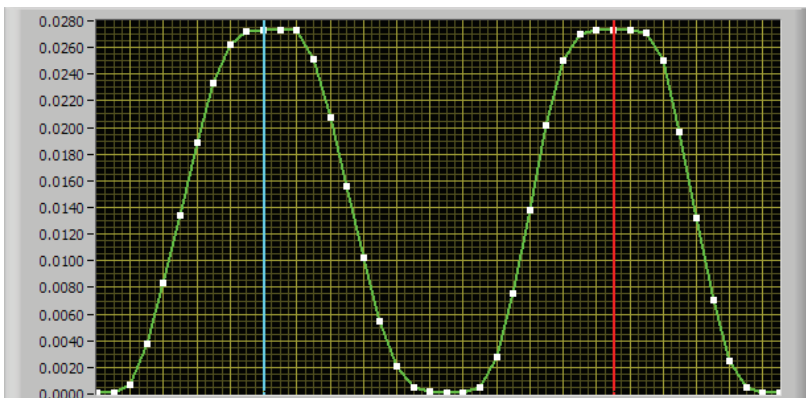
Fig. 34. Example of centering the standard detector. The sensitive area has a diameter of 5 mm. The left and right perpendicular lines correspond to the center (X,Y =0) of the detector. One division is equal to 1 mm.
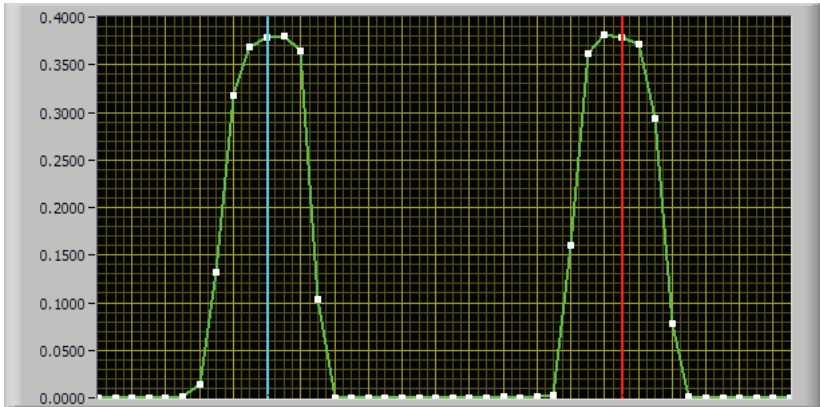
Fig. 35. Incident beam profile in the X (Left) and Y directions. The left and right perpendicular lines correspond to the center (X,Y = 0) of the detector. One division is 1 mm.

Where pyroelectric detectors are not used or AC measurements are not needed, the spectral instrument with the related optics does not have to be optimized for power throughput. Also, in many cases, full automation is not necessary.

The power responsivity scale-extension to the IR and UV ranges, including pyroelectric, InSb, and HgCdTe detector calibrations, are discussed in Sections 3, 4, and 5 of Voulme 3.

2.3.3. IR scale realizations, extensions, comparisons, and validations

As an example, the realization and comparison of independently realized infrared spectral power responsivity scales is discussed here. The measurements were performed at the NIST monochromator-based Infrared Spectral Calibration Facility (IR-SCF).

A spectral power responsivity reference scale was realized from 2 μm to 14 μm on a low-NEP single-element pyroelectric transfer standard. An InSb working standard developed in 1998 was re-calibrated in 2012 against the NIST reference scale for both power and irradiance responsivity. Both the power and irradiance responsivities of the InSb working standard have been validated against a sphere-input extended-InGaAs power-to-irradiance converting

transfer standard. This transfer standard gave the traceability to the radiant power measuring cryogenic ACR which is a primary standard. The aperture at the sphere-input was measured at the NIST Aperture Area Measurement Facility.

The InSb working standard was also calibrated at the National Physical Laboratory (NPL) of United Kingdom in 1999. The spectral power responsivity disagreements at the 1999 scale comparison were within 2 %, well within the combined (coverage factor k=2) responsivity uncertainties. The InSb working standard has an input aperture of known area to determine its spectral irradiance responsivity as well.

2.3.3.1. The pyroelectric detector spectral responsivity

A single-element pyroelectric hybrid-detector with a noise equivalent power (NEP) of 5 nW/Hz$^{1/2}$ [57] was used as a reference detector at the NIST IR-SCF [25]. The organic-black coated detector was built from a 100 μm thick LiTaO$_3$ crystal. The preamplifier and the crystal are located in the same metal can. The picture of this hybrid reference detector is shown in Fig. 36. The temperature coefficient of responsivity is 0.14 %/^{o}C. In order to perform good long-term stability, the temperature of the detector-can was stabilized at 26 ^{o}C using thermoelectric heating/cooling. The max-to-min spatial non-uniformity of response of the 5 mm detector was about 1 % at the tested 785 nm and 10.6 μm wavelengths.

The relative spectral response was determined from spectral reflectance measurement of the organic black detector-coating. The response is proportional to the absorption which is equal to 1-reflectance if the transmission is zero. The relative curve was converted into absolute, using absolute responsivity (tie) points. The tie points were obtained from substitution to a sphere-input extended-InGaAs transfer standard radiometer [53, 55]. The low-NEP pyroelectric transfer standard radiometer was used at the output of the f/4 grating monochromator of the IR-SCF in the 830 nm to 19.7 μm wavelength range.

Fig. 36. Picture of a temperature-controlled low-NEP pyroelectric hybrid detector standard.

Figure 37 shows the output beam arrangement of the monochromator [25]. Two off-axis parabolic mirrors can image the output beam of the monochromator to the detectors in power measurement mode where the detectors are underfilled by the incident radiation. For irradiance mode measurements, the imaging output optics is substituted with a 100 mm diameter gold coated integrating sphere to overfill the detectors with a uniform field of radiation. The spectral power responsivity of the pyroelectric transfer standard as measured at 10.5 Hz is shown in Fig. 38. The upper 3 dB roll-off frequency of this pyroelectric transfer standard is 100 Hz. The responsivity uncertainty is 1 % (k=2) between 2.5 μm and 13 μm. The uncertainty, because of the increased noise (caused by the signal decrease), is 1.3 % (k=2) at 2 μm and 1.2 % (k=2) at 14 μm [55].

The properties of pyroelectric detectors were discussed in detail in Section 5 of Volume 1.
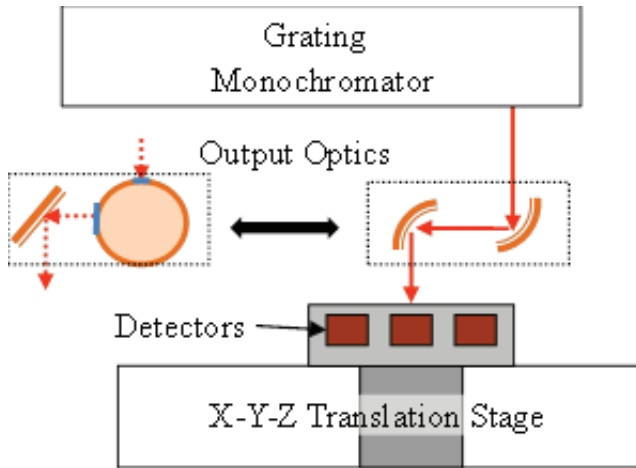
Fig. 37. IR-SCF monochromator output optics for power (right side) and irradiance (left side) responsivity calibrations.
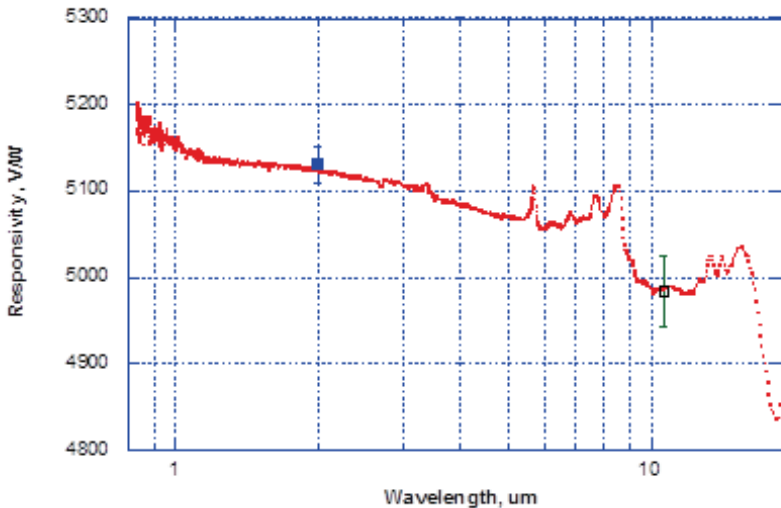
Fig. 38. Spectral power responsivity of a low-NEP single-element pyroelectric transfer standard.
The filled square is the tie point from the sphere-input EIGA radiometer and the open square is the tie point from a dome-input pyroelectric reference detector. The error bars show the expanded responsivity uncertainties of the two tie points.

The uncertainty budget for the 5-mm hybrid (the detector and the preamplifier are combined in the same metal-can) organic-black coated pyroelectric standard is shown in Table 4.

Table 4. Responsivity uncertainty budget for a low-NEP hybrid pyroelectric reference detector.

Uncertainty component	Type A, %	Type B, %	Combined, %
Tie points responsivity			
Sphere Ext-InGaAs (2 μm)	0.4		
Dome pyro (10.6 μm)	0.8		
Pyroelectric radiometer gain		0.04	
Pyroe. temperature dependence		0.04	
Radiometer frequency dependence		0.08	
Spatial non-uniformity of resp.		0.5	
Pyroe noise dominated uncertainty		0.5	
Expanded combined uncertainty (2 μm)			0.82
Expanded combined uncertainty (10.6 μm)			1.06
Relative response from reflectance data	0.5		
Overall expanded (k=2) at 2 μm			1.0
Overall expanded (k=2) at 10.6 μm			1.2

Hemispherical dome-input pyroelectric radiometers with gold black and organic black coatings are also used to extend the spectral responsivity scale to the LWIR. The design considerations of a reflecting dome is discussed in Section 3.1.3.2 of Volume 2. The gold coated dome can increase the detector absorptance and to minimize spectral structures in order to obtain a close to constant spectral response for the dome-input detector. The efficiency of the dome-trap mainly depends on the optical properties of the black coating on the detector, such as the reflectance and distribution of the reflected light in the wavelength range of interest. The dome-trap efficiency for specular and diffuse detector coatings can be obtained from reflectance measurements performed with and without the dome. For this test, the NIST Complete Hemispherical Infrared Laser-based Reflectometer (CHILR) was used at 1.56 μm, 4 μm, 5 μm, 9.5 μm, and 10.6 μm. The detector absorptance with dome is determined by using the trap efficiency to correct the spectral reflectance of the bare coating of the detector using the NIST Fourier Transform Infrared

Spectrophotometry (FTIS) facility [59]. The relative spectral responsivity associated to absorptance and the absolute tie-point method could determine the absolute spectral responsivity of the dome input radiometer. The direct calibration of the dome-input pyroelectric radiometers with organic black coating using the Infrared Spectral Comparator Facility (IRSCF) and traditional sources can be conducted with dome/without dome to make a comparison with the reflectance measurements from the CHILR and the FTIS. This comparison can help to understand the loss of the reflected light outside the detector inside the dome. The main conclusion of the dome-input application is that the dome can be efficient only if the reflectance of the detector coating is high which may be typical in the the long-wave IR range.

The picture of a dome-input pyroelectric reference radiometer is shown in Fig. 39. The top cover that includes an aperture of 3.5 mm diameter, is removed for better illustration.
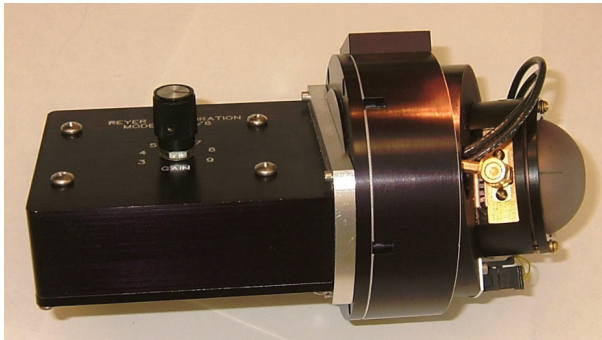
Fig. 39. Photo of a dome-input pyroelectric reference radiometer. The top cover is removed for better illustration.

2.3.3.2. Pyroelectric power-responsivity extension to far-IR

The organic-black coated hybrid pyroelectric detectors were analyzed for extension of their low-uncertainty spectral power responsivity to the far (long-wave) IR. A responsivity scale for this wavelength range is important for detector-based infrared calibrations. An example is accurate measurement of Earth infrared radiations.

An organic-black coted pyroelectric hybrid detector is suitable for long-wave IR measurements. The goal here is the produce calibrated spectral responsivity for these low-NEP pyroelectric hybrid detectors for the IR to 30 μm as a continuation of the above discussed UV-to-SWIR responsivity scale.

The measured reflectance and calculated absorptance curves of an organic-black coat, deposited on a thin glass plate, are shown in Fig. 40. The two curves on the left side of the graph (labeled Sample purple and Sample green) were measured at the NIST STARR monochromator-based reflectance measurement facility [60] between 250 nm and 2500 nm. The other two curves on the right side (both labelled R s Mean) were measured using the Infrared Reference Integrating Sphere (IRIS) in the Fourier Transform Infrared Spectrophotometry (FTIS) Lab [61] in two steps. First, the measurement was performed from 800 nm to 3 μm (circles) and then between 3 μm and 18.5 μm (crossed-squares). These IRIS-based measurements were performed before the responsivity extension to 30 μm. The deviation between the monochromator-based and the FT-based measurements in the SW-IR where the two results overlap is about 0.25 %. This deviation is small because the absorptance is about twenty times higher than the measured reflectance values resulting in low absorptance uncertainties.
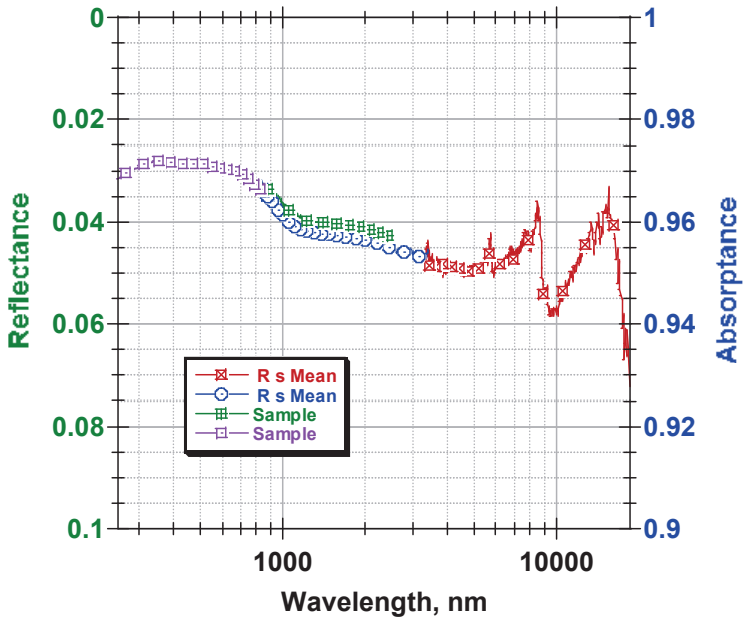
Fig. 40. Absorptance deviation obtained from monochromator (left curve to 2500 nm) and FT (right curve 3 μm and 18.5 μm) measured spectral reflectance data of the same organic-black paint coating.

The expanded uncertainty (*k*=2) of absorptance for the organic-black coating evaluated at the IRIS/FTIS facility between 1 μm and 18 μm is shown in Fig. 41. The ~5 % spectral reflectance below 15 μm was measured with ~3 % (*k*=2) uncertainty. This uncertainty converts to ~0.2 % (*k*=2) for the ~20 times higher absorptance (~95 %). This is the main conclusion/message of the here applied reflectance based determination of the IR relative spectral response of organic-black coated pyroelectric detectors. The uncertainty of absorptance (which is proportional to response) increases to 0.9 % (*k*=2) at 18.5 μm when performing the traditional IRIS/FTIS measurements.
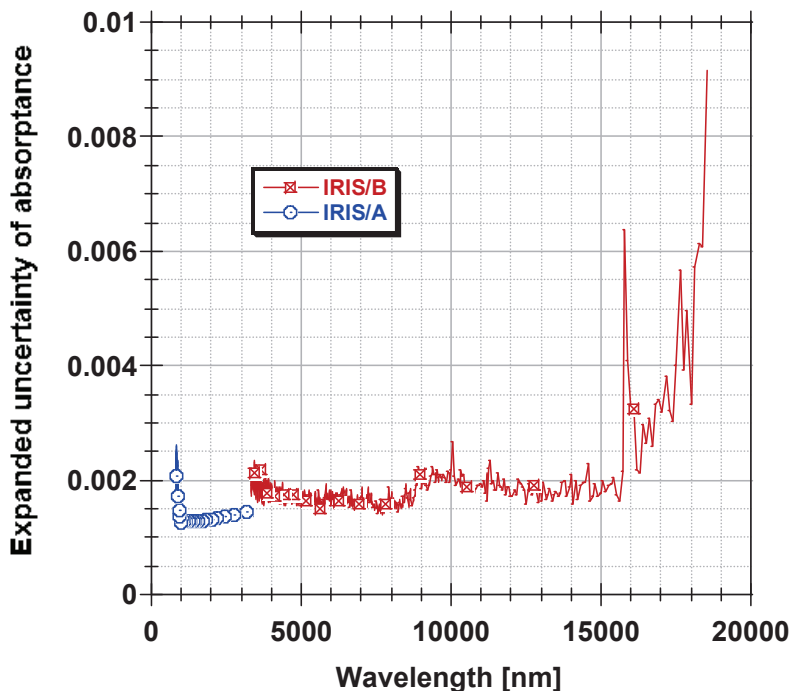
Fig. 41. Expanded uncertainty (*k*=2) of the absorptance of the organic-black coating when measured with the IRIS sphere at the FTIS Lab.

To utilize the low uncertainty of the relative pyroelectric response, shown above, the uncertainty of the tie point(s) used for the conversion of the relative spectral response curve into an absolute one, should also be 0.2 % (*k*=2) or smaller to obtain reasonably low uncertainty for the realized IR (absolute) spectral power responsivity.

To extend the spectral reflectance measurement to 30 μm, a second FTIS/IRIS reflectance measurement facility was used. The spectral reflectance measurements for pyroelectric detectors were performed using a newer custom integrating sphere for detection. The sphere's high efficiency and spatial throughput uniformity enables lower uncertainties for the extended wavelength range.

The sphere was interfaced to a Bruker Vertex 80V [2] Fourier Transform Spectrometer (FTIR) with an internal SiC source, was employed. This integrating sphere is an upgraded copy of the IRIS sphere used in the FTIS facility. The gold-coated diffuse interior surface of the sphere has a superior diffuse character at wavelengths longer than 10 µm. Measurements were performed using a liquid-Helium-cooled blocked-impurity-band boron-doped silicon (Si:B) detector, which has responsivity from 5 µm to 30 µm. The detector's near-normal spectral absorptance is obtained by subtraction from 1 of the near-normal (8 degree) hemispherical reflectance measurements. The sphere reflectance measurements were made in a relative mode, with a bare gold-coated mirror reference, separately calibrated at the FTIS facility to 18 µm. A black-paint coated 5 mm aperture was placed over the sphere sample port, and the detector element was centered on the aperture with a minimal gap of 0.5 mm between them. A good quality bare gold mirror has essentially (within 0.001) constant reflectance over the range of 15 µm to 30 µm, based on handbook data. The relative reflectance of the detector is multiplied by the gold mirror reflectance values to obtain the detector reflectance values. Two additional characterization measurements were performed: 1) an "empty port" measurement to characterize the degree of scattered light overfilling the sphere sample port, and 2) a comparison measurement of a diffuse gold reference and the gold mirror reference to provide a correction for the diffuse character of the detector coating and its interaction with the sphere.

The spectral reflectance R, measured between 5 µm and 30 µm, is shown in Fig. 42. The absorptance 1-R, also shown in Fig. 42, was calculated from the measured R. The relative 1-R curve was tied to the IRIS data to obtain the spectral power responsivity shown in Fig. 43. The uncertainty determination here for the extended wavelength range is similar to that discussed for Fig. 41 at wavelengths shorter than 15 µm. We estimate that 5 % of the 0.1R level between 18 µm and 30 µm on Fig. 42 gives 0.5 % (k=2) uncertainty for the 1-R between 18 µm and 30 µm.

---

[2] Certain commercial equipment, instruments, or materials are identified in this certificate to adequately describe the experimental procedure. Such identification does not imply recommendation or endorsement by the author, nor does it imply that the materials or equipment is the best available for the purpose.

The disagreement (in the overlap region to 19 μm) to the spectral power responsivity obtained above with the old reflectance measurement system (FTIS) is less than 1 %.
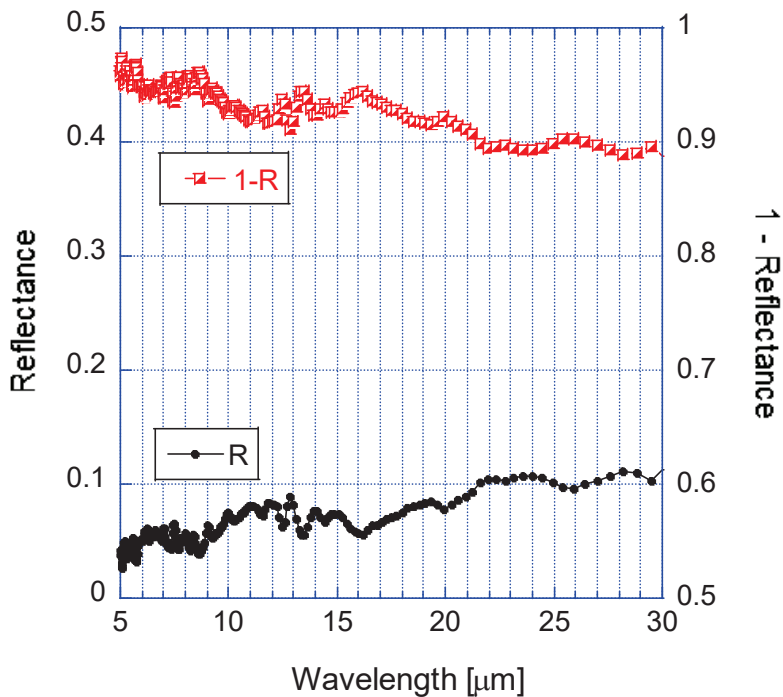
Fig. 42. The measured reflectance R and the calculated 1-R absorptance of an organic-black coated pyroelectric detector versus wavelength.
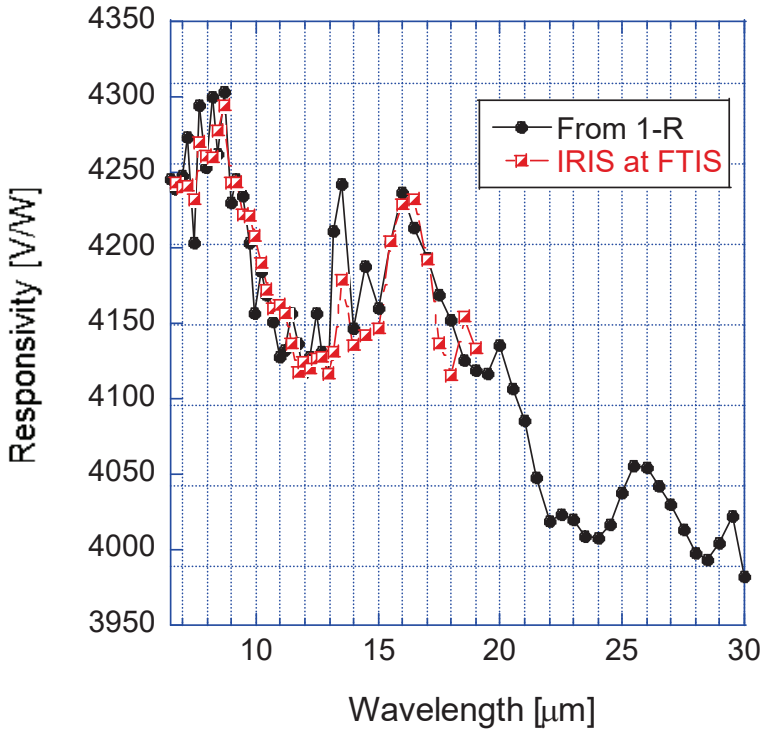
Fig. 43. Spectral power responsivity of an organic-black coated pyroelectric detector between 6.5 μm and 19 μm (IRIS at FTIS) and the extended responsivity to 30 μm (from 1-R).

Even if the spectral power responsivity of the discussed low-NEP pyroelectric detectors was determined to 30 μm, their utilization for IR calibrations at NIST (during the time of these measurements) ends at 24 μm because of signal-to-noise ratio problems at the monochromator output of the IR-SCF facility.

2.3.3.3. InSb detector spatial and spectral power responsivity

The here discussed InSb detector is used as a spectral power and irradiance measuring working standard. A 7 mm diameter InSb detector with a 6.4 mm diameter aperture, 1 mm away from the detector was mounted in a liquid-nitrogen cooled dewar as shown in

Fig. 44.
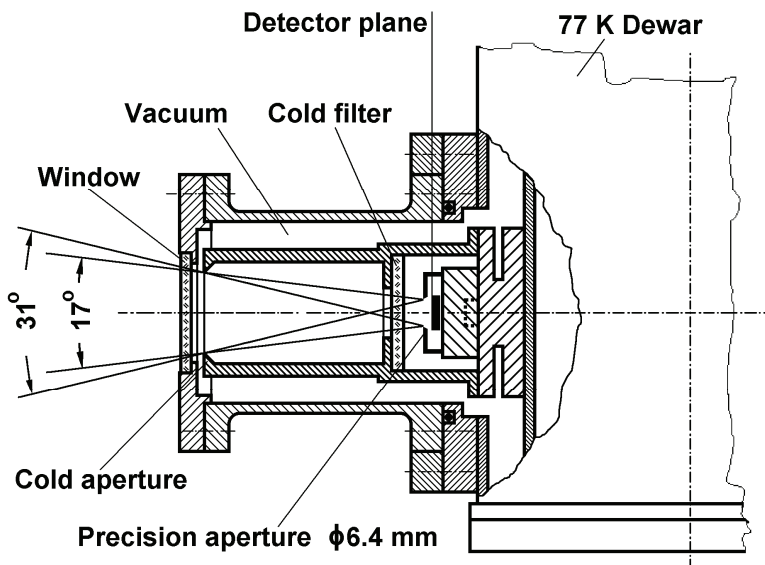
Fig. 44. InSb working standard detector.

The dewar has a sapphire window. There is a cold long-pass filter with a cut-on wavelength of 1850 nm inside of the dewar to minimize InSb flashing [62].

Before power responsivity calibration, the spatial uniformity of the InSb detector was measured within the input aperture. All spectral measurements were performed at the IR-SCF. A near-Gaussian profile beam with full-width-half-max (FWHM) of 0.35 mm was used for the spatial scan. The measured relative response along the detector diameter is shown in Fig. 45. The assessable detector diameter was about 5.6 mm where a response non-uniformity of less than 1 % was measured. When using a centered beam spot with a diameter of 4 mm or less, the non-uniformity of response can be decreased to less than 0.2 %.
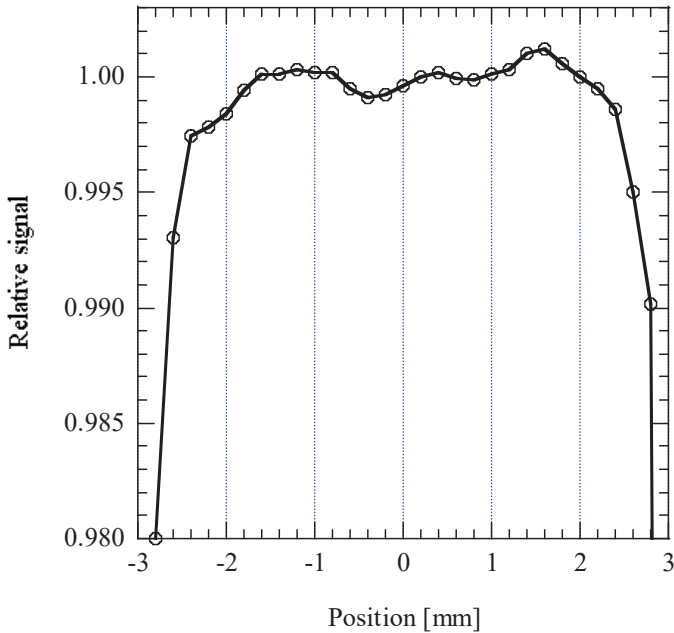
Fig. 45. Spatial non-uniformity of response of the InSb working standard along the detector diameter.

The InSb working standard previously calibrated against a cryogenic bolometer [63] was recalibrated against the low-NEP single-element pyroelectric transfer standard. The obtained spectral power responsivity at a signal gain of 2.957 x 10^4 V/A (using a nominal 30 kΩ feedback resistor) is shown in Fig. 46. For validation, this InSb detector was also calibrated for power responsivity against the sphere-input extended-InGaAs transfer standard radiometer. The extended-InGaAs transfer standard was calibrated against the cryogenic ACR when both measured the same total power of several stabilized laser beams. The power responsivity of the InSb detector was determined against both the pyroelectric and the extended-InGaAs transfer standards. The obtained two InSb power responsivities are compared in the spectral range where the InSb and the extended-InGaAs detectors overlap. The spectral responsivity determinations are shown at the same wavelengths (in the overlap interval) where the ACR-based laser calibrations were performed. For this comparison at the IR-SCF, the grating

monochromator was used with a 1100 ℃ blackbody radiator as a
stable source to perform the spectral power responsivity calibrations.
The two sets of spectral power responsivities of the InSb working
standard as derived from the two transfer standards at the same
wavelengths used at the ACR calibrations are shown in Fig. 47. The
differences are well within the 0.92 % (from the extended-InGaAs)
and the 1.17 % (from the pyroelectric) uncertainties (*k*=2) of the two
power responsivity determinations.
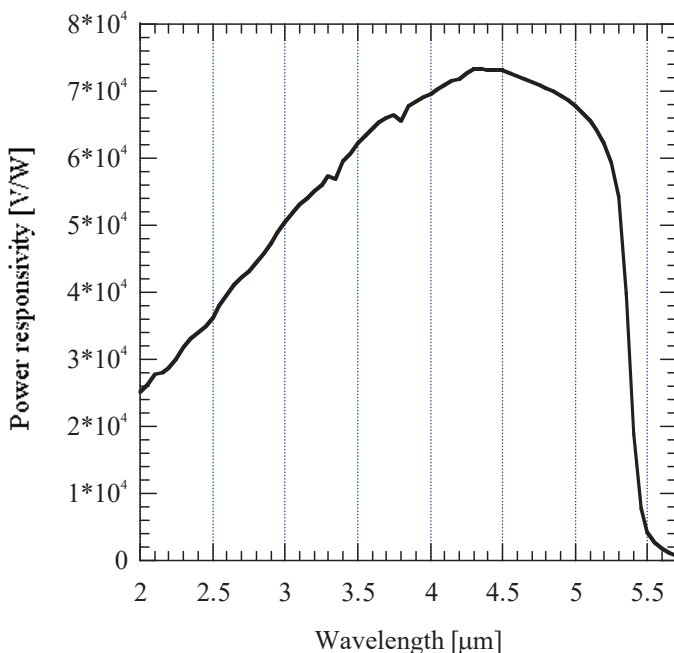
Fig. 46. Spectral power responsivity of the InSb working standard as
derived from the low-NEP single-element pyroelectric transfer standard.
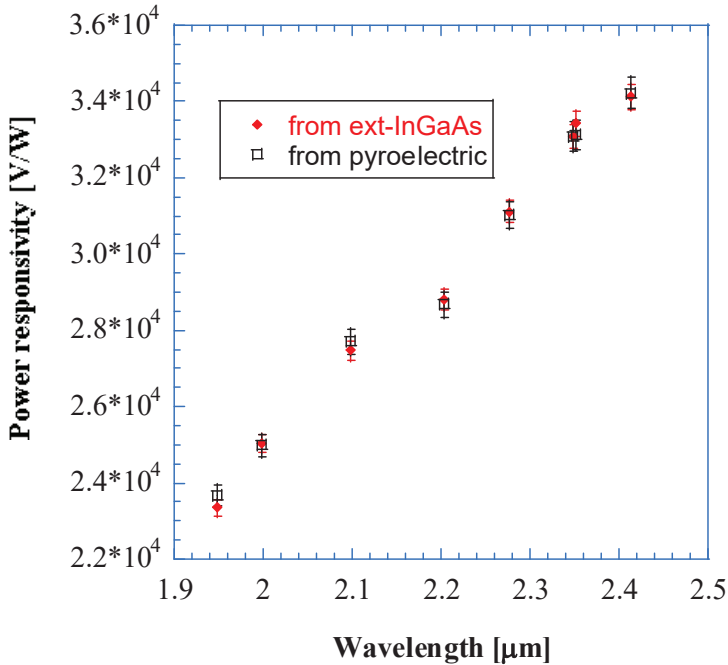
Fig. 47. Two sets of power responsivities of the InSb working standard as determined against the sphere-input extended-InGaAs and the pyroelectric transfer standards. The error bars show the expanded uncertainties.

The uncertainty of the spectral power responsivity of the InSb working standard was dominated by the power responsivity uncertainties of the reference detectors, which is 0.7 % (*k*=2) using the sphere-input extended InGaAs transfer standard in AC mode from 1.7 μm to 2.4 μm (discussed in DC mode in Section 2.3.1.2 above) and 1 % (*k*=2) from 2.5 μm to 13 μm and 1.2 % (*k*=2) at 14 μm for the low-NEP single-element pyroelectric transfer standard. An additional uncertainty component of 0.6 % (*k*=2) comes from the power responsivity transfer from the reference detectors. This component includes spatial non-uniformity of responsivity of the reference and test detectors and fluctuations (noise and drift to 2.4 μm and noise only in the AC measurements above 2.4 μm). The combined uncertainty of the spectral power responsivity (using the InSb working standard), obtained as the square root of sum of square of uncertainty components, is 1.2 % (*k*=2) between 2 μm and 5.2 μm.

The good matching of the data in the overlapping wavelength ranges of the different detectors validated the independently established spectral responsivity scales.

2.4. Spectral Irradiance Responsivity

The measurement geometry of practical (such as field) applications is more complicated than the total-power measurement in an incident beam described above in radiant-power measurement mode. Irradiance and illuminance (the photometric equivalent of irradiance) are the most widely measured radiometric and photometric quantities. The advantage of irradiance measurements is that even spatially non-uniform detectors can be used for low uncertainty measurements. The non-uniformity of the spatial responsivity can be averaged out if a uniform incident radiation overfills the active area of the detector. Also, detectors with small active area can be calibrated in irradiance mode. At the same time, a small area detector may not be calibrated in radiant-power measurement mode if the incident beam is too large to underfill the detector.

Spectral irradiance responsivity calibrations are made with a narrow optical bandwidth and the responsivities are determined with certain wavelength increments.

The measurement geometry of irradiance measurements and the Cosine-law of detector irradiance measurements were discussed in Section 3.2. of Volume 2.

Application considerations of adding an integrating sphere to a monochromator output for irradiance responsivity calibrations was discussed above in Section 2.3.3.1 where IR signal measurement modes were described. An advantage of the sphere applied method is that the irradiance is free of polarization effects. Larger irradiance levels can be obtained if integrating spheres are not used at the output of the monochromator. In this case, the irradiance field created by the monochromator itself is used for irradiance responsivity calibrations. The signal measured at the same distance between source and detector indicated about 300 times higher irradiance at the detector compared to the irradiance coming from a gold-coated 100 mm diameter sphere-source at a wavelength of 4.5 μm. The irradiance increased by a factor of 840 at 0.85 μm where a sphere with polytetrafluoroethylene (PTFE) coating was used [14]. Using the PTFE coating, the reflection losses were higher inside of

the sphere and also the scattering angle from the sphere exit port was higher compared to the related angle defined by the monochromator f-number.

Since the spatial uniformity of the irradiance field is a basic requirement for responsivity calibration, the response variations are to be measured. The spatial uniformity should be measured at a few wavelengths because it is wavelength dependent. As an example, the normalized signal changes obtained with the sphereless irradiance measurement method are shown in Fig. 48 at 4.5 μm at a distance of 250 mm from the monochromator. The scans were made in two orthogonal directions (i.e. along the X-axis and Y-axis) through the approximate center of the beam. The non-uniformity results can be utilized in the estimation of the uncertainty budget of irradiance responsivity measurements.
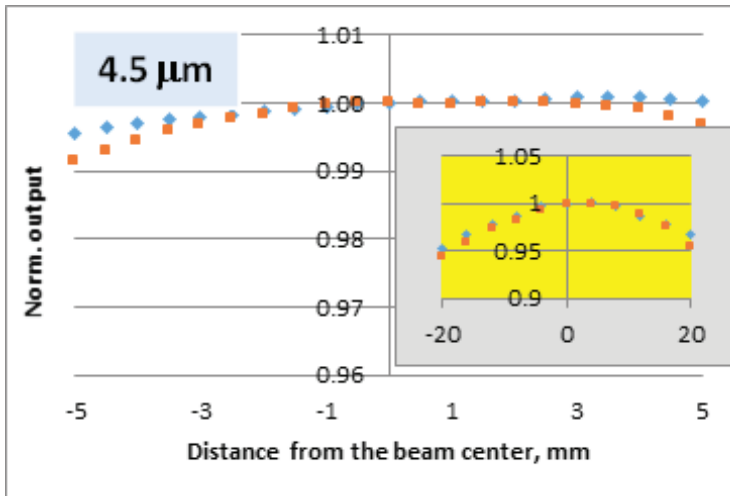
Fig. 48. Irradiance non-uniformity at 25 cm from monochromator in X (squares) and Y directions from center, measured by a 5 mm detector.

A spectrally calibrated irradiance meter can be used as a standard to calibrate test irradiance meters by substitution in a large enough, spatially uniform monochromatic field. As discussed above, the irradiance can be realized by either a collimator, or an integrating sphere coupled to the output of a monochromatic radiation source, or by the output radiation from a monochromator. The laser based

sphere sources were also discussed above.

The stray light from the edge of the aperture and the aperture holder (that can reach the detector) should be kept at a low level. Irradiance meters are to be substituted for an irradiance standard meter at the same distance to perform an irradiance responsivity transfer. During the substitution, both irradiance meters have to be aligned such that their apertures are placed at the same reference plane. Both detectors are to be overfilled with the same uniform field of radiation. In an irradiance responsivity transfer, the source-to-detector distance does not have to be the same for the standard and test detectors if the source is operated as a point source (having negligible spatial extension and Lambertian angular distribution). In this case, the inverse square law can be utilized and the radiant intensity of the point source has to be determined as an intermediate calibration step. The radiant intensity must be constant during a calibration transfer or corrected for stability using a monitor radiometer.

The aperture areas of irradiance meters can be measured in different ways. The effective aperture area of an irradiance or illuminance meter may not be equal to the geometrically measured aperture area. When the point source geometry is used in an irradiance responsivity transfer, the aperture area determination also should be made with point-source geometry. In this situation, the geometrically measured detector-aperture area can be used for conversion from radiant power responsivity into irradiance responsivity. From the irradiance transfer standard, the irradiance responsivity will propagate to working standards and test devices.

The advantage of using point source geometry is that it produces a uniform irradiance with a collimated beam shape within the aperture of the irradiance meter. Ideal and real beam shapes and different detector input geometries for irradiance measuring radiometer inputs are shown in Section 3.2.2 of Volume-2.

IR irradiance responsivity calibrations are needed in many applications, such as calibration of IR collimators. Irradiance measuring radiometers can be used as reference detectors to calibrate field radiometers in both irradiance and radiance measurement modes. In irradiance mode, smaller detectors with high shunt resistance, such as 1 mm diameter EIGA detectors can be used. Measurement of noise equivalent currents (NEC) are performed to evaluate noise

equivalent power (NEP) and D*.

The cosine law of detector irradiance measurements is discussed in 3.2.1 of Volume-2.

2.4.1. Measurement Methods and Irradiance Responsivity Transfer

Irradiance meters can be calibrated for irradiance responsivity in three different ways. The calibration method selected can depend on the construction of the meter to be calibrated.

2.4.1.1. Relative response determination

Frequently, irradiance meters are calibrated for relative spectral responsivity when they are underfilled by the monochromatic incident beam. This calibration can be done against a power measuring responsivity standard. During the spectral scan, the incident beam should be positioned to the same location, possibly to the center of the aperture (or detector) to reduce possible influence of spatial non-uniformity.

When using pyroelectric detectors for standards, their relative response can be determined from spectral reflectance measurement of the black-coating (as discussed in Section 5.3.1 of Volume 1). A pyroelectric hybrid detector coated with 50 μm thick coating was selected for low-uncertainty UV-to-SWIR responsivity scale realization. The spectral absorptance was determined as 1 – reflectance. Since the detector response is proportional to the absorptance (when the transmittance is negligibly small), the spectral absorptance can be used as a relative response function.

2.4.1.2. Absolute tie points against standard irradiance meters

The relative spectral response of an irradiance meter can be converted into absolute irradiance responsivity by making a tie point against a standard irradiance meter. A tie point means the determination of the absolute irradiance responsivity of the test irradiance meter at one wavelength only. The tie point can be used to make the relative to absolute spectral responsivity conversion.

In order to get the lowest relative measurement uncertainty, irradiance meters are to be calibrated with a point source geometry.

The point source should be located in the optical axis of the meter and the reference plane (the aperture) of the meter should be perpendicular for the incident radiation. Test irradiance meters can be calibrated against standard irradiance meters utilizing the inverse square law.

The irradiance responsivity for the organic-black coated pyroelectric detector, discussed in 5.3.1.2 of Volume-1, could be determined between 250 nm and 2500 nm. For the shown 250 nm to 2000 nm wavelength range in Fig. 49, several tie points were applied to evaluate the uncertainty after converting the relative spectral response into (absolute) spectral irradiance responsivity. Tie points from different irradiance measuring reference detectors were evaluated. The 2.6 % (k=2) uncertainty [9] of the tie points in the near-IR and SW-IR ranges are shown with red (error) bars. These tie points were derived from a sphere-input extended-InGaAs irradiance meter which is a power-to-irradiance converting transfer standard. The tie point and uncertainty-bar at 365 nm (blue color) were determined from indirect responsivity measurements using 365 nm LED irradiance sources calibrated against an FEL spectral irradiance lamp-standard. The uncertainty of this tie point is 1.6 % (k=2) [9]. The irradiance responsivity tie point with the smallest uncertainty is located at 660 nm (shown with green color). This tie point was derived with direct comparison of the pyroelectric detector to a Si trap irradiance standard at a distance of 1843 mm. The irradiance responsivity uncertainty of this Si trap-detector is 0.1 % (k=2) and it was derived from the cryogenic radiometer in power measurement mode. The area of the aperture was separately determined [32]. The tie point was used for the relative to absolute spectral responsivity conversion. The tie point uncertainty budget with its resultant uncertainty of 0.5 % (k=2) is shown in Table 5. The 0.5 % (k=2) uncertainty propagated for the 250 nm to 2500 nm wavelength range. This calibrated pyroelectric detector was used as a standard for spectral irradiance responsivity calibrations in the UV-to-SWIR wavelength range.
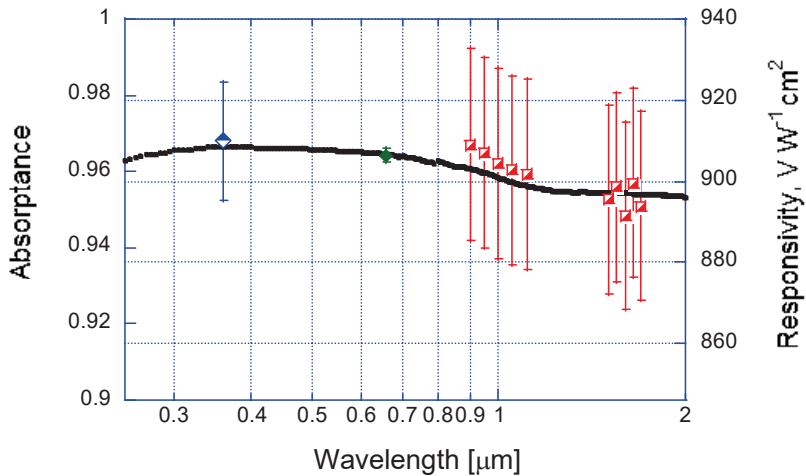
Fig. 49. Spectral absorptance and irradiance responsivity of an organic-black-coated hybrid pyroelectric detector between 250 nm and 2000 nm. The tie points with their uncertainty bars, obtained from three different transfer standard detectors, are shown. The final tie point used for the response curve conversion was at 660 nm.

Table 5 - Uncertainty budget of the organic-black coated pyroelectric detector at the 660 nm irradiance responsivity tie point.

Relative uncertainty components	[%]
$\Delta\lambda$	0.03
Distance	0.04
Target spot non-uniformity	0.10
Spectral response change	0.18
Output signal ratio	0.10
Reference Si-trap	0.10
Combined (*k*=1)	**0.25**
Expanded (*k*=2)	**0.5**

The uncertainty components in Table 5 originate from distance, wavelength error, target spot spatial nonuniformity, and signal (ratio) measurement errors. To keep the uncertainties originating from distance measurement and target-spot irradiance-nonuniformity small, an increased separation was used between the LED irradiance source and the irradiance measuring detectors. Figure 50 shows the

optical geometry for irradiance responsivity measurements using a collimated LED source peaking at 660 nm. This source was used only for irradiance responsivity transfer and it is not a standard. In this discussed example, the standard was a Si trap-detector with known power-responsivity and area of its front aperture.
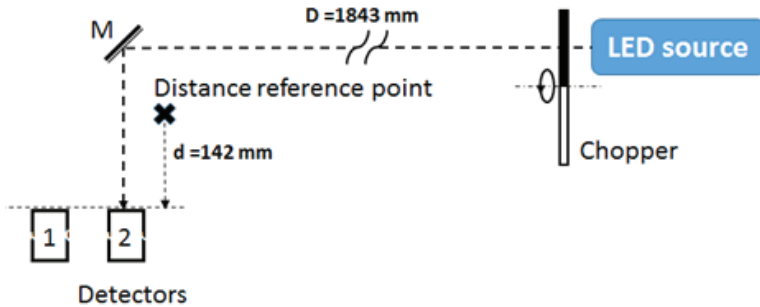
Fig. 50. Optical geometry for irradiance responsivity measurements using a collimated red LED (transfer but not standard) source.

For the required low-uncertainty distance measurement, an arbitrary distance-reference-point was used. The distance measurement error for the shown d = 142 mm distance is about 1 mm. However, when moving the LED source further away, the increased distance D = 1843 mm can be measured with a decreased uncertainty even if a simple tape measure is used. Detector 1 is the transfer standard Si-trap with the irradiance responsivity uncertainty of ~0.1 % (k=2). This irradiance responsivity is transferred to Detector 2 which is the above discussed pyroelectric hybrid detector. The transferred tie point converts the relative spectral response of the pyroelectric detector into spectral irradiance responsivity.

For power responsivity calibration of the above pyroelectric detector in the UV-to-SWIR, the tie point can be derived from the power-responsivity of the same Si trap-detector (where the above irradiance responsivity was derived from) also at 660 nm but both detectors are to be underfilled by the incident-beam from the 660 nm LED.

2.4.1.3. Power to irradiance responsivity conversion with aperture

The irradiance responsivity is equal to the product of the radiant power responsivity and the area of the aperture added to the front of the meter.

The aperture addition method works best on trap detectors where no radiation is reflected back to the aperture. Trap detectors equipped with aperture are the irradiance measuring transfer standards which can be calibrated with the lowest associated relative standard measurement uncertainty. However, their acceptance angle (FOV) is limited to several degrees.

Example: A relative standard measurement uncertainty of 0.05 % associated to the irradiance responsivity value can be achieved with point-source geometry [54].

2.4.1.4. Effective area determination with raster scan

This method, called the raster scan, was described using Fig. 53 in Section 3.2.6 of Volume-2. Using this method, the effective area of the irradiance meter can be determined. The effective area determination is very important for diffuser input irradiance meters where the effective area can be very different than the geometrically measured area. The raster scan method should be applied with special care if the beam has wings.

Figure 51 shows the scanning path of a beam over the aperture area in the raster scan method. The effective aperture area, A, is the ratio of the total signal, i, summed over the scanned area (total irradiance responsivity) to the product of the total beam power, Φ[W], and average spectral responsivity, $s(\lambda)$, within the active area of the aperture where Δx and Δy are the small steps taken to completely over-scan the aperture:

$$A = \frac{\sum i(x,y)\Delta x \Delta y}{\Phi \cdot s(\lambda)}$$

(20)
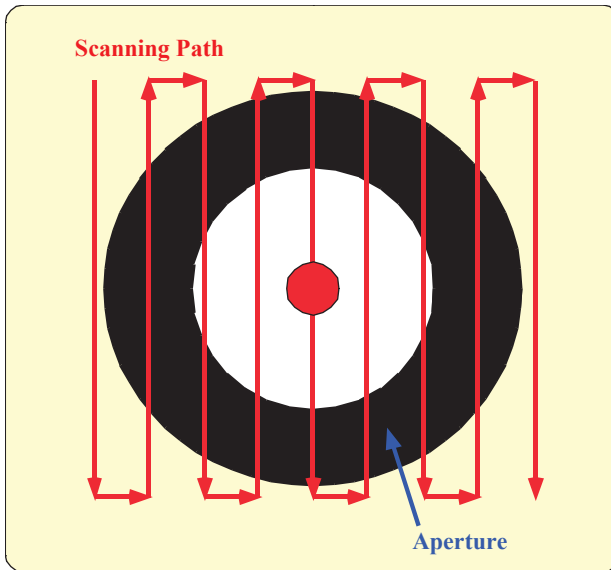
Fig. 51. Scanning path of a beam over the input aperture.

2.4.1.5. Irradince meter substitution method using inverse square law

Test irradiance meters can be calibrated against standard irradiance meters using the substitution method. If the reference planes of both the standard and test meters are in the same plane they measure the same irradiance and the responsivity can be transferred from the standard to test device. If the locations of the meter reference planes are not known, or the distances of the two meters from the source are different, the inverse square law can be used to determine the source-detector distances, provided the source is a point source, the angular distribution is Lambertian and the minimum distance is large enough compared to the size of the detector. A two-parameter curve fit to the data points measured at different meter distances will result in the zero offset of the point source position:

$$\frac{I_T}{I_{MT}} = \frac{I_{e,0}}{(x - x_0)^2}$$

(21)

where I_T / I_{MT} is the ratio of the irradiance produced signal to the source-monitoring detector-signal and *x* is the position of the moving detector stage. The two fit parameters are $I_{e,0}$ the constant radiant intensity of the measured point source, and x_0 the zero offset of the fixed (point) source. The signal ratio measurements minimize the effect of the intensity fluctuation of the source.

The difference of the zero offset from the reading of the detector position (where the detector stage is attached to the distance measuring ruler) will give the correct source-to-detector distance.

Note: The value should be taken only after verification with an uncertainty budget. Even when all readings are well within 10^{-4}, the measurement uncertainty of the distance varies by mm.

2.4.2. SI traceable calibration of IR quantum detectors

The SI traceability for the below discussed spectral irradiance responsivity calibrations was obtained from the NIST absolute cryogenic radiometer (ACR) and the here discussed power-to-irradiance converting transfer standard radiometers calibrated against the ACR.

2.4.2.1. IR-enhanced Si

The 5 mm diameter IR-enhanced Si photodiode (discussed in Section 2.3.1.1 above) can be used for irradiance measurements as well. Positioning a precision aperture in front of the photodiode (as shown in Fig. 52), it can be used as a power-to-irradiance responsivity converter. The irradiance responsivity will be equal to the product of the power responsivity and the aperture area. The spectral irradiance responsivity is the reference scale for tunable laser applied calibration facilities which are used for spectral irradiance and radiance responsivity calibrations [34]. A thin aperture (or an aperture with a thin land at the input hole) can sit on the top of the photodiode to avoid unwanted reflections between the aperture and the detector. Another solution for irradiance mode measurements is to use a front adapter similar to the one shown in Fig. 52. The goal in irradiance mode measurements is to limit the angular response of the photodiode to obtain a cosine function response within the limited field-of-view (FOV) of the detector. The FOV can be much larger than

with trap detectors.
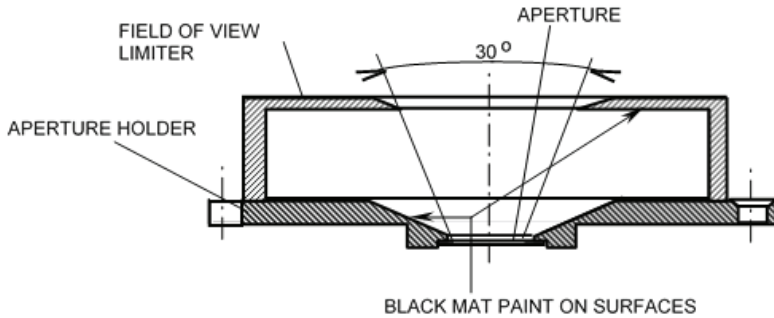
Fig. 52. Irradiance measuring input optics for an IR enhanced Si photodiode.

2.4.2.2. Sphere-input extended-InGaAs

An extended-InGaAs detector with an integrating sphere attached to its input was used as a transfer standard to transfer the irradiance responsivity scale to the InSb working standard discussed below. The characteristics of this transfer standard are discuseed in Section 3 of Volume 3 of this book series.

The scale transfer described here, gives the traceability to the NIST primary standard absolute cryogenic radiometer (ACR).

The extended-InGaAs radiometer was calibrated against the cryogenic ACR in radiant power measurement mode. The expanded uncertainty of the power responsivity transfer was less than 0.5 %. The integrating sphere attached to the detector input produced a non-uniformity in the spatial responsivity of less than 0.5 %. From these two uncertainty components, the uncertainty of the spectral power responsivity was 0.7 % (k=2). This transfer standard is a power-to-irradiance responsivity converter. The area of the precision aperture at the entrance port of the integrating sphere was determined at the Aperture Area Measurement Facility of NIST [32]. The measured area was 50.04 mm^2 with a 0.1 % (k=2) measurement uncertainty. The spectral irradiance responsivity is the product of the aperture area and the spectral power responsivity. The spectral irradiance responsivity is shown in Fig. 53 between 1725 nm and 2525 nm. The absolute irradiance responsivity tie points derived from the cryogenic

ACR are shown with square dots. These absolute tie points fit the spectral power responsivity derived from the pyroelectric transfer standard. The uncertainty of this relative function is 1 % (*k*=2). The uncertainty of the spectral irradiance responsivity of the sphere-input extended-InGaAs transfer standard is 1.23 % (*k*=2) between 1725 nm and 2413 nm.
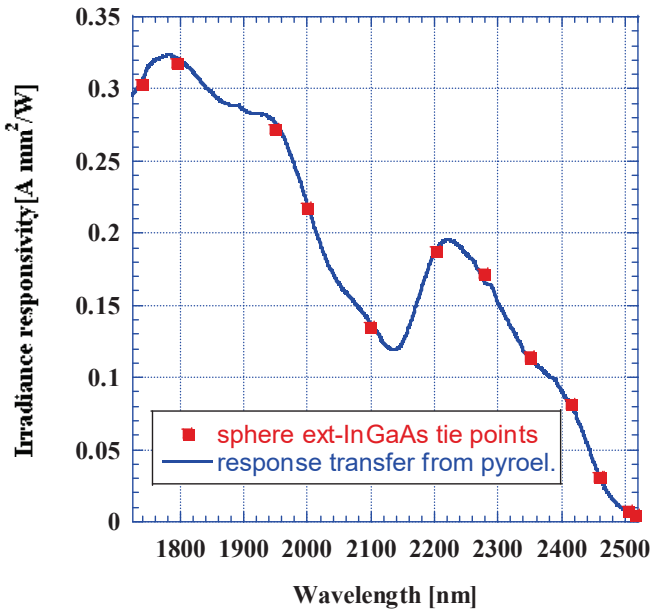
Fig. 53. Spectral irradiance responsivity of the sphere-input extended InGaAs transfer standard.The square tie points give the traceability to the primary standard cryogenic ACR. The relative curve (solid line) was derived from the pyroelectric standard.

2.4.2.3. InSb

While a low-NEP pyroelectric transfer standard is used only for radiant power measurement, an InSb working standard can be used in irradiance measurement mode as well. A good quality InSb detector has a current responsivity of about 2.5 A/W at the 4.4 μm peak. This is a factor of 5 x 10^6 higher than the current responsivity of a low-NEP pyroelectric transfer standard. However, the signal-gain of the InSb detector cannot be higher than 3 x 10^4 V/A because

of the large DC background current (to avoid saturation of the preamplifier). In contrast, the signal gain of the pyroelectric detector is 10^{10} V/A. The 7.5 x 10^4 V/W voltage responsivity of the InSb working standard (around the peak) is still 15 times higher than the roughly 5 x 10^3 V/W responsivity of the pyroelectric transfer standard. This higher voltage responsivity makes it possible to perform irradiance measurements with satisfactory signal-to-noise ratios.

The InSb spectral power responsivity after derived from a low-NEP pyroelectric transfer standard, was multiplied with the 0.3205 cm^2 area of the aperture in front of the InSb detector. The product resulted in the spectral irradiance responsivity of the here discussed InSb working standard. Since the InSb detector spatial non-uniformity close to the aperture edges is not known, estimation of the uncertainty of this spectral irradiance responsivity determination is a problem. To avoid this problem, the spectral irradiance responsivity of the InSb working standard was also derived from the sphere-input extended-InGaAs transfer-standard in the wavelength interval where the InSb working standard and the extended-InGaAs transfer standard overlap. This irradiance responsivity transfer was also performed at the monochromator-output of the NIST IR-SCF using a 100 mm diameter gold coated integrating sphere shown in Fig. 37.

The sphere-input extended-InGaAs reference detector and the InSb detector (as a test detector here) were positioned at a distance of 300 mm +/- 1 mm away from the exit port of the sphere source. Using this geometrical arrangement, the spatial non-uniformity of the irradiance was less than 0.3 % inside the apertures of both irradiance meters. The main uncertainty components of the irradiance responsivity transfer from the extended-InGaAs transfer standard to the InSb working standard are shown in Table 5.

Table 5. Dominant uncertainty components of the irradiance responsivity transfer from the extended-InGaAs transfer standard to the InSb working standard between 1.95 μm and 2.35 μm.

Uncertainty factor	Type A [%]	Type B [%]	Combined [%]
Ext-IGA irradiance responsivity	1.23		
Distance		0.66	
Ext-IGA signal noise and drift		1.5	
InSb signal noise		1.5	
Expanded combined uncertainty ($k=2$)			2.5

The 2.5 % ($k=2$) uncertainty of the irradiance responsivity of the InSb working standard was extended to 5.2 μm based on the agreement of the spectral power responsivities (derived from the sphere-input extended-InGas and the pyroelectric transfer standards) shown above.

The comparison of the previously determined spectral irradiance responsivity (from the product of the InSb power responsivity and its aperture area) and the here determined (transferred from the sphere-input extended-InGaAs transfer standard) spectral irradiance responsivity is shown in Fig. 54. Only the high responsivity tie points of the ext-InGaAs radiometer between 1948 nm and 2413 nm were used for this irradiance responsivity comparison. The uncertainty of the scale transfer (from the ext-InGaAs to the InSb) increased from 2.0 % ($k=2$) at 1948 nm to 2.5 % ($k=2$) at 2413 nm. The comparison at 2.5 μm, where the uncertainty of the irradiance responsivity transfer is 9.9 % ($k=2$) (caused by the low signal of the extended InGaAs transfer standard) could not be made with a low enough uncertainty. The InSb spectral irradiance responsivities from the two different realizations agree within the reported irradiance responsivity uncertainties. These results validate that the previously used spectral irradiance responsivity determination (the product of the power responsivity and the aperture area) gives a comparable result to the irradiance responsivity derived from the sphere-input extended-InGaAs transfer-standard. The good agreement also verifies that the spatial non-uniformity of the InSb working standard close to the

aperture edges is about the same as the non-uniformity around the detector center.
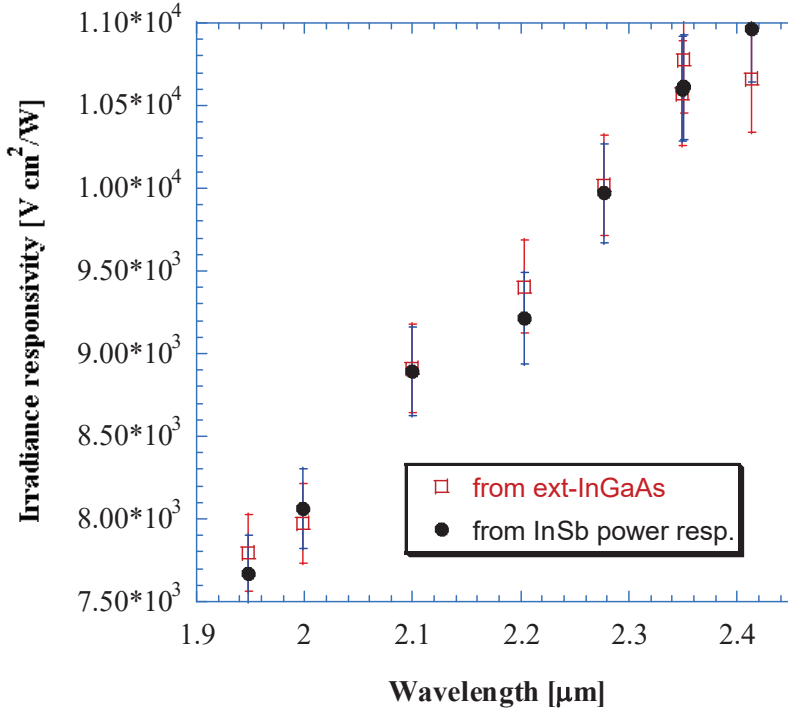
Fig. 54. Comparison of two different sets of irradiance responsivity data of the InSb working standard. The open squares were derived from the sphere-input ext-InGaAs transfer standard and the full circles were obtained from the InSb power responsivity derived from the pyroelectric transfer standard. The error bars show the expanded uncertainties.

2.4.2.3.1. Narrowband (selective) InSb

Four narrow-band InSb irradiance meters have been developed at different times. They were used to calibrate infrared target simulators instead of traditionally using blackbody source standards. The goal of the here described work was to update the infrared spectral irradiance responsivity scales and the compare previously measured spectral irradiance responsivity results.

Two of the four irradiance meters (InSb #5 and #7) were calibrated for spectral irradiance responsivity in 2003 against the InSb working standard using tunable lasers at the Infrared Spectral Irradiance and Radiance Responsivity Calibrations using Uniform Sources (IR-SIRCUS) facility. That time, the InSb working standard was calibrated against a cryogenic bolometer [64]. Irradiance meters InSb #5, #8, and #9 were calibrated in 2007 at the improved IR-SIRCUS [65] using tunable laser sources.

Figure 55 shows the 2011 spectral irradiance responsivity results of four narrow-band InSb irradiance meters. All four irradiance meters were calibrated against the broadband InSb working standard at the NIST IR-SCF.

Figure 56 shows the comparison of the 2007 and the 2011 spectral irradiance responsivity calibrations as an example for InSb #9. The two spectral curves agree within the reported uncertainties. The 3 % (k=2) uncertainty bars for both the 2007 and the 2011 irradiance responsivity calibrations are shown for both curves. The graph also shows that the monochromator measured spectral shape is slightly different from the laser source measured one because of the different spectral resolutions produced by the two different monochromatic sources. However, the integral responsivity with both spectral resolutions is the same (within the reported uncertainties).
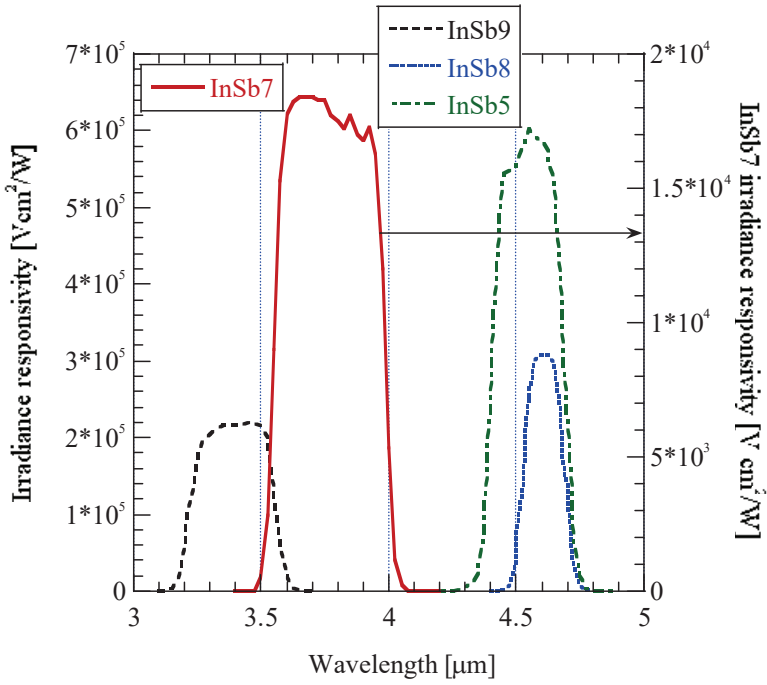
Fig. 55. Spectral irradiance responsivities of four narrow-band InSb irradiance meters calibrated against the broadband InSb working standard.
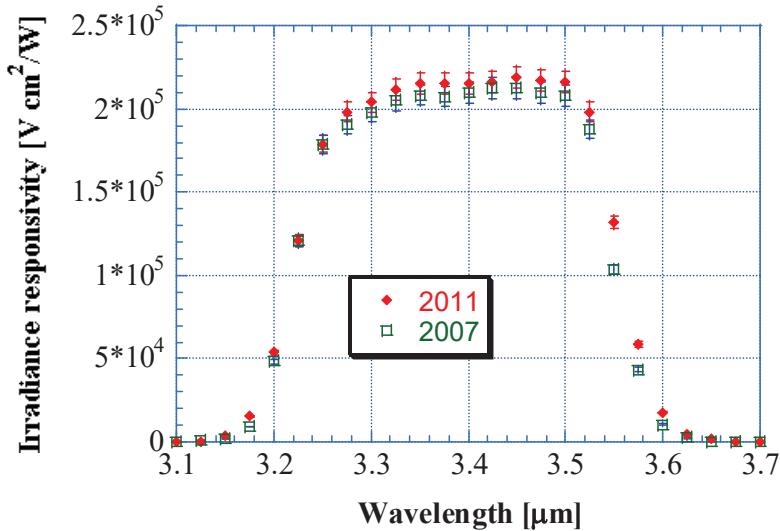
Fig. 56. Comparison of the 2007 and 2011 spectral irradiance responsivities of the InSb#9 irradiance meter. The error bars overlap.

2.4.2.4. HgCdTe (MCT)

Since the noise equivalent power (NEP) of pyroelectric transfer-standards is too small (less than 10 nW/Hz$^{1/2}$), irradiance mode measurements (where the signal is much smaller), even with low-NEP pyroelectric detectors, cannot be performed at the output of monochromators. Instead, MCT detectors can be used.

The main advantages of MCT detectors is broad wavelength coverage, low-NEP, and good long-term stability.

PV-MCT (single-element) detectors are small, typically 1 mm, but not larger than 2 mm. With 4-stage thermoelectric coolers, the PV-MCT detectors can be operated between -70 °C and -85 °C. As a result of this cooling, selected short-wave PV-MCT detectors with the bandgap wavelength at 2.8 μm can have a large shunt resistance (about 10 MΩ). Typically, the shunt resistance of small area PV-MCT detectors is around a few-hundred ohm. The low shunt resistance should be avoided because it causes high noise-amplification. Characteristics and application issues of PV-MCT detectors are discussed in Section 7.1 of Volume 2. PV-MCT detector based

working standards are discussed in Section 5.3.3.1 of Volume 3: Optical Detector and Radiometer Standards of this book series.

As an example, a large-area multi-junction PV-MCT radiometer was characterized for spectral responsivity, spatial uniformity of response, detector shunt resistance, signal-to-noise ratio, DC output signal, and output noise. This 4 x 4 mm detector seemed to be a good candidate for the extension of the spectral irradiance responsivity scale. The evaluation work is discussed in Section 5.3.3.1.1 of Volume 3. The NEP evaluations were performed at different signal-gains and frequencies. The noise tests indicated that amplifier gains higher than 10^4 V/A cannot improve the NEP of the PV-MCT radiometer. The equal NEPs at the 10^4 V/A, 10^5 V/A, and 10^6 V/A gains were obtained because the dominant noise was the highly amplified amplifier-noise which proportionally increased to the gain increase. A solution was proposed to better utilize the high, 0.008 A/W current-responsivity of the PV-MCT detector. This can be done if the amplification for the input noise is decreased using a bootstrap (shunt-resistance increasing) amplifier. In that case, the amplifier gain could be increased to 10^7 V/A that produces a DC output voltage close to the saturation limit of the amplifier. At this gain, the NEP could be decreased not only because of the increased gain (and responsivity) but also because of the decreased output noise. Then, the decreased output noise component should be equalized to the background current produced output noise. The equalization should be made after the background produced current is reduced with a cold field-of-view limiter positioned around the PV-MCT photodiode. The result of the suggested noise equalization would be a significantly decreased NEP that would be low enough for spectral irradiance responsivity measurements. The suggested NEP improvement can be applied to many other PV-MCT detectors including small-size detectors with low shunt resistance.

PC-MCT working standards are discussed in Section 5.3.3.2 of Volume 3. PC-MCT detector characteristics are discussed in Section 3.2 of Volume 1. The size of these detectors can be 3 mm or 4 mm. The 4 mm detector is suitable for power mode calibrations and measurements. These detectors are operated in liquid nitrogen cooled dewars and have spatial non-uniformities of several times ten percent. Power mode measurements can be applied if the beam size and beam position are always the same on the surface of the detector. Typically, the beam is centered using a computer program.

The PC-MCT detectors are operated with DC bias current to sense the photogenerated conductance change, which is proportional to the radiant power on the detector. In a traditional biasing and measuring circuit, a DC source is connected to the detector through a load-resistor. The resistance of the detector is low, usually less than 100 Ω. The load resistor keeps the biasing current constant and the voltage change on the detector is measured. The measured voltage is a nonlinear function of the conductance change [58]. To eliminate this response nonlinearity, current mode measurements should be applied (instead of voltage mode). A linear current mode amplifier is described in Section 8 of Volume 2. In this preamplifier ten current-to-voltage converters are connected parallel to produce 10 x 5 mA = 50 mA DC bias current for the PC detector. The preamplifier does not need any compensating source to zero the effect of the bias current for the output of the preamplifier.

MCT radiometers after charcterizations and selections are usually calibrated against low-NEP pyroelectric reference radiometers. This calibration transfer is performed in power mode. The power response can be converted into irradiance responsivity using tie points from calibrated irradiance meters at the wavelength interval(s) where the reference and test detectors overlap.

2.4.2.4.1. Responsivity extension using sphereless beam

Here, the issues of the irradiance responsivity scale extension are discussed to cover the wavelength range from 5.2 μm to the long-wave (LW) IR. As discussed earlier, high quality IR detectors are available for irradiance responsivity calibrations at wavelengths shorter than 5.2 μm. Extended-InGaAs radiometers [66] are used between 950 nm and 2.5 μm and InSb radiometers [67] are used to ~5 μm. For scale extension, it is important to use MCT detectors with NEP lower than that of the "low-NEP" pyroelectric standards used for spectral power responsivity calibrations.

At the extension of the irradiance responsivity scale to the LW-IR, the irradiance level at the monochromator output must be high to obtain high signal-to-noise ratios and spatially uniform to obtain low responsivity uncertainties. The previously used 10 cm diameter gold-coated sphere produced high spatial irradiance uniformity in the reference planes of the detectors (discussed above in Fig. 37 of Section 2.3.3.1). The radiation uniformity was obtained due to the

multiple reflections inside the sphere. However, the radiation loss for the output was significant. In monochromator applications, this problem becomes significant for wavelengths above 5 μm where most IR detectors do not have a sufficiently low NEP needed for accurate irradiance measurements. In the below discussed example, the irradiance level was significantly increased [14]. The sphere was removed and the extended beam of the monochromator was used instead.
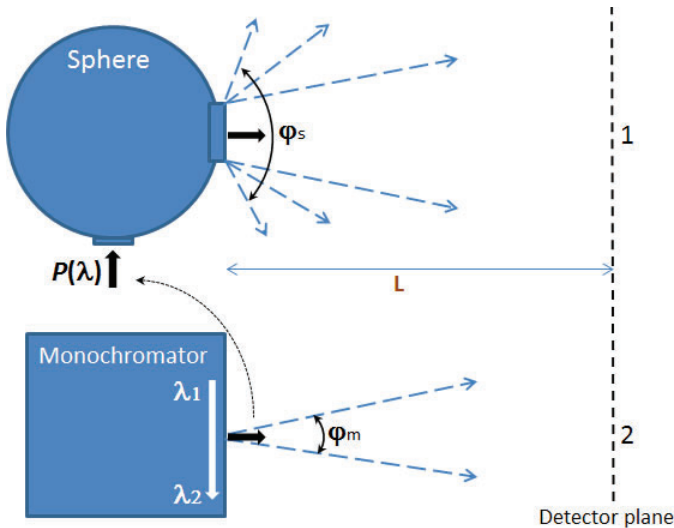
Figure 57. Different beam geometries for the irradiance responsivity measurements.

Figure 57 shows two optical geometries used for irradiance responsivity measurements [14]. In the upper portion, where an integrating sphere is used, the monochromator output is directed to the input port and radiation from the output port configures the irradiance field applied to a detector in position 1. In the alternative solution (in the lower part of the scheme), the irradiance field is created directly by the monochromator beam (in detector position 2). Signal measurements performed at 4.5 μm at a constant distance L between source and detector show an irradiance at the detector about 300 times higher for the direct (lower) case, compared to the

gold-coated 100 mm sphere application. A signal increase by a factor of 840 was measured at 0.85 µm, using a sphere with a high reflectance polytetrafluoroethylene (PTFE) [13] coating. This result was expected because of the reflection losses inside of the sphere and the nearly hemispherical output angle φ_s compared to the output angle φ_m defined by the monochromator *f*-number.

The spatial non-uniformity of the irradiance field was measured at a few fixed wavelengths in two orthogonal directions (i.e. along X and Y axes). Figure 48 (above) shows an example. The scans were made through the approximate center of the detector.

In a direct comparison of irradiance responsivity measured with both geometries [14] the output radiation from the monochromator was reduced to a level where noise-related features were clearly seen in the measurements using the sphere. Using the same output of the monochromator for the extended beam geometry, a less noisy spectrum was obtained.

It should be noted that one disadvantage of a sphereless geometry is the polarization of the output beam, as compared to the sphere geometry. This factor can be taken into account in the uncertainty budget.

The sphereless geometry was used for the responsivity scale extension to 12.5 µm. The 4 mm x 4 mm PC-MCT detector was used at a modulation frequency of 10.5 Hz. The MCT detectors are known to have a large spatial non-uniformity of response. However, this kind of non-uniformity was not critical for calibration of irradiance responsivity. The extension of the irradiance calibration scale above 5.5 µm where the reference standard was not available, was based on three data sets for the MCT detector: power responsivity in the range of 3 µm to 12.5 µm, irradiance responsivity in the range of 3 µm to 5.5 µm and a spectral ratio of outputs in both radiant power and irradiance modes. The latter was necessary to check a possible spectral non-uniformity that may limit the application of the sphereless method. The normalized ratio for irradiance mode to power mode showed a difference of less than a 1.5 %. Therefore, the spectral shape of the irradiance responsivity will be similar to that of the known power responsivity within the expected uncertainty budget.
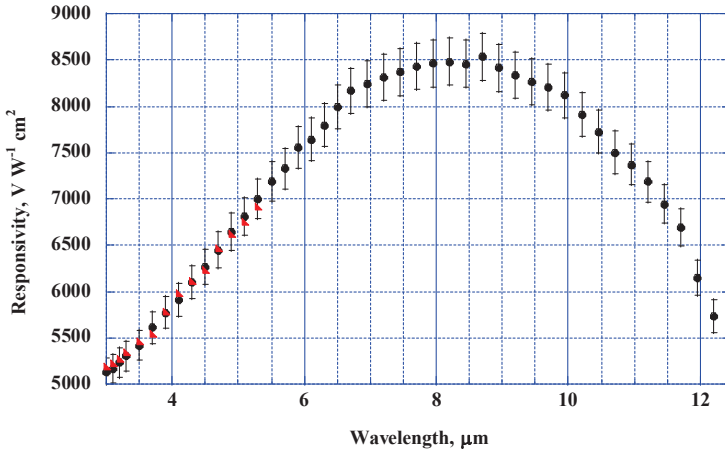
Figure 58. Spectral irradiance responsivity of a PC-MCT detector.
The error bars indicate the expanded uncertainty (*k*=2).

Thus, once the irradiance responsivity of the MCT detector is directly calibrated in the range up to 5.5 μm, the remaining piece of the range may be characterized by the shape of the radiant power responsivity prorated to the known irradiance responsivity value below 5.5 μm. The demonstration of this method is shown in Fig. 58 where the best match of two data sets was provided in the overlapped range below 5.5 μm. The estimated uncertainty of this calibration was 3 % (*k* = 2).

2.4.2.4.2. Irradiance responsivity uncertainty

The NIST IR-SCF allows responsivity calibrations in irradiance mode from 0.6 μm to 24 μm with uncertainties to 3 % (*k* = 2). The basic components of the uncertainty budget for irradiance responsivity measurement of a PC-MCT detector are shown in Table 6. It should be noted that the most significant contribution originates from the scale transfer.

Table 6. Calibration uncertainty budget (%) for irradiance measurements of PC-MCT detectors.

Wave-length range [μm]	Δλ	Dist.	Field non-uniformity	Outp ratio	Stdard	Comb. Uncert. ($k = 1$)	Exp.unc ($k = 2$)
5.3 - 12.5	.08	0.6	0.8	0.5	1	1.5	3.0

In the long-wavelength range or at the edges of the spectral sub-ranges the available signal to noise ratio becomes noticeable as well. On the other hand, usually the observed deviation of the experimentally measured data from the responsivity fitting function is lower than the combined uncertainty presented in Table 5. It is anticipated, therefore, that upon reduction of these two components, an uncertainty better than 1 % ($k = 2$) may be achieved in future calibrations for the entire spectral range. The estimate of the uncertainty component related to the ageing effect of the reference detector is problematic since it may occur slowly over a long period. Using group policy for the detector standard(s) and periodic comparison of different standard detectors in the spectrally overlapping regions is helpful to identify this effect, assuming that ageing effects for different detectors would unlikely be the same.

2.4.3. DSR use for spectral irradiance responsivity

A test method for spectral responsivity measurements of photovoltaic devices has been published in the ASTM E 1021 – 06 standard. This test method is to be used to determine either the absolute or relative spectral responsivity of a single-junction photovoltaic device. This test method requires the use of a bias light [68].

The differential spectral responsivity (DSR) method [69], as already discussed in Section 9.4.1.4 of Volume-1 for testing non-linearity, is a spectral calibration method based on the measurement of the DSR $\tilde{s}(\lambda)$ as a function of wavelength in the presence of steady-state bias irradiance E_b setting the operating point of the device, expressed by its photocurrent $I_{sc}(E_b)$:

$$\widetilde{s}(\lambda) = \frac{\Delta I_{sc}}{\Delta E(\lambda)}\bigg|_{E_b}$$

$$(22)$$

$\widetilde{s}(\lambda)$ is equal to the slope of the photocurrent I_{sc} versus irradiance characteristic $E(\lambda)$ at the bias irradiance E_b. It is measured using a modulated quasi-monochromatic irradiance $\Delta E(\lambda)$ yielding a photo-generated AC photocurrent ΔI_{sc}.

It should be noted that the low signal spectral responsivity, which is typically measured using setups without bias radiation is only applicable if the test detector is perfectly linear up to the irradiance levels used ($\widetilde{s}(\lambda, E_b) \equiv s(\lambda)$ independent of E_b).

In practice, a dual-beam optical arrangement is used (as shown in Fig. 60 which is a repeat of Fig. 106 in 9.4.1.4 of Volume 1) to measure DSR distributions of a detector, a photometer or any radiometer at a series of discrete operating points. The operating points are set with a steady-state bias irradiance at levels between 1 μW/cm² and 200 mW/cm², depending on the application for which the detector is used. A chopped monochromatic radiation $\Delta E(\lambda)$ from the output of a double grating monochromator as the second beam is finally measured at the DUT with lock-in technique. The DUT is measured against standard detectors using substitution method, where the standard detector is not exposed to the bias radiation and its responsivity is linear. A monitor detector is used to correct for fluctuations of the monochromatic source.

Without the bias radiation, the DSR setup works like a classical setup for irradiance / radiance responsivity measurements of linear devices. For measurements of a non-linearity of the responsivity the type of bias irradiance, which is applied for the measurement of the DSR signal, depends on the process causing the non-linearity within the detector. The non-linearity of the popular Hamamatsu S1227 and S1337 diodes is illustrated in Fig. 59 at high irradiance levels [70]. The relative response, *s*, is shown versus the bias-current produced by the irradiance levels at different wavelengths. The non-linearity is caused by ohmic losses within the device and it is nearly independent of the spectral distribution of the bias radiation.
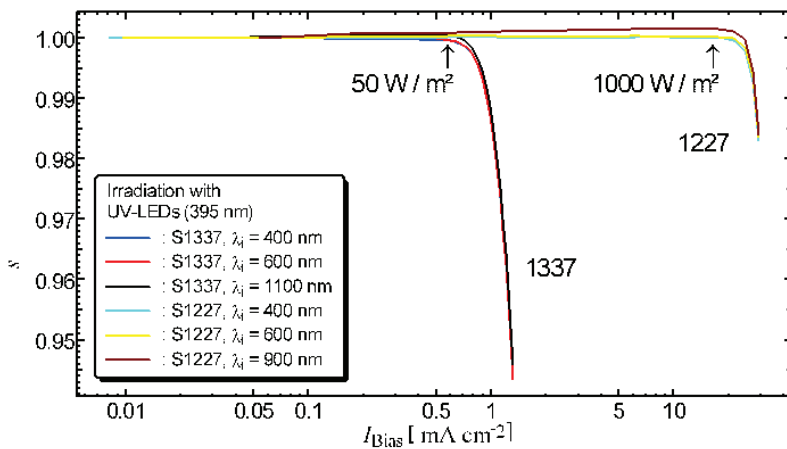
Fig. 59. Non-linearity of Hamamatsu S1227 and S1337 photodiodes at high irradiance levels with respect to the spectral responsivity at different set wavelengths.

x   y

plate with photometer
and reference radiometer

z

36 bias lamps
with dichroic
mirrors for
relative
calibration

focus

beam splitter

monitor
photodiode

aperture

shutter

f = 125 mm

condensor lens

chopper

FEL lamp
Xe lamp
Hg lamp

monochromator with
triple grating turrets

210 nm - 1900 nm
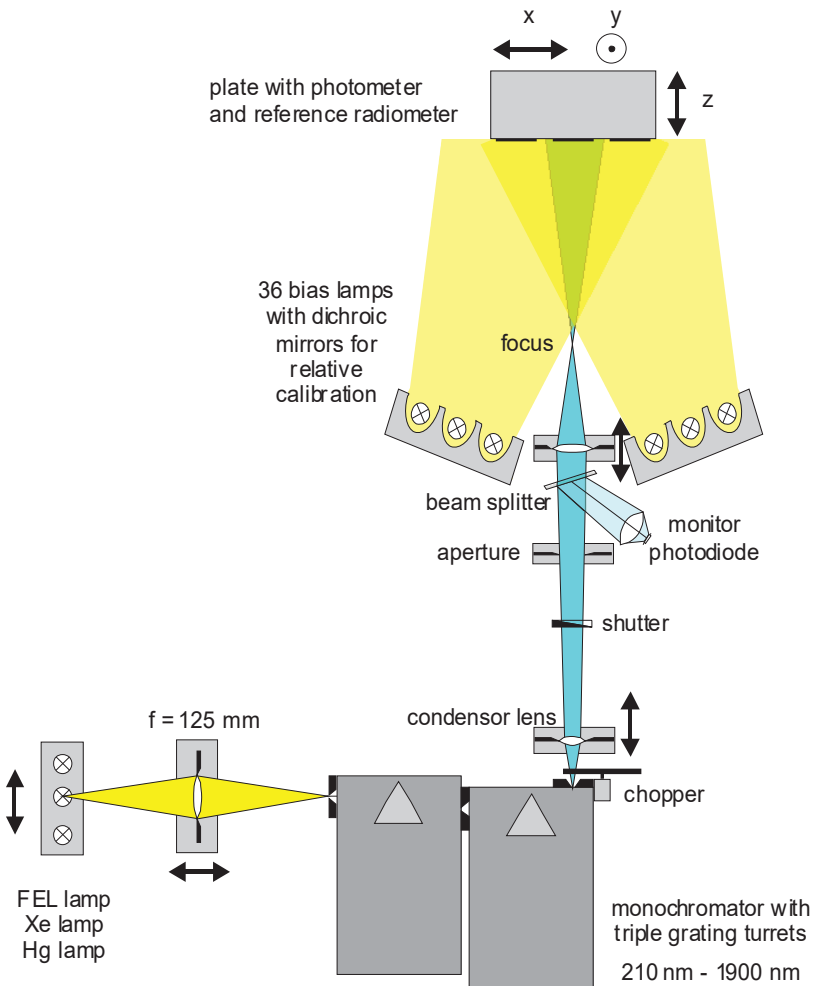
Fig. 60. Optical arrangement of a differential spectral responsivity (DSR)
setup. Depending on the z-position of the detector it is possible to switch
between spectral irradiance responsivity and spectral radiant power
responsivity.

2.4.4. Noise-equivalent-irradiance (NEI)

The NEI is derived from the NEP when the input quantity to be measured is irradiance. The radiant-power (measured directly by the detector) responsivity can be converted into irradiance responsivity using a conversion factor a. (Irradiance responsivity transfers are discussed in Section 2.4.1 above.) The power-responsivity should be multiplied by a to obtain the irradiance responsivity. The NEI is:

$$NEI = \frac{NEP}{a} = \frac{NEC}{a \cdot R}$$

(23)

where NEC is the noise-equivalent current and R is the responsivity. The dimensions are A/W for R and m^2 for a

2.4.4.1. Low-NEI of EIGA irradiance meters

While the dominant noise at the output of silicon photodiode current meters is the resistor (Johnson) noise (using a few seconds or shorter integration time constants), the dominant output noise will originate from the operational amplifier of the photocurrent meter (1/f noise) when the photodiode shunt resistance is low and the upper wavelength cut-off is limited to about 2.5 micrometer. This long-wavelength limitation is important to get out from the background limited noise operation of infrared detectors. The low shunt resistance will dominate the source resistance (the parallel connected feedback and shunt resistances) when the applied feedback resistors are higher than the photodiode shunt resistance. In this case, the resistor noise remains constant not like with silicon and other high shunt resistance photodiodes where the resistor noise increases when the feedback resistors are increased (up to about the value of the shunt resistance). Low source resistance produces low resistor noise and low shunt resistance produces high (closed-loop) voltage gain: (Rf+Rs)/Rs, where Rf is the feedback resistor and Rs is the shunt resistance. It is important to minimize this voltage gain that amplifies the amplifier noise from its input to its output. The highest signal-to-noise ratio will be reached at the output of the current meter when the feedback resistor is equal to or somewhat higher than the shunt resistance of the photodiode. Further increase of the feedback resistor will not improve the signal-to-noise ratio at the current meter output. The signal and the noise will be amplified equally.

It is always the first amplifier-stage (after the detector) that determines the signal-to-noise ratio of the detector-amplifier system. If the first stage (the current-to-voltage converter) design is not done properly, the following lock-in amplifier cannot correct the poor signal-to-noise ratio introduced by the first stage. Consequently, the photodiode shunt resistance must be increased to the highest possible value. This can be done by decreasing the area of the photodiode and also by making photodiode selections for the highest shunt resistance value. Shunt resistances between 3 Mohm and 3.6 Mohm can be routinely performed (during fabrication) on 3 mm diameter EIGA photodiodes at -85 degree C. In this case, a 10 Mohm feedback resistor as a maximum can optimize the output signal-to-noise ratio. If the diameter is decreased by a factor of 3, the shunt resistance can be increased by about a factor of 10 as well. This means, that a feedback resistor of 100 Mohm is the maximum value that will optimize the signal-to-noise ratio for the output. However, if the photodiode could be further cooled (e.g. using liquid Nitrogen) the shunt resistance would also increase. In this case, manual or electronic (auto) compensation of the relatively low background current is possible for the operational amplifier of the current meter and the feedback resistor could be increased further. Similar feedback resistor increase cannot be performed in traditional background-noise limited infrared measuring systems. As an example, 40 fW dark-NEP was measured at the output of a 3 mm diameter EIGA photodiode current meter at chopping frequencies between 15 Hz and 40 Hz with 1 s integration time constant. In comparison, the dark-NEP of a cold-filter and cold-stop (17 degree field-of-view) limited 4 mm InSb photodiode current meter (with the limiting background noise) was about an order of magnitude higher at similar operating conditions.

Care should be taken because further increase of the feedback resistor will equally increase both the signal-gain (current-to-voltage gain) and the noise gain (the closed-loop voltage gain will amplify the input noise of the operational amplifier). The noise-equivalent-irradiance (NEI), which is derived from the NEP (see above), includes the measurement geometry (flux transfer) of the input optics. The NEI can be increased with well designed input geometry where the flux transfer from irradiance mode to radiant-power mode is high. The noise should be decreased for the output of the current meter as it was discussed above. But, the irradiance responsivity should be increased with optical methods.

The application of short-wave infrared (SWIR) (2.0 μm to 2.5 μm) detectors for infrared irradiance detection is described here. The performance of such detectors with thermo-electric (TE) cooling in measuring a blackbody source is compared with traditionally used cryogenically-cooled and sensitivity optimized InSb mid-wave infrared (mid-IR) radiometers. The preliminary laboratory measurements demonstrated that significantly better irradiance sensitivity could be achieved even with the unselected and not optimized SWIR detectors as compared with liquid nitrogen cooled, peak-performance mid-IR InSb irradiance detectors because the detector shunt-resistance of SWIR detectors increases to much higher values with TE cooling than the maximum achievable shunt resistance of InSb detectors with cryogenic cooling. As a result of the shunt resistance increase, the noise and drift amplification for the output of the photocurrent amplifier decreases. At the same time, because of the tremendously decreased background current of the SWIR detector (as compared to the InSb), the signal-gain (responsivity) of the photocurrent preamplifier can be increased. Decreased output noise and increased irradiance responsivity results in highly decreased NEI which is the radiometric key-parameter for heat-seeking sensors. The SWIR detectors can be wavelength sensitivity modified (or tuned) to operate in a clear, atmospheric window between 2.0 μm and 2.5 μm. Additionally, in contrast to other IR bands, allows the use of inexpensive and easily fabricated ambient-temperature glass or plastic, refractive or diffractive optics to optimize radiometric performance at a decreased cost. The optical path linkage between the image plane of a large collecting input lens and the SWIR detector can be achieved with the use of SWIR-transmissive fibers, allowing the detector to be optimally placed in the system. As an example, it is demonstrated here using a TE-cooled ext-InGaAs photodiode that such irradiance measuring devices can achieve significantly better irradiance sensitivity than cryogenically-cooled InSb radiometers. As an example, these detectors could be used in future forward-looking infrared (FLIR) devices with extremely low NEI without the need for cryogens, providing greatly increased operational hours for heat-seeking sensors, as well as a more compact, low-cost and light-weight design. Optimized detectors with low NEI will also allow a longer range for locking in on targets in heat-seeking missiles and other similar applications.

By the selection of the wavelength region of detection, the noise floor of the radiometer is tuned out from the thermal background-limited range (of traditional infrared radiometers) and the NEI is minimized by: (1) Increasing the irradiance responsivity using both large acceptance area input optics and increased signal-gain (to reach the maximum value of the current-to-voltage converting feedback resistor) by compensating the remaining background current of the detector for the radiometer output, (2) Decreasing the output noise of the radiometer by tuning out from the 1/f noise spectrum using signal modulation (chopping) and also decreasing the closed-loop voltage gain for the input noise and drift of the radiometer using photodiodes with small active area that are selected and maximized for shunt resistance, and also by applying reverse-bias voltage for the photodiode (if necessary) to further increase shunt resistance.

Short-wave infrared (SWIR) sensitive detectors with responsivities from 2.0 μm to 2.5 μm are improved replacements for cryogenic-cooled quantum detectors such as InSb and HgCdTe detectors in heat-sensing applications. Since the SWIR detectors can be cooled with thermo-electric (TE) cooling, the limitations due to cryogen supply will be eliminated. Furthermore, the sensors can be active at all times, allowing, for instance, more rapid targeting and firing of heat-seeking missiles.

The selection and then application of these detectors is followed by the selection of the wavelength region. The relationship of the Planck blackbody radiances and the atmospheric transmission to determine the optimal balance between background discrimination and sensitivity is discussed. The ability to use small, < 1.0 mm diameter photodiodes will result in high shunt resistance and low junction capacitance and signal-gains of 10^8 V/A or lower, necessary for a fast time response. As an example, application of such detectors demonstrates that low-temperature blackbodies with small apertures can be measured using TE-cooled ext-InGaAs detectors. Two candidate detector materials are identified, extended InGaAs and short-wave HgCdTe, and provide further testing information on the ext-InGaAs photodiode.

Due to the rapid improvements in InGaAs material fabrication driven by the optical fiber communications, the InGaAs photodiodes are the preferred detectors in the 900 nm to 1700 nm range. With modification of the fabrication process, InGaAs can be made to be

sensitive to infrared radiation from 900 nm to 2500 nm, with the long-wavelength bandgap occurring at around 2.5 μm. But with the extension of the longer wavelength sensitivity limit, the ext-InGaAs diodes will have lower shunt resistances than the regular InGaAs photodiodes. The low shunt resistances of the ext-InGaAs can be increased by cooling the diode with 1-stage to 4-stage thermo-electric (TE) coolers.

The advantages of using SWIR detectors for heat seeking applications is also realized in short-wave HgCdTe (MCT) photodiodes in operating in photovoltaic mode. The MCT photodiodes can be fabricated to optimize sensitivity from 2.0 μm to 2.5 μm with long-wavelength cutoffs near 2.5 μm, distinct from the usual 10 μm to 12 μm operation of these devices. The shunt resistances of the SWIR MCT detectors can also be increased by TE cooling the detector, and such detectors can be substituted for ext-InGaAs.

Any detectors meeting the technical requirements as described here can be suitable for these applications in heat-sensing systems.

These experimental results indicate that the shunt impedances for the ext-InGaAs detector can be increased by about a factor of 1000, resulting in 1×10^6 Ω to 3×10^6 Ω with the detector cooled to -85 $^\circ$C (188 K). The increase in the shunt impedance to $3 \times 10^6\,\Omega$ with cooling to -85 $^\circ$C have experimentally been measured for 3 mm diameter ext-InGaAs diodes.

As the shunt resistance depends on the resistivity of the photodiode material(s), it can be fabrication batch dependent. Therefore, the shunt resistance can be further increased by individual photodiode selections. The shunt resistance can be measured and the highest values are to be selected. Also, the shunt resistance depends on the photodiode bias. With the application of a few V reverse bias voltage to the photodiode, the shunt resistance will further increase.

The decrease in the output noise with just TE cooling and without the need for cryogens will increase the utility of such detectors, and is critical for the proposed application to replace standard mid-IR InSb systems used in IR collimator applications.

2.4.5. Calibration of IR collimators

Many types of military sensors are used to detect the thermal radiation from objects at long distances. For testing these systems, infrared collimators are used with small sources to simulate the long-range target to the sensor which is at close proximity to the collimator. Up to now, the calibrators of such collimators have utilized the mid-infrared or thermal-infrared wavelength detectors with the use of cryogenically-cooled sensors which require both the maintenance of the vacuum and the cryogens. The detectors which operate in the mid- or long-wavelength infrared are also sensitive to the ambient or the room-temperature background radiation which limits the low-noise performance of these calibrators due to the noise from the background. Furthermore, these calibrators typically utilized reflective optics which can be difficult to align and prone to scatter from the central obscuration as in a cassegrainian collector. Although the advantages of operating the calibrators in short-wave infrared (SWIR) wavelength region have been long recognized studies with experimental systems have been lacking. Below, SWIR (ext-InGaAs-based) and MWIR (InSb-based) calibrations are described and compared.

The use of SWIR detectors and regular-glass optics is also described here to construct a calibrator for infrared collimators. SWIR detectors with thermo-electric cooling can be used instead of cryogenically-cooled IR detectors. Diffraction-limited imaging is obtained using off-the-shelf achromats for rejection of stray radiation and for collection of the thermal radiation. The design of the calibrators is shown and the noise-equivalent irradiances (NEI) are determined using a separately calibrated, off-axis infrared collimator.

2.4.5.1. Use of refractive or diffractive optics

Since the short-wave infrared (SWIR) wavelength region is used with ext-InGaAs detectors, refractive lenses with better optical imaging performance could be utilized. Many optical materials transmit to 2.5 μm. The transmittance of BK7 glass is shown in Fig. 61. Typical achromats using BK7 and a flint glass with center thickness of < 10 mm could be used to collect the SWIR radiation. Such lenses could be easily optimized for diffraction-limited optical performance.
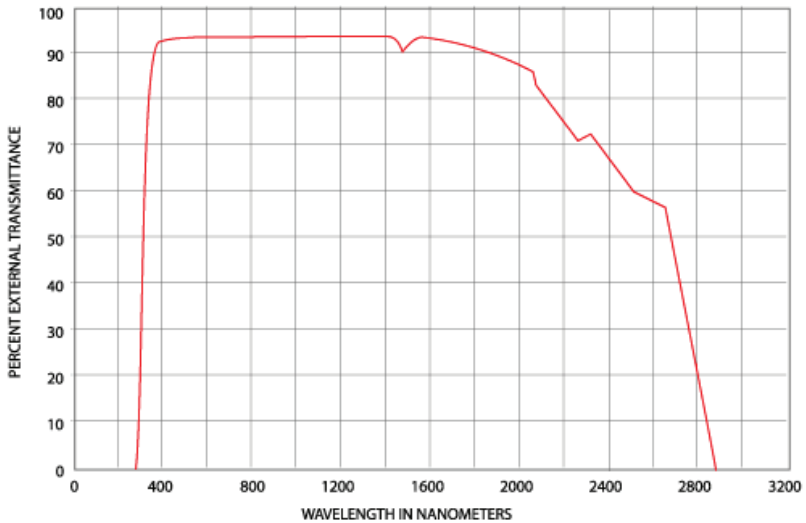
Fig. 61. The transmittance of 10 mm thick BK7 glass. Typical lenses are about 10 mm thick only at the center.

It is also possible to use infrared, plastic lenses in a diffractive, Fresnel-lens geometry. An example of a SWIR transmissive plastic material is shown in Fig. 62. The use of plastic lenses would reduce the mass and cost of the optical-sensor assembly.
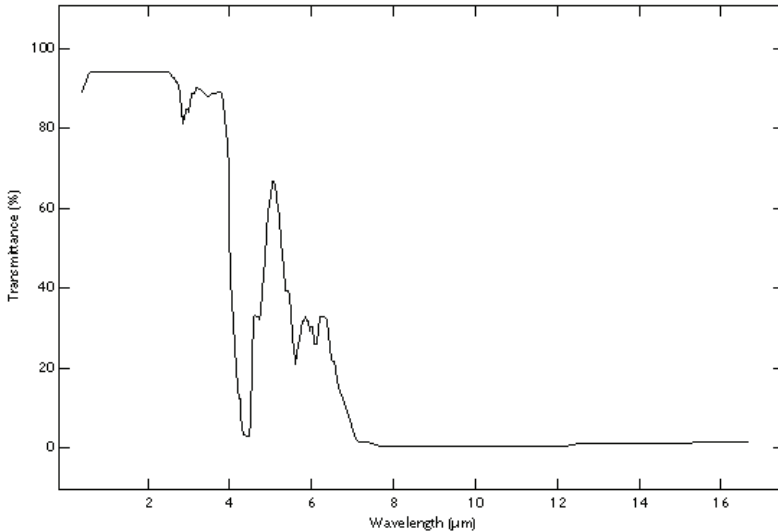
Fig. 62. Transmittance 0.81 mm thickness of PolyIR5 material from Fresnel Technologies [71].

2.4.5.2. Time response and gain increase using EIGA

The time responses of radiometers built with ext-InGaAs are important characteristics for detecting objects in rapidly changing environments. The time response of detectors are given by the feedback resistance and the feedback capacitance of the transimpedance amplifier along with the junction capacitance of the diode. The time constant, τ, is given by

$$\tau = \frac{(C_j + AC)R}{A} \approx CR \quad ,$$

(24)

where A is the open loop gain of the operational amplifier in the transimpedance amplifier, C is the feedback capacitance, R is the feedback resistance and C_j is the junction capacitance. If the loop gain A is ~ 1 x 10^6, then the time constant is just the product of the feedback capacitance and feedback resistance. At a feedback resistance of R = 1x10^7 Ω, with a feedback capacitance of C = 2 pF, the resultant time constant is, τ = 20 μs. This corresponds to a 3 dB upper roll-off frequency, f, for the responsivity of the detector current

meter of

$$f = \frac{1}{2\pi RC} = 8\,kHz$$

.   (25)

The stray capacitance can be lowered from 2 pF to 0.2 pF if the printed circuit board of the current-to-voltage converter is optimum designed for stray capacitances between the output and the inverting input of the operational amplifier (parallel to the feedback resistor). In this case, the feedback resistance can be increased to $10^8\ \Omega$ and the upper roll-off frequency still remains 8 kHz.

The radiometer background current can be electronically compensated by subtracting a current from the background current which is equal to the background current and has an opposite polarity. The subtraction can be done at the input of the current-to-voltage converting operational amplifier. The compensation can be done manually or automatically. Manual compensation can work for constant or slowly changing background signals. In case of large and fast background current changes (such as in airplane and missile applications), the compensation can be done with an analog control loop that monitors the DC output signal of the radiometer, compares it to a zero reference voltage, and then adjusts the compensating current such that it controls the DC output signal component of the radiometer very close to zero. The useful AC (chopped or modulated) signal component (which is superimposed on the DC output signal) can be measured by a lock-in amplifier synchronized by the chopper.

After the DC output voltage of the radiometer is compensated to zero, the maximum value of the feedback resistor in the current meter can be $10^9\ \Omega$. This huge gain increase can be applied only to the compensated photocurrent meters of SWIR detectors because of their low background current. SWIR radiometers can use this high signal-gain also in DC (useful) signal measurement mode if manual background current compensation can be made (the background current is steady or slowly changing). Using the 10^9 V/A gain, the upper roll-off frequency decreases to about 1 kHz (the parallel stray capacitance can be decreased to about 0.1 pF with a careful printed-circuit-board design). The $10^9\ \Omega$ feedback resistor is three orders of magnitude higher than the maximum feedback resistor of background optimized InSb detector amplifiers (when cryogenically

cooled f/4 field-of-view limiter and cold band-pass filters are used). The reason for this large (3 decades) gain (and voltage per watt responsivity) increase is the large difference in the background signals between the InSb (responds to 5.5 µm) and the ext-InGaAs (responds to 2.6 µm only) detectors. This gain increase will produce a factor of 1000 responsivity increase for the ext-InGaAs radiometer (relative to a background optimized InSb radiometer) that will result in 3 decade decrease in the NEP or a 3 decade increase in the D*. Together with the roughly 2 orders of magnitude optical signal-gain (irradiance responsivity) increase of the ext-InGaAs input optics, a total of about five orders of magnitude responsivity increase can be achieved (relative to a background optimized InSb irradiance meter) with the optimized TE-cooled ext-InGaAs irradiance meter. When the ext-InGaAs photodiode is cryogenically cooled to 77 K, the feedback resistor can be increased to 10^{10} Ω (as a result of the further decreased voltage amplification for the input noise and drift caused by the further increased shunt resistance). In this case, the 3 dB upper roll-off frequency is 160 Hz if the parallel stray capacitance (to the 10^{10} Ω feedback resistor) is 0.1 pF, making the responsivity of the ext-InGaAs irradiance meter comparable to a silicon photodiode radiometer (with fW level NEP) but operating in the 2 to 2.5 µm infrared range. As an example, the above mentioned background optimized InSb radiometer has an NEP of 1 pW/Hz$^{1/2}$ with a 3.5 mm diameter input aperture [72]. The optical gain of the ext-InGaAs irradiance meter can be a factor of 200 higher than that of the referenced InSb irradiance meter. Also, the peak responsivity of an ext-InGaAs photodiode is 2 to 3 times higher than the peak responsivity of a silicon photodiode.

2.4.5.3. Irradiance detection limits using EIGA

As examples of the ext-InGaAs sensitivity for near-room-temperature objects, measurements of objects were taken with a 3 mm diameter, 4-stage cooled ext-InGaAs detector at –85 °C. The detector was mounted in a heat sink without restricting the 60° field-of-view. Due to the sensitivity of the detector to 2.5 µm, the signals with the object at room temperature can be affected by the changes in the SWIR emissivity. When the ext-InGaAs diode was placed on top of a liquid-nitrogen dewar, the photocurrent reduced to about 2.6 nA. The photocurrent under a room temperature environment is about 13.7 nA, as measured using the black-polymer-covered Al plate. The

warm temperature of the human hand immediately results in an increase in the signal to 22.6 nA. The immediate increase in the signals with the introduction of the human hand with low standard deviations indicates the sensitivity of the detector. The calculation of the noise-equivalent irradiance can be obtained from using the standard deviations of the signal converted to noise-equivalent current of

$$250 \text{ fA} = 2.5 \times 10^{-6} \text{ V} / 10^{7} \text{ V/A} . \qquad (26)$$

The noise-equivalent power can be obtained from the power responsivity of the ext-InGaAs of roughly 1 A/W, such that the NEP is 250 fW. Since the effective area is increased by the 50 mm diameter lens, the noise-equivalent irradiance is

$$NEI = 0.13 \text{ fW/mm}^2 = 250 \text{ fW} / 3.14 * (25\text{mm})^2, \qquad (27)$$

which is comparable to the irradiance responsivity of Si photodiode irradiance meters.

2.4.5.4. Using InSb

In many applications, the radiometric performances of imaging and non-imaging sensors which are used to detect targets at long distances need to be calibrated. For these calibrations, the knowledge of the angular divergences, in addition to the spectral intensity of the sources used for the calibrations is important. Collimators are used to generate a scene or a point source with low angular divergence for producing a controlled, virtual source at infinity. These collimators are, in turn, used for calibration of telescopes or imaging radiometers designed for measurement of targets at far distances. For instance, collimators are used to test telescopes for imaging quality and to test radiometric quantities such as spectral irradiance response of sensors. This type of testing is especially critical for military applications where the sensor is detecting and locating a small target at far distances.

The collimators are constructed from a variable-temperature blackbody equipped with a precision aperture, collimating mirror and folding mirrors. These collimators have different sizes and can be transported to the sensor under test. Until now, the spectral irradiance from these infrared collimators has been determined only by using the knowledge of the individual component parameters such

as the blackbody temperature and emissivity, the area of the aperture, the focal length and the reflectance of the collimating mirror and folding mirrors, and any optical aberrations of the setup. Since the irradiance at the output of the collimator is calculated from the individual components, the total uncertainty of the irradiance depends on the measurement uncertainties of the individual components and any changes or errors in the individual component values or their alignments could lead to unknown changes in the final irradiances.

An alternative, detector-based, system-level calibration is discussed here that does not rely upon knowledge of the individual component parameters except the blackbody temperatures and emissivities. This approach requires the use of calibrated, spectrally- filtered, infrared radiometers and can lead to lower uncertainties than the piece-parts approach. Two of the non-imaging InSb selective radiometers (similar to those mentioned in Section 2.4.2.3.1) were used here for SI traceable calibration of IR collimators. The bandpass of the two radiometers was centered at 3.4 μm and at 4.6 μm using filters with 400 nm and 260 nm band-pass, respectively. The radiometers have cold, field-of-view limiters to reduce the background signal, and the broad-band filters were also held at cryogenic temperatures to further reduce the contribution from the ambient background. The radiometers were calibrated in irradiance mode at the NIST Infrared Spectral Irradiance and Radiance Responsivity Calibrations using Uniform Sources (IR-SIRCUS) facility. The calibrated radiometers were then used to determine the irradiance at the output of an infrared collimator, and the measured irradiances were compared to the calculated irradiances of the collimator. The implementation of the SI traceable calibrations of the collimators resulted in total uncertainties of < 3 % (k = 2) in the infrared spectral irradiances.

The scheme of the collimator, used in the experimental setup, is shown in Fig. 63.
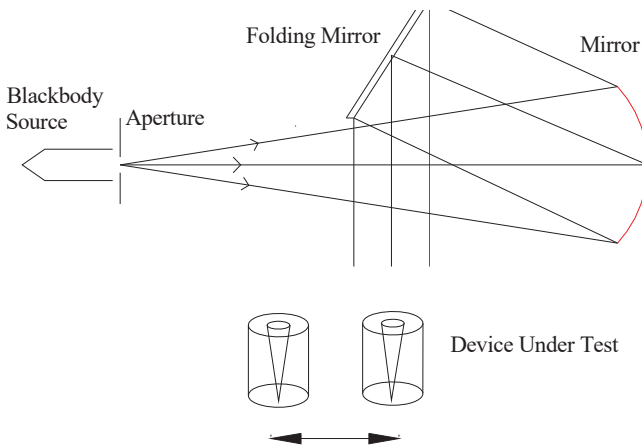
Fig. 63. A basic configuration of a collimator for testing infrared sensors. The blackbody source is defined by a precision aperture and the source is collimated by a spherical or a paraboloid mirror and the radiation is folded into the device under test.

The blackbody serves as a spatially and angularly uniform source which is equipped with a precision aperture placed directly in front of the blackbody source. The area of the aperture is imaged by a spherical or paraboloid mirror and the exting optical radiation is collimated. To reduce the physical dimensions of the collimator, one or more folding mirrors can be used. If the imaging performances of focal plane arrays or lenses are tested, then the circular aperture in front of the blackbody could be replaced with a set of bar-pattern target for assessing the image quality.

For radiometric calibrations of devices, the spectral irradiance at the output of the collimator must be determined. Assuming a point-source geometry since the area of the aperture is much smaller than the area of the collimating mirror, the optical power incident on the collimating mirror is given by

$$\phi_{mirror} = \varepsilon \cdot L(\lambda, T) \cdot A_S \cdot \omega \tag{28}$$

where ε is the spectral emissivity of the blackbody, $L(\lambda, T)$ is the radiance from the blackbody and A_s is the area of the precision aperture and ω is the solid angle of the collimating mirror. The solid

angle is

$$\omega = \frac{A_{mirror}}{(d)^2},$$

(29)

where d is the focal length of the collimating mirror. The irradiance at the collimating mirror is the incident optical power divided by the total area of the collimating mirror,

$$E_{mirror} = \frac{\phi_{mirror}}{A_{mirror}} = \varepsilon \cdot L \cdot \frac{A_S}{(d)^2}.$$

(30)

The irradiance at the output of the collimator is the irradiance at the collimating mirror convolved with the reflectances, ρ, of any folding mirrors,

$$E = \rho \cdot E_{mirror}.$$

(31)

This calculated irradiance from the individual parameters does not account for increased uncertainties from effects such as diffraction, imperfect imaging of the collimating mirror, spatial uniformity of the mirrors and the edge quality of the precision aperture. Since many of these individual component characteristics could also change during the time of operations, it is difficult to reduce the final uncertainties of the spectral irradiances from these collimators. Due to the recognition that the uncertainties in the irradiances could not be reduced using the piece-parts approach, filter radiometers for direct substitutional calibrations have been developed and used. The design of the InSb radiometers is discussed in Section 5.3.2 of Volume 3 and also in Section 2.3.3.3 above. A single element InSb detector was used in a cryogenic dewar. The spectral filter was held at cryogenic temperatures and a field-of-view restricting cold shield was used to reduce the background signal. A precision aperture was placed in front of the detector to act as a limiting aperture. The extension of the cold shield limited the field-of-view to < 17 °. Since the radiometer was designed for measurement of collimated sources, the limited field of view did not affect its operation. In order to reduce the 10^{-3} out-of-band scatter from the cold interference filters, an additional cold filter was added to further reduce the out-

of-band scatter to 10^{-6}.

The detector-based irradiance responsivity calibration of the InSb radiometers was performed at the NIST Spectral Irradiance and Radiance Responsivity Calibrations using Uniform Sources (SIRCUS) facility [34]. The scheme of the IR-SIRCUS setup is shown in Fig. 64 [65]. The periodically-poled lithium-niobate (PPLN) optical parametric oscillator (OPO) laser is used to generate a tunable monochromatic source. The laser is intensity stabilized using optical feedback, and the wavelength of the source is measured using the interferometric wavemeter. Any speckle measured by the device-under-test (DUT) is reduced by using the rotating mirror to change the incident beam-position on the wall of the diffuse-gold coated integrating sphere at a rate faster than the integration time of the DUT. Since the detectors are sensitive to the background thermal radiation, the incident laser radiation is modulated by the chopper for lock-in detection. The radiation inside of the integrating sphere is monitored to remove drift in the laser sources.

The integrating sphere is fitted with a precision 50.8 mm diameter aperture which is separately measured by non-contact techniques. Two intermediate baffles of 101.6 mm diameter are located within the 1.4 m separation between the sphere-opening and the radiometers to reduce the scattered (stray) radiation. Since the radiometers collect radiation from a 17° field-of-view, any source of radiation within this field-of-view will affect the measured signal. The irradiance responsivity calibration of the InSb DUT is performed by direct substitution to the reference InSb radiometer of the same construction without the spectral interference filters. Using the direct substitution-type calibrations in the same irradiance plane, the measurements minimize issues such as the spatial and angular non-uniformity of the sphere and also possible diffraction effects. The substitution between the standard radiometer and the DUT is repeated for each setting of the laser wavelength until the entire spectral irradiance responsivity is determined. The different types of lasers utilized in the IR SIRCUS for coverage of the infrared wavelength region are shown in Fig. 65. Since these measurements were performed in the wavelength region from 2.5 μm to 5.0 μm mostly the PPLN OPO laser was used.
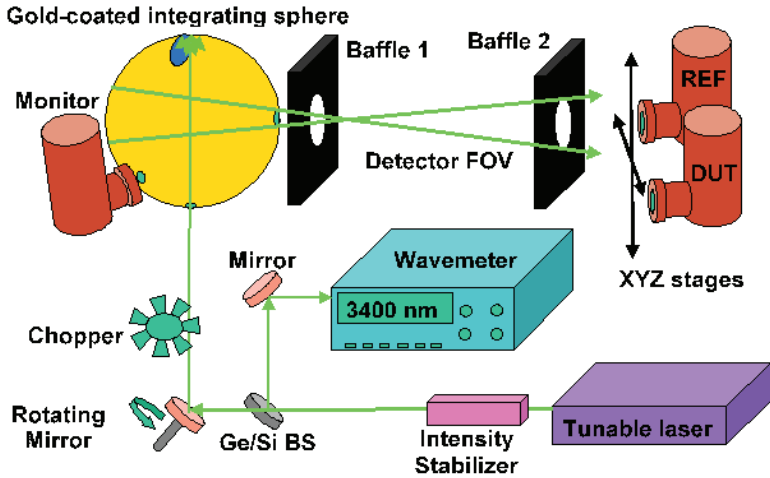
Fig. 64. **C**alibration scheme at the NIST Infrared Spectral Irradiance and Radiance Responsivity Calibrations using Uniform Sources Facility (IR-SIRCUS).
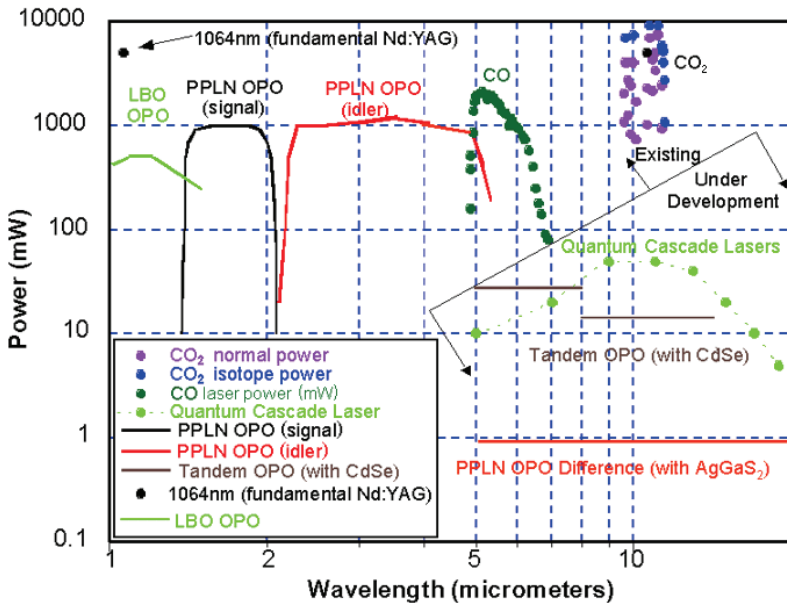
Fig. 65. The wavelengths and optical powers of the tunable laser sources used at the NIST IR-SIRCUS [89].

The measured irradiance responsivities of the selective InSb #5 and InSb #6 radiometers [65] are shown in Fig. 66. The center wavelengths and spectral bandwidth of the radiometers were chosen to avoid atmospheric absorptions. The large dynamic range of the irradiance responsivities are due to the use of the double interference filters and the use of the high-power laser sources at the IR SIRCUS.
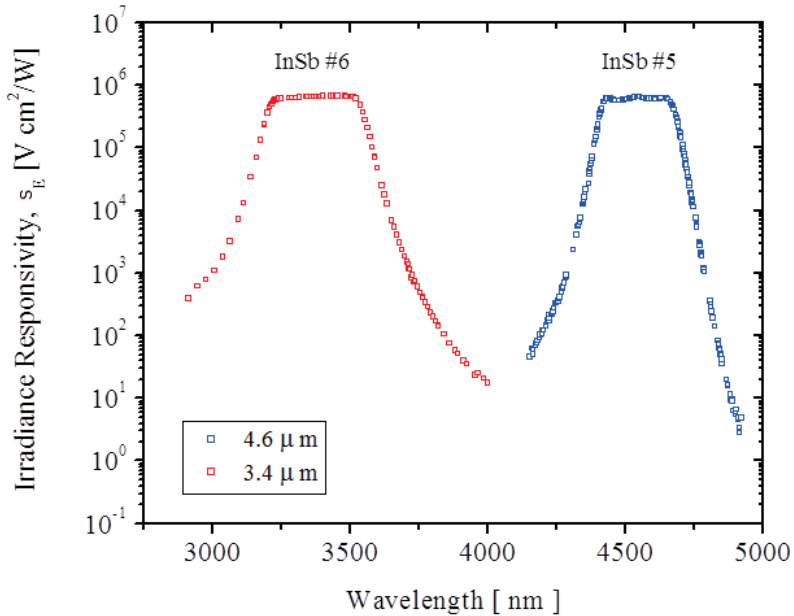
Fig. 66. Irradiances responsivities of the selective InSb #6 and InSb #5 infrared radiometers [89].

The uncertainties of the irradiance responsivity calibration for any wavelength are shown in Table 7. The shown uncertainties are equally applicable to both radiometers. The largest uncertainty component is related to the transfer standard. The transfer standard is the broad-band, unfiltered InSb radiometer which was calibrated using the cryogenic bolometer discussed in Section 4 of Volume 1. This component includes the initial uncertainties of the responsivity calibration and the added uncertainties due to the possible long-term change related to the initial calibrations. The InSb standard was calibrated in under-filled mode for spectral power responsivity. The spectral irradiance responsivity was determined using the known

area of the precision aperture placed in front of the detector and also by determining the spatial uniformity of responsivity. The spatial uniformity of the sphere output is especially critical in the infrared since the diffuse-gold coating is much less (both spatially and angularly) uniform than the PTFE coatings used in the visible and the near-infrared wavelength regions. The uncertainty components 3 and 4 are related to the physical alignment of detector and source and also reproducibility of the alignment. The low uncertainties of the repeatability and the distance are attributed to the radiometers being placed on computer-controlled motorized stages. The laser intensity and spectral fluctuations are determined from the characteristics of the laser-intensity stabilizer and the temperature-stabilized OPO crystal. The total expanded uncertainty of the calibrations are estimated to be < 3 % (k=2). The long-term repeatability of the InSb #5 radiometer compared to the InSb standard can be seen in Fig. 67. The differences in the averaged irradiance responsivities are well within the 3 % (k=2) uncertainties.

Table 7. Total expanded uncertainties of the irradiance responsivities of the InSb filter-radiometers when calibrated at the IR SIRCUS [65].

	Uncertainty component	(%)
1	Transfer Standard	1.30
2	Sphere Spatial uniformity	0.40
3	Alignment of detector	0.01
4	Ratio of distance square	0.20
5	Laser intensity stability	0.40
6	Laser spectral fluctuation	0.02
7	Repeatability	0.30
8	Combined (k = 1)	1.46
9	Expanded Uncertainty (k = 2)	2.93
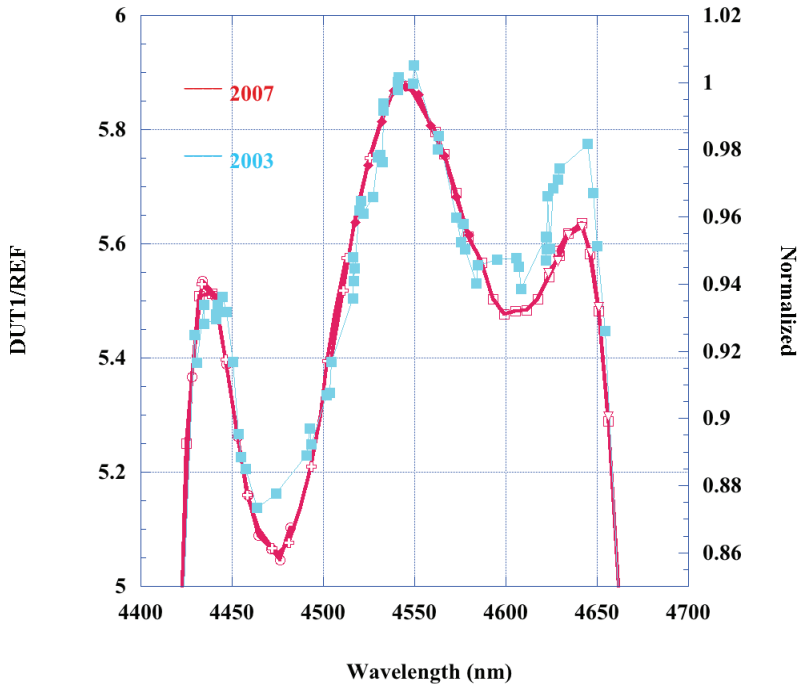
Fig. 67. The signal ratios of the InSb #5 to the InSb standard radiometer as measured in 2003 and in 2007. The differences in the irradiance responsivities are well within the 3 % (*k*=2) total uncertainties of each measurement [65, 89].

2.4.5.4.1. Utilization of irradiance responsivity

Due to the broadband irradiance responsivity of the filter radiometers, measurement of irradiances from a blackbody sourcerequire knowledge of the blackbody temperatures and its emissivity [89]. From the measured spectral irradiance responsivity, s_E, and the spectral irradiance of the source, E_λ , the integrated irradiance response (signal) v_{calc} can be calculated:

$$v_{calc} = \int s_E \cdot E_\lambda d\lambda \,.$$

(32)

If the throughput and the solid angle of the source are known then the measured signal is

$$v_m = \int s_E \cdot E_\lambda = \tau \cdot \Omega \int s_E \cdot L_\lambda(T) d\lambda$$

(33)

where v_m is the measured voltage and Ω is the solid angle relating the radiance to irradiance and τ is the transmittance of the source setup. The transmittance factor accounts for diffraction losses, mirror reflectance losses and imperfect imaging of the collimating mirror. The integral in Eq. 33 is the band-averaged radiance which is needed since the broad-band filter-radiometers measure broad-band radiances from blackbody sources. The band-averaged radiances can be calculated for a range of blackbody temperatures as shown in Fig. 68. The band-averaged radiances found using the InSb #5 filter radiometer are greater than those found using the InSb #6 radiometer since the peak of the Planck radiance shifts to longer wavelengths at lower temperatures.

If the emissivity and the temperature of the blackbody, used as collimator source, is known, then the measured voltage, v_m, can be used in conjunction with the band-integrated radiance in Eq. 33 to determine the solid angle and the transmittance of the collimator. The knowledge of the transmittance, τ, and the solid angle, Ω, would specify the spectral irradiance averaged over the InSb #5 and InSb #6 wavelengths.
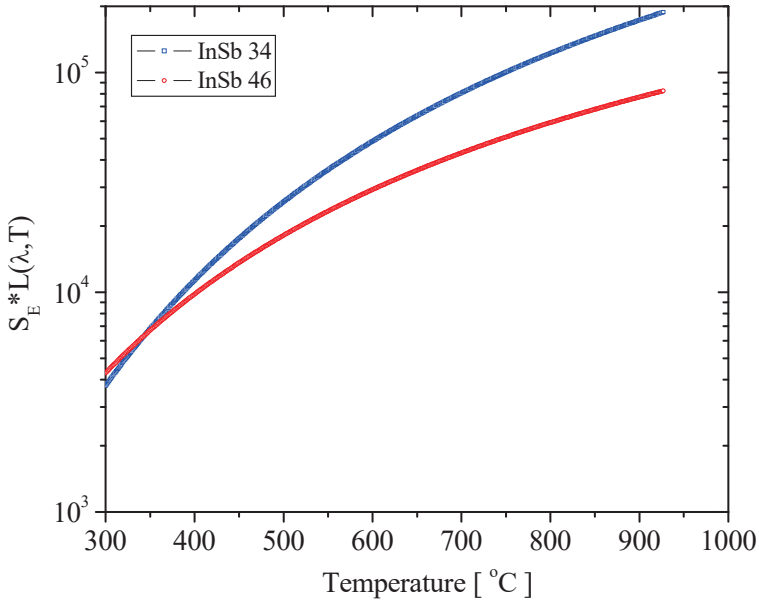
Fig. 68. The band-integrated radiances using the 2003 calibrations as a
function of the blackbody temperature for the InSb #5 (4.6 μm center) and
InSb #6 (3.4 μm center) filter-radiometers [89].

2.4.5.4.2. Interpolation functions for band-weighted radiances

Since integral must be determined for all the blackbody
temperatures, the calculated temperatures can be fitted with a
modified Planck function [89]:

$$i = \frac{A}{\exp\left(\dfrac{c_2}{B*T+C}\right)-1},$$
(34)

where T is the temperature in kelvin, c_2 is the second radiation
constant, and A, B, and C are the fitting parameters. The nonlinear
minimization to determine the fitting parameters can be performed
using Excel fitting program. The fitted function and the parameters
are shown for InSb #6 in Fig. 69 [89]. The modified Planck function
with the three fitting parameters is used for interpolations.The fitting

parameters can be saved to quickly determine the integral for any blackbody temperatures.
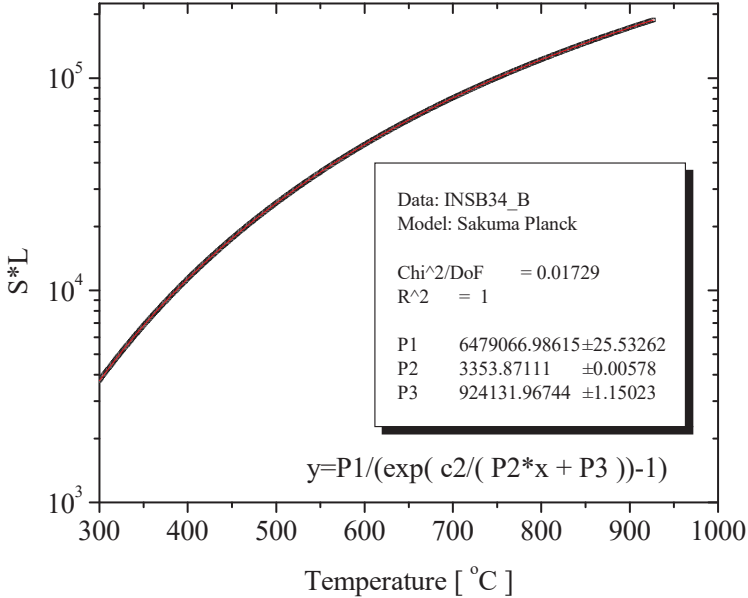
Fig. 69. Calculated and fitted S*L for InSb #6 with 3.4 μm center.

2.4.5.4.3. Source-based validations of the detector-based irradiance responsivity

Although the uncertainties in the detector-based irradiance responsivity calibrations can be assessed independently of other experimental setups, a source-based validation can provide further confidence in the total uncertainties [89]. The source-based validations utilized a setup shown in Fig. 70.
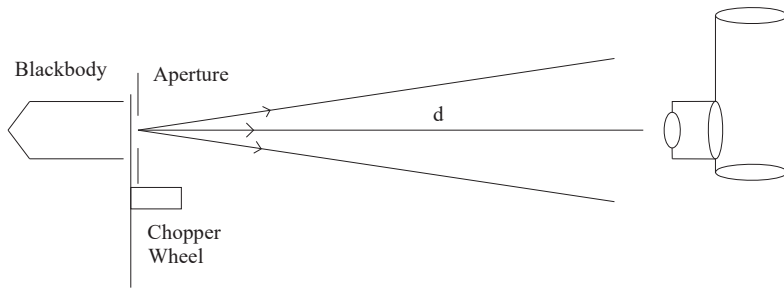
Fig. 70. Scheme of the setup used for the source-based validation
of the detector-based irradiance responsivity calibrations.
A variable-temperature blackbody fitted with a precision aperture
was set at a known distance from the InSb filter radiometers.

For a point-source geometry as shown in Fig. 70, with the source of
area, A, the solid angle is related to the distance from the source to
the entrance aperture plane of the filter radiometer, d, by

$$\Omega = \frac{A}{d^2}.$$

$$(35)$$

The solid angle term can be modified by additional factors such as
the reflectance of mirrors if they are in the optical path from the
radiance source to the irradiance measurement plane. No additional
mirrors were used for these experiments. The InSb #5 and InSb #6
filter radiometers were used to measure the irradiances of a
blackbody with a precision aperture with area, A, set at a distance, d,
from the blackbody aperture to the reference plane of the filter
radiometer. The parameters and the measurement results used in
the source-based validation are listed in Table 8 and Table 9. The
calculated signal is the product of the solid angle and the band-
weighted radiance, $S*L$.

Table 8. The measurement parameters for the InSb #6 filter-radiometer [89].

InSb #6 (3.4 μm)	
Blackbody (BB) T (° C)	840
BB Aperture diameter, (mm)	0.9939
BB Aperture area , A (cm^2)	0.00775836
BB to InSb distance, d (cm)	57.19
Solid angle (sr)	2.37208E-06
$S*L$ (V/sr)	141933.6
Calculated signal, V_c (V)	0.33668
Measured signal (V)	0.15085
Lockin DC to AC conversion factor	2.221
Measured * Lockin factor, V_m (V)	0.33504
Percent difference 100*(V_m-V_c)/V_c	**-0.49**

Table 9. The measurement parameters for the InSb #5 filter-radiometer [89].

InSb #5 (4.6 μm)	
Blackbody (BB) T (° C)	840
BB Aperture diameter (mm)	0.9939
BB Aperture area, A (cm^2)	0.00775836
BB to InSb distance, d (cm)	57.19
Solid angle (sr)	2.37208E-06
$S*L$ (V/sr)	66305.5
Calculated signal, V_c (V)	0.15728
Measured signal (V)	0.07144
Lockin DC to AC conversion factor	2.221
Measured * Lockin factor, V_m (V)	0.15867
Percent difference 100*(V_m-V_c)/V_c	**0.87**

For these validations, a variable-temperature blackbody was set at 840 °C as measured with a thermocouple embedded into the blackbody. The emissivity of the blackbody was assumed to be unity. A 1 mm diameter aperture was placed in-front of the blackbody and the distance was measured using a calibrated micrometer. A chopper wheel was placed between the aperture and the blackbody for the lock-in detection. The band-integrated radiances were determined for the blackbody temperatures, and the calculated signals were determined using Eq. 33 with the transmittance set to unity. Since the irradiance responsivity calibrations are performed with a standard radiometer which was calibrated in direct-current (DC) mode, the alternating-current (AC) modulated signals need to be multiplied with a conversion factor. The conversion factor will depend on the exact operation of the lock-in amplifier. The percent differences between the measured and the calculated signals are shown to be < 1 % for both radiometers. The agreement is well within the absolute uncertainties which are at least > 3 % (k=2) as indicated in the uncertainties of the responsivity calibrations in Table 7.

2.4.5.4.4. Field comparison of the detector-based and source-based calibrations

After the detector-based calibrations and the source-based validations, the InSb #5 and InSb #6 filter radiometers were transported to a laboratory with a collimator consisting of a variable-temperature blackbody with a measured emissivity and fitted with a set of precision apertures set at a distance of 2.5 m from a gold-coated off-axis parabolic mirror. The InSb radiometers were set at a distance of 2.5 m from the mirror to result in a total separation of 5 m from the blackbody sources. Since the atmospheric transmittance in the infrared could be affecting the measured signal, the attenuation due to the atmosphere was modeled using MODerate resolution atmospheric TRANsmission (MODTRAN) model with the results shown in Fig. 71 [89].
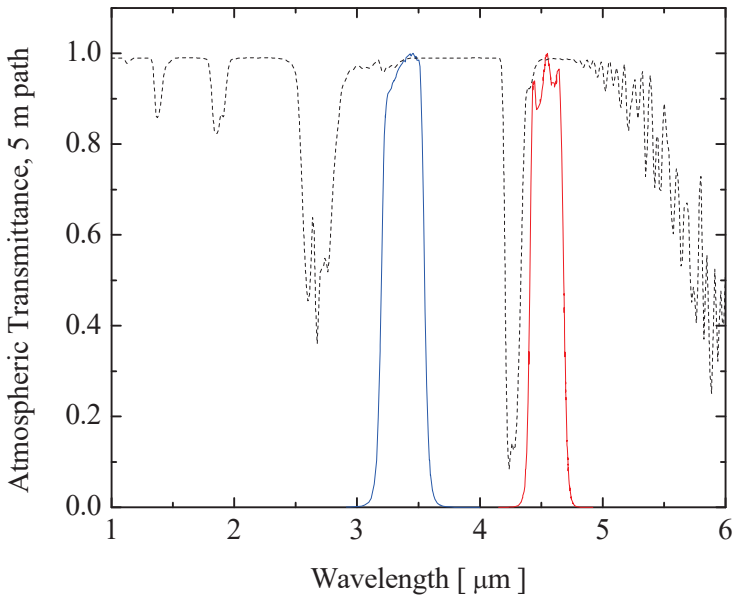
Fig. 71. The irradiance responsivities of the InSb #5 and InSb #6 filter radiometers plotted along with the 5 m path air transmittance at sea level convolved with the gold-coated mirror reflectance.

For these measurements, the temperature of the variable-temperature blackbody was set at 450 °C, 800 °C and 1000 °C and 5 different sized apertures were placed in front of the blackbody. The calculated signals were determined from the convolved responsivities of the InSb filter radiometers with the atmospheric transmittances and the spectral reflectance of the gold coating. The diameters of the apertures in this setup were determined using a microscope calibrated using metal-deposited on glass, dimensional standards. Due to the small aperture diameters and the operations in the infrared wavelength region, diffraction corrections were also applied. The total expanded uncertainties of the spectral irradiances is 6 % with the combined uncertainties of the measurements at 6.7 % ($k=2$). The results of the comparisons are shown in Figs. 66 and 67 for the InSb #6 and InSb #5 respectively. The overlap between the runs at different temperatures as a function of the aperture diameter indicates that the temperatures are determined with low uncertainties. The systematic dependence of the ratios with the aperture diameters

for both filter radiometers indicates that the aperture measurements could be the cause of the characteristic shape seen in Figs. 72 and 73 [89].
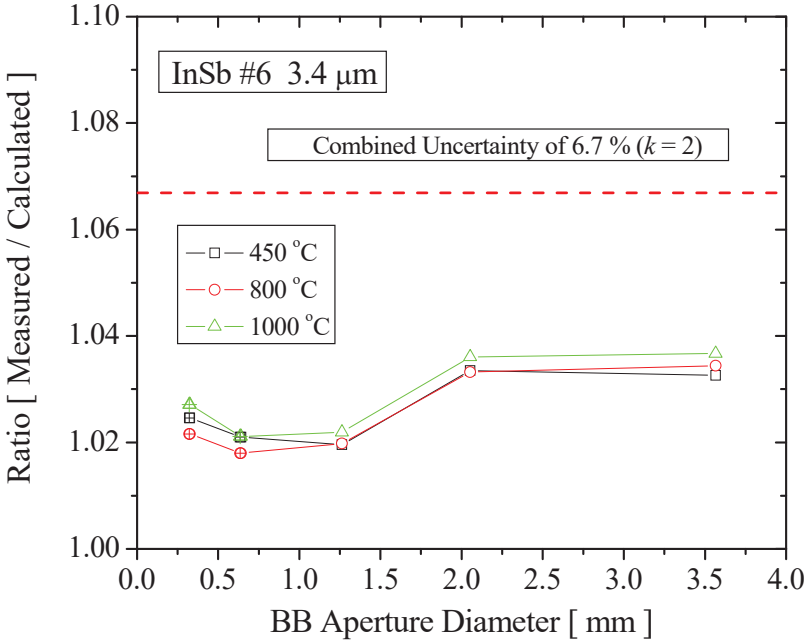
Fig. 72. The ratios between the measured and the calculated signals from the 2.5 m focal length collimator using the InSb #6. The measurements are within the expanded combined uncertainties of 6.7 % which include the dominant uncertainty components from the piece-parts irradiance calculations of the collimator.
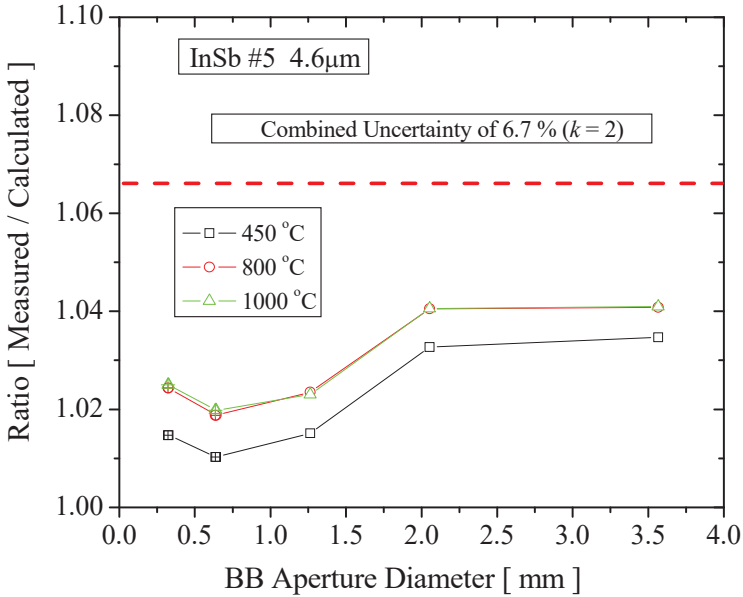
Fig. 73. The ratios between the measured and the calculated signals from the 2.5 m focal length collimator using the InSb #5. The measurements are within the expanded combined uncertainties of 6.7 % which include the dominant uncertainty components from the piece-parts irradiance calculations of the collimator.

In summary, the above non-imaging InSb filter radiometers were calibrated for irradiance responsivity using spectrally tuned laser radiation at the NIST IR-SIRCUS facility. These radiometers can be used to determine the irradiances from infrared collimator and can also be used to determine the radiometric characteristics of infrared collimators to result in lower uncertainties in the spectral irradiance than had been possible with piece-parts calibration approach. For instance, instead of relying on external aperture measurements, it would be possible to use the filter radiometers to assign aperture areas based upon the measured signals either directly or as ratios from the largest apertures where the uncertainties in the aperture diameters are lowest and thus eliminating the need to measure the area of the smallest apertures.

These filter radiometers can be used for a variety of different tasks. The InSb filter radiometers can be used to perform comparison of collimator scales at different facilities when such comparisons would be difficult to perform due to the use of large, multiple mirrors in the configuration which cannot be transported. The radiometers have also been used to determine the beam divergence of the collimated radiation. A well collimated beam should not have any distance dependence and any such dependence is due either to the optical aberrations or the poor optical design, fabrication or setup of the collimator system. Similarly, the collimated output should be spatially uniform within the collimated beam diameter. The InSb filter radiometers have been used to perform x- and y-scans to measure spatial non-uniformity problems.

2.4.5.5. Detection comparison of EIGA- and InSb-radiometers

An important application of infrared detectors is their use in calibrations of collimators. Infrared collimators are often used as in-lab sources for optical testing, but portable versions can be used for in-field testing of FLIR and seeker systems. The basic setup for an infrared collimator without the folding mirror was shown above in Fig. 70. In this setup the blackbody was used in point source measurement geometry for simplicity [90]. The SWIR radiometer and the InSb detector were substituted for each other at a distance of 62.5 cm between the source aperture and the detector plane.The chopper was needed for the InSb detector. The SWIR radiometer had an internal chopper wheel. The aperture diameters were ranging as shown in Fig. 74. They were changed with the blackbody temperature varied to determine the noise equivalent irradiance and the radiometer performance.

As discussed above, background-signal optimized InSb band-pass radiometers have been constructed with center wavelengths at 3.4 μm and at 4.6 μm. The AC-mode InSb radiometer centered at 3.4 μm and operated at gain 10^7 V/A measured the signals from blackbodies with the apertures and temperatures as shown in the legend of Fig. 74. The linear behavior with aperture area indicates that only the radiation from the aperture was detected.

The measurements of point-source geometry targets using these radiometers can be compared with similar measurements using extended-InGaAs radiometers for comparisons of detector performance.

A variable-temperature blackbody ranging in temperatures from over 300 °C to 850 °C is placed behind the apertures.
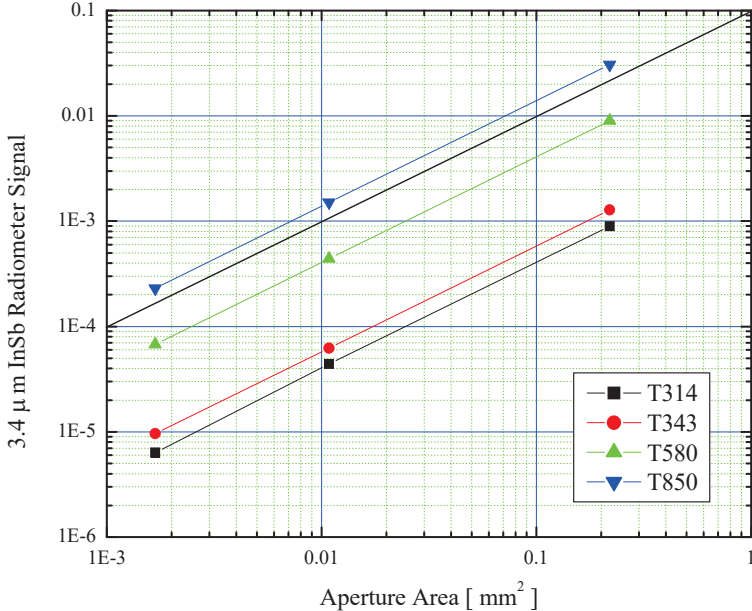
Fig. 74. Signals of an AC-mode InSb radiometer (at gain 10^7 V/A and centered at 3.4 μm) from the blackbodies with the respective apertures and temperatures as in the legend. The linear behavior with aperture area indicates that only the radiation from the apertures is detected.

A tuning-fork chopper was used to modulate the signal which was detected using phase-sensitive (lock-in) detection. The linear signal dependence on the aperture area indicates that chopping between the blackbody and the aperture eliminates detection of radiation outside of the aperture area.

A similar setup but without the chopper using a blackbody in point-source geometry with apertures were used to determine the sensitivity of the extended-InGaAs radiometer, and the results are shown in Fig. 75. In order to increase the collection efficiency (irradiance responsivity), a 50 mm diameter, achromatic objective lens was used to collect the radiation at a distance of about 60 cm from the apertures. The collected radiation was focused into a 3 mm

diameter extended-InGaAs photodiode which was TE-cooled to a temperature of -85 °C. The measurements were performed in DC mode. The dark signal was determined by blocking the radiation with an anodized aluminum plate of room temperature. The photocurrent from the extended-InGaAs photodiode was converted to voltages using a transimpedance amplifier at a gain setting of 10^7 V/A. The linear behavior with aperture areas indicates that DC measurements of collimators should be possible with low uncertainties.
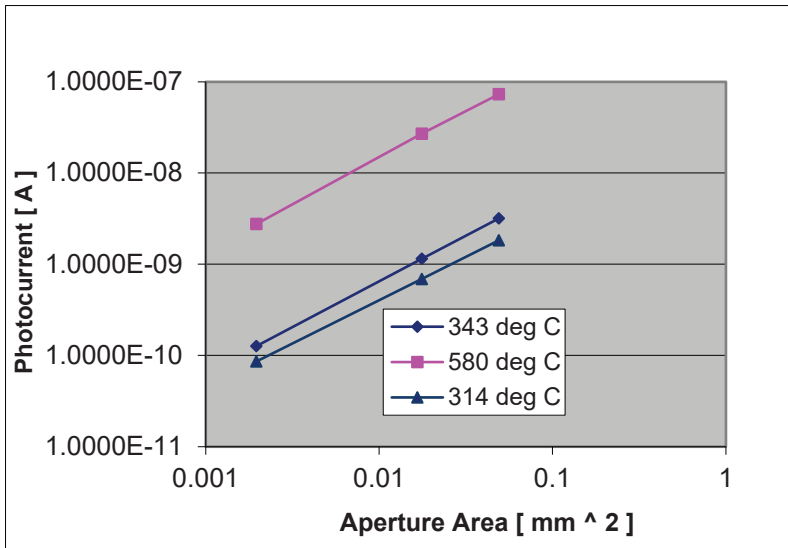
Fig. 75. The signals from the same setup as in Fig. 74 but with the DC-mode extended-InGaAs radiometer at gain 10^7 V/A. The linear behavior with aperture area indicates that the signal from the aperture is effectively discriminated by the extended-InGaAs radiometer.

Using this extended-InGaAs radiometer in AC mode, the NEP can be further decreased, resulting in further improved signal-to-noise ratios. As an example, a noise-equivalent-irradiance (NEI) < 5 fW/cm^2 was obtained using this optimized extended-IGA radiometer. The radiometer was successfully used to measure thermal radiation using regular glass optics and short-wave IR detectors [73].

The above work demonstrated that SWIR detectors sensitive from 2.0 μm to 2.5 μm can be used as a new generation of sensors for FLIR devices and heat-seeking sensors. It was demonstrated that

although the cut-on at 2.0 μm can be accomplished with a filter, the cut-off at around 2.5 μm must be intrinsic to the material from the fabrication process to avoid large background currents. These detectors can be used in a spectral wavelength region where the atmosphere has a clear window from 2.0 μm to 2.5 μm, leading to the possibility of using refractive-glass or diffractive-plastic optics without central obscurations. In this SWIR window, objects at long distances can be measured without substantial attenuation of the signal. According to Planck's law, the radiance contrast between the object and the ambient (like sky-background temperature) is greatly enhanced at this short-wavelength window. This enhancement of the radiance contrast can result in radiometer constructions that have low sensitivity to ambient temperature changes. The optical path between the detector and the objective lens assembly can also be linked using fiber-optic coupling.

In the described process a 4-stage TE-cooled extended-InGaAs photodiode was used. The Planck radiation for blackbody temperatures of interest leads to operations of the extended-InGaAs photodiode at gains of 10^8 V/A or smaller leading to time constants of detection shorter than 20 μs. Comparison measurements on the same point-source geometry using AC-mode InSb radiometer showed that better performance can be obtained using 1/f noise dominated DC mode extended-InGaAs radiometers. The performance can be further improved using AC-mode (Johnson noise dominated) extended-InGaAs irradiance meters. Most importantly, these performance metrics can be achieved with thermo-electric cooling to -85 °C without the need for cryogenic cooling as for the InSb detector. Furthermore, equivalent or better infrared detection capability than the InSb detector can be achieved in a compact, low-maintenance design which would open up the use of heat seeking sensors to low payload platforms and a fundamental change in the deployment of such devices.

It should be noted that use of detectors which operate in the SWIR are not always desired if the FLIR must discriminate the target from reflected or direct solar radiation since the spectral irradiance of the sun is quite substantial at these wavelengths.The utilization of these SWIR detectors should be considered in situations where the solar radiation is not present or minimized. These detectors are already proving useful as in-lab or field-based calibrators for radiation thermometry and for spectral irradiance under well-controlled

environments where the stray radiation can be minimized.

It was shown in this study that the irradiances in a point-source geometry can be measured with > 100 x better signal-to-noise ratios than with traditionally used mid-IR detectors.

2.5. Spectral radiance responsivity

Radiance (or luminance) is a source characteristic and radiance (or luminance) responsivity is a detector characteristic. The radiance of extended sources can be measured with radiance meters. The requirement from a standard quality radiance meter is to have a well-defined measurement angle to measure the source target area only. Radiance and luminance meters have input optics to image a given surface of a light source to the detector of the meter. In radiance and luminance meters, the field stop (usually the aperture in front of the detector) is overfilled by the measured radiation. Accordingly, measurements can be made even with detectors of spatially non-uniform responsivity if the radiance (or luminance) of the target area (of a source) is spatially uniform.

Typically, spectral radiance responsivity calibrations are made with a narrow spectral bandwidth and the responsivities are determined with certain wavelength increments.

2.5.1. Radiance Measurement methods and transfer

The measurement geometry of radiance mode measurements was discussed in 3.3 of Volume 2. Radiance is defined as radiant power per area per solid angle as shown in Fig. 54 in Volume 2. The radiance responsivity of a radiance meter is equal to the ratio of the meter's output signal to the radiance of the measured source.

As an example, the simplified optical/mechanical design of a radiance meter is shown in Fig. 76. A radiance meter like this can be used as a transfer or working standard. The radiance measuring input optics can be attached to a power or irradiance measuring radiometer.

EYEPIECE   FIELD STOP   HEAT   ADAPTER &   OUTPUT
           MIRROR   SINK   CONNECTOR

CAMERA   APERTURE   SECOND   PHOTO   CURRENT-   GAIN
LENS   STOP   IMAGING   DIODE   TO-VOLTAGE   SWITCH
                                       CONVERTER
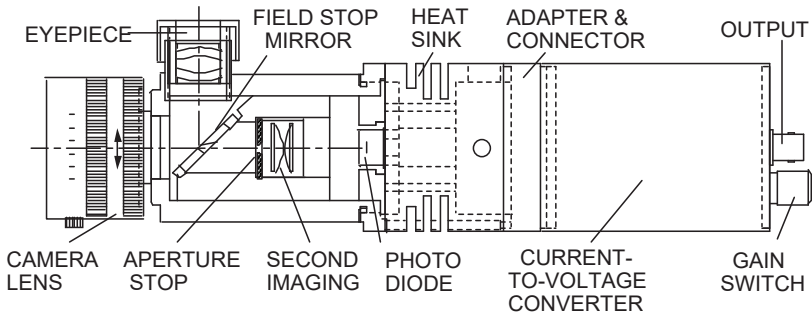
Fig. 76. Scheme of a radiance meter. The imaging input optics is attached
to a Si photodiode power meter.

The bevelled aperture mirror serves as a field stop, and it is positioned into the focus of a camera lens. Bevelling minimizes stray radiation. The camera lens has a broad-band anti-reflecting (AR) coating, resulting in high transmittance in the visible (and NIR) ranges. The surroundings of the source target area can be viewed through the eye-piece. The target radiation is imaged to the same center position of the photodiode through a second imaging optics. The second imaging optics produces a well-defined FOV and a very efficient out-of-FOV blocking. The original aperture (used for irradiance measurement) stays in front of the Si photodiode, and it is underfilled (not used as a field stop) in radiance measurement mode. There is a dominant aperture stop in front of the second imaging optics in order to keep the flux response of the optics constant for different target distances of the adjustable-focus camera lens.

The spectral radiance responsivity of a radiance meter can be determined in a few ways. Three methods will be discussed here as examples. The spectral radiance responsivity can be derived from the spectral power responsivity of the detector used in the radiance meter if the front geometry of the meter is well defined. Also, the absolute spectral radiance responsivity can be determined from the relative spectral radiance responsivity of the radiance meter when radiance responsivity tie points make the relative to absolute conversion. The third method is to determine the spectral radiance responsivity (or the absolute tie points) against an irradiance-meter standard that calibrates the radiance of a monochromatic point source(s).

2.5.1.1. Power responsivity based geometrical calibration

While irradiance (or illuminance) can be measured with one aperture, radiance (or luminance) mode measurements need two apertures. An example was described in 3.3.2 of Volume 2, where an input tube with two baffles between the two apertures is attached to the front of a radiometer/photometer for radiance and luminance mode measurements [74]. The two apertures determine the radiance (luminance) measurement angle.

2.5.1.2. Relative spectral radiance responsivity

Relative spectral radiance responsivity measurements can be made with two different beam geometries.

The first one is a simple, non-imaging method that can be used for radiance meters where a second imaging optic projects the beam always into the same position on the detector (as shown in Fig. 76). In this case, the target spot of the radiance meter is not defined [75]. The relative radiance responsivity determination can be used on a conventional monochromator-based calibration facility in radiant power responsivity (underfilled) measurement mode. A relative standard measurement uncertainty associated to the values of the relative radiance responsivity of the radiance meter of 0.11 % could be achieved between 450 nm and 900 nm using this method. However, the above non-imaging method is not correct for relative radiance responsivity measurements.

A modified arrangement for relative spectral radiance responsivity calibration is shown in Figure 77 [75]. As an example, an f/9 converging beam from the monochromator, before the two lenses, produces a 1.1 mm diameter spot (which is on the surface of the power measuring detector in the standard arrangement). In the modification, a camera lens of 35 mm focal length is used as a relay lens to magnify this spot into a 15 mm diameter image, inside an achromatic collector lens of 350 mm focal length. The corrected lens collects the radiation exiting from the relay lens and projects it into the center of the camera lens of the radiance meter. The distance of the radiance meter from the collector lens has to be adjusted until the diameter of the target spot of the radiance meter is equal to the diameter of the reference detector that is positioned directly after the collector lens. The reference detector has to be circular (e.g. a 1 cm^2 silicon detector). In the eyepiece of the radiance meter, the black

(measured) spot has to be in the center of the 15 mm diameter image inside the collector lens. The relative radiance responsivity of the meter will be the power responsivity of the reference detector times the ratio of the radiance meter output signal to the output signal of the reference detector.
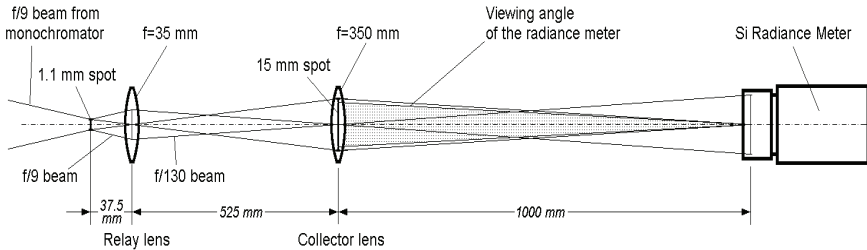
Figure 77. Example for an optical arrangement to measure relative spectral radiance responsivity of a radiance meter.

2.5.1.3. Calibration against uniform and monochromatic extended sources

The absolute radiance responsivity of a radiance meter can be determined against an irradiance meter standard. First, the radiant intensity of a monochromatic Lambertian (uniform) source is be determined from the spectral irradiance responsivity of the standard meter and the distance between the apertures of the standard meter and source. The distance should be large enough to utilize point source geometry. In this case, the radiant intensity will be equal to the product of the irradiance (in the aperture plane of the irradiance meter standard) and the square of the distance. The radiance within the source aperture (at a given wavelength) will be the ratio of the radiant intensity to the source aperture area. When calibrating a radiance meter against the source, its target area (the measured spot) has to be within the source aperture. The radiance responsivity of the meter will be the ratio of its electrical output signal to the measured source radiance. This calibration can be made at a few wavelengths to obtain tie points to a relative spectral radiance responsivity curve or can be done at a large number of wavelengths (by tuning the laser introduced into the sphere source) to obtain the spectral radiance responsivity curve in a given wavelength range.

2.6. Directional errors of detectors and radiometer standards

The accuracy of primary standard radiometers has significantly improved in the past decades. In order to benefit fully from these improvements, the accuracy of the derived radiometric scales needs to be improved. Greater accuracy in the scales means that some effects, formerly negligible, have become more important. One such effect is the directional response error of the detectors/radiometers. At calibration, the directional distribution of optical radiation (beam geometry) from a source may differ from that in subsequent tests of optical detector standards. These changes in beam geometry can be significant: here they are treated as equivalent to uncertainties in detector responsivity. Such uncertainties, caused by non-ideal detector input characteristics and changes in input beam geometry, can be reduced significantly by correcting the detector response to a reference input beam geometry. A collimated beam normally incident on the detector surface makes a practical choice for reference geometry.

As an example, an irradiance meter measures irradiance in its reference plane which is usually the surface of its aperture. When the angle of incidence changes away from the normal, the irradiance in the plane of the aperture changes by the cosine of the incidence angle. Consequently, the detector measures less for larger incident angles. The requirement from an accurate irradiance meter is to measure the irradiance in the aperture plane, that is to obtain a constant ratio of the output-signal to the input irradiance. As the irradiance in the aperture plane changes by the cosine of the incidence angle, the response of the irradiance meter should change according to the the cosine of the incidence angle. As the realization of a perfect cosine angular response is not easy, the CIE directional $f_2(\varepsilon,\varphi)$ error has to be determined. When a calibrated beam is measured from a given direction, the $f_2(\varepsilon,\varphi)$ should be known (measured) for that ε and φ. If this $f_2(\varepsilon,\varphi)$ is known, the correction for those ε and φ (only) can be applied. If $f_2(\varepsilon,\varphi)$ is known for the hemisphere (or at least for a range of that) and also the distribution of the measured source $L(\varepsilon,\varphi)$ is known, then for this given source distribution the directional error can be calculated and a correction can be applied. If the source is uniform and circular, the calculation of the correction will be easier. In a proper design, the detector should be also circularly summetric to simplifiy the calculation of the correction. Asymmetric detector design should be avoided. A good

solution is to use a symmetrical detector even if the errors are larger and then apply the correction.

An integral directional error can be determined for radiant power, luminous flux, irradiance and illuminance detectors by calculating the weighted integral of the product of the measured source radiance and the directional error over the solid angle produced by the light source. A conical directional error has been introduced, and used to describe the case of circular and uniform radiant sources (e.g. exit port of an integrating sphere) and circularly symmetric detectors [ref]. Evaluation of the conical directional error and the directional response correction factor, the results of directional response measurements, and directional response correction factors for practical standard detectors (such as diffuser-input InGaAs and integrating-sphere-input silicon irradiance meters, silicon photodiode, and pyroelectric radiant power and irradiance measuring detectors) are discussed below.

A conical directional error, $f_d(\alpha)$, and a directional response correction factor, C_d, are introduced [76] which can easily be derived from the directional error, $f_2(\varepsilon, \varphi)$, as defined by the International Commission on Illumination (CIE), for spatially uniform and circularly symmetric calibration sources [77, 78].

2.6.1. Calculation of directional response correction factor

The directional response correction factor C_d of a radiometric detector is a quantity that corrects the detector response measured for the beam geometry S_b to the collimated beam response S_c:

$$S_c = S_b / C_d .$$

(36)

An integral directional error quantity f_2 defined by the CIE [77] is given by:

$$f_2 = S_b / S_c - 1 .$$

(37)

It follows from Eqs. (36) and (37) that

$$C_d = 1 + f_2 .$$

(38)

References [77, 78] describe a method for determining the directional

characteristics of irradiance, illuminance, and radiance meters in terms of the directional error $f_2(\varepsilon,\varphi)$. For irradiance and illuminance meters, the CIE defined directional error is:

$$f_2(\varepsilon,\varphi) = \frac{E_{reading}(\varepsilon,\varphi)}{E_{reading}(\varepsilon=0°)\cdot\cos\varepsilon} - 1 \quad,$$

(39a)

where φ is the azimuth angle (rotation around the detector axis), and ε is the angle of incidence. $E_{reading}(\varepsilon,\varphi)$ and $E_{reading}(\varepsilon=0°)$ are the readings for an irradiance or illuminance, E, arriving at the angles of incidence ε and $0°$, respectively.

As the denominator shows, the response of an ideal irradiance or illuminance meter follows the cosine function. For radiant power and directional luminous flux meters, for which the ideal response is independent of direction, the directional error $f_2(\varepsilon,\varphi)$ is:

$$f_2(\varepsilon,\varphi) = \frac{E_{reading}(\varepsilon,\varphi)}{E_{reading}(\varepsilon=0°)} - 1 \quad.$$

(39b)

References [77, 78] describe how to calculate the integral directional error f_2 from the directional error $f_2(\varepsilon,\varphi)$. The integral directional error f_2 which describes the response measurement error originating from the directional error of the detector. The CIE defined integral directional error f_2 for irradiance and illuminance meters is:

$$f_2 = \int_\Omega f_2(\varepsilon,\varphi)\cdot L(\varepsilon,\varphi)\cdot\cos\varepsilon\cdot d\Omega \left/ \int_\Omega L(\varepsilon,\varphi)\cdot\cos\varepsilon\cdot d\Omega\right.$$

(40a)

where $L(\varepsilon,\varphi)$ is the source radiance, $d\Omega$ is the elementary solid angle, and Ω is the total acceptance solid angle (field of view) of the detector.

For radiant power and directional luminous flux meters, for which the ideal response is independent of direction, the error f_2 is defined as:

$$f_2 = \int_\Omega f_2(\varepsilon,\varphi)\cdot L(\varepsilon,\varphi)\cdot d\Omega \left/ \int_\Omega L(\varepsilon,\varphi)\cdot d\Omega\right.$$

(40b)

$$.$$

Using only angles ε and φ, Eq (40a) can be written as:

$$f_2 = \int_0^{\pi/2}\left[\int_0^{2\pi} f_2(\varepsilon,\varphi)\cdot L(\varepsilon,\varphi)\cdot\cos\varepsilon\cdot 2\pi\cdot\sin\varepsilon\cdot d\varphi\right]\cdot d\varepsilon \left/ \int_0^{\pi/2}\left[\int_0^{2\pi} L(\varepsilon,\varphi)\cdot\cos\varepsilon\cdot 2\pi\cdot\sin\varepsilon\cdot d\varphi\right]\cdot d\varepsilon\right.$$

(41)

References [77, 78] describe the cases in which the irradiation comes from the $\Omega=2\pi$ hemisphere or the total $\Omega=4\pi$ sphere. Their considerations may be applied to detector calibrations, if spatially uniform and circularly symmetric calibration sources are used and the source center is on the optical axis of the detector. For irradiance and illuminance meter calibrations, such radiation sources can be realized with integrating spheres. The radiance or luminance of the exit port of a high-quality integrating sphere may be considered to be spatially uniform. In this case $L(\varepsilon,\varphi)=L$, for $\varepsilon < \alpha$, and $L(\varepsilon,\varphi)=0$ for $\varepsilon >\alpha$, where α is the half angle of the field-of-view determined by the radius of the light source (the exit port of the integrating sphere) and the distance to the aperture center of the detector.

In the case of spatially uniform and circularly symmetric calibration sources, the integral directional error f_2 depends on the half angle α of the field-of-view of the radiation (extended) source, that is, $f_2=f_2(\alpha)$. To avoid confusion with the CIE $f_2(\varepsilon,\varphi)$ (and later $f_2(\varepsilon)$), a conical directional error $f_d(\alpha)$ is introduced instead of $f_2(\alpha)$ [76].

The conical directional error $f_d(\alpha)$, using spatially uniform and circularly symmetric sources, for irradiance and illuminance meters is:

$$f_d(\alpha) = \int_0^{\alpha}\left[\int_0^{2\pi} f_2(\varepsilon,\varphi)\cdot\cos\varepsilon\cdot 2\pi\cdot\sin\varepsilon\cdot d\varphi\right]\cdot d\varepsilon \left/ \int_0^{\alpha}\left[\int_0^{2\pi}\cos\varepsilon\cdot 2\pi\cdot\sin\varepsilon\cdot d\varphi\right]\cdot d\varepsilon\right.$$

(42)

The calculation is simplified if the detector directional response is also circularly symmetric (i.e. the response is independent of azimuth angle φ) resulting in $f_2(\varepsilon,\varphi)=f_2(\varepsilon)$. In this case, the conical directional error for irradiance and illuminance meters is:

$$f_d(\alpha) = \int_0^\alpha f_2(\varepsilon) \cdot \sin 2\varepsilon \, d\varepsilon \bigg/ \int_0^\alpha \sin 2\varepsilon \cdot d\varepsilon$$

(43a)

Similar evaluation of Eq. (40b) results in the conical directional error for radiant power and directional luminous flux meters:

$$f_d(\alpha) = \int_0^\alpha f_2(\varepsilon) \cdot \sin \varepsilon \, d\varepsilon \bigg/ \int_0^\alpha \sin \varepsilon \cdot d\varepsilon .$$

(43b)

For radiant power and directional luminous flux meter calibrations, where the incident beam underfills the detector aperture, the uniform source can be realized by projecting a point source on to the detector entrance with a lens.

In accordance with Eq. (38), the conical directional error can be compensated for all types of radiometer by applying the directional response correction factor C_d:

$$C_d = 1 + f_d(\alpha)$$

(44)

2.6.2. Application of conical directional error and directional response correction factor

Determination of detector directional response characteristics is frequently needed in radiometric and photometric calibrations and measurements [3, 80]

For practical applications, the directional response correction factor C_d is used to correct the detector response for the reference beam geometry, which is the axially incident parallel beam. Because C_d is close to unity, the conical directional error $f_d(\alpha)$ gives better visual information.

The CIE $f_2(\varepsilon)$ directional errors were measured, and the conical directional errors $f_d(\alpha)$ and the directional response correction factors C_d were calculated for a number of detector standards. Table 10 summarizes the results of four tested detectors. As an example, Fig. 78 shows the CIE directional error $f_2(\varepsilon)$ and the conical directional error $f_d(\alpha)$ of a radiometer that has an InGaAs photodiode with input

optics consisting of a flashed opal glass diffuser, a precision aperture, and a field-of-view limiter. The characterization of the input optics and the directional response measurement results of this irradiance standard have been described [80]. The detector directional response characteristics were measured with an incandescent lamp irradiation.

The figure can be used to determine the directional response correction factor C_d. If the half angle α of the field-of-view of the source from the detector center is known, the value of the conical directional error $f_d(\alpha)$ can be read from the right vertical axis. The directional response correction factor can then be calculated using Eq. (44). The corrected detector response can be calculated from Eq. (36).
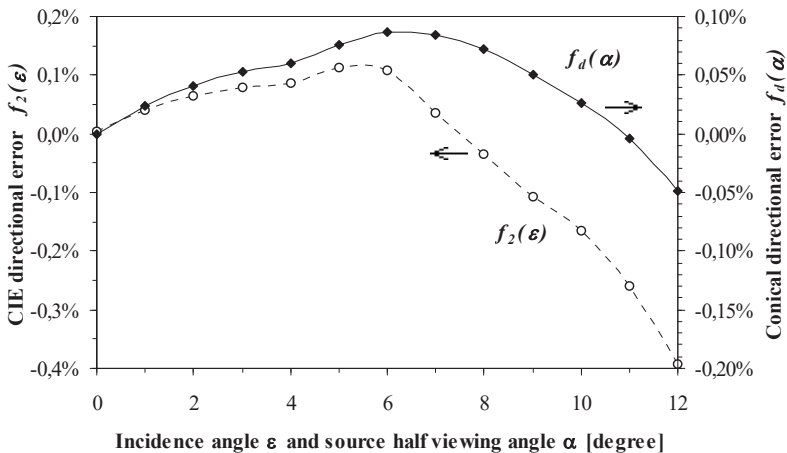
Figure 78. Directional error $f_2(\varepsilon)$ (dotted line with open circles) and conical directional error $f_d(\alpha)$ (solid line with black diamonds) of a diffuser input InGaAs irradiance meter. The uncertainties are less than 0.025 % for $f_2(\varepsilon)$ when $\varepsilon \leq 6°$ and less than 0.023 % for $f_d(\alpha)$ when $\alpha \leq 9°$ (k=1).

In addition to the InGaAs radiometer, the test results of the following detectors are summarized in Table 10:

Table 10. Conical directional errors $f_d(\alpha)$ and directional response correction factors C_d of several irradiance and radiant-power detector standards for $f/9$ and $f/4$ incidence beam geometries. The relative uncertainties of the error determinations are also given, ($k = 1$).

Detector type	Irradiance mode				Radiant flux (power) mode			
	$f/9$ beam, α =3.18º		$f/4$ beam, α =7.13º		$f/9$ beam, α =3.18º		$f/4$ beam, α =7.13º	
	f_d	C_d	f_d	C_d	f_d	C_d	f_d	C_d
Sphere-input Si (1)	+0.033 % ±0.007 %	1.00033	+0.166 % ±0.005 %	1.00166				
Diffuser-input InGaAs	+0.055 % ±0.010 %	1.00055	+0.081 % ±0.016 %	1.00081				
Gold-black coated pyroelectric (2)	+0.036 % ±0.046 %	1.00036	+0.022 % ±0.033 %	1.00022	-0.003 % ±0.005 %	0.99997	-0.006 % ±0.004 %	0.99994
Si photodiode with window (3)	+0.076 % ±0.033 %	1.00076	+0.175 % ±0.026 %	1.00175	-0.009 % ±0.038 %	0.99991	+0.037 % ±0.026 %	1.00037

(1) Integrating-sphere-input silicon irradiance meter. A Si photodiode was attached to the exit port of a 50 mm diameter integrating sphere. A previous design of this irradiance meter was published earlier [81]. In the present version, a smaller (3.5 mm diameter) input aperture is used, and an additional light-tight cover is added to the housing. The directional characteristics were measured using an incandescent lamp.

(2) Pyroelectric radiant power and irradiance measuring detector. A gold black coated $LiNbO_3$ pyroelectric detector [3] was tested. The detector has an 8 mm diameter aperture with 1 mm separation from the detector surface. The power-mode directional measurements were performed with a laser beam focused on the detector. The irradiance-mode directional characteristics were measured using an incandescent lamp source.

(3) Silicon photodiode. Si photodiodes are the most frequently used transfer standards for the near-UV, visible, and near-IR spectral

ranges [5, 51, 79]. Their directional characteristics were measured on a widely used standard photodiode which has a window and circular photodiode of 1 cm^2 area. The tests were made using incandescent lamp irradiation.

The results show that even for well-designed (optimized) radiometer standards, the uncertainty associated with the conical directional error $f_d(\alpha)$ can exceed the 0.1 % (k=1). In order to achieve uncertainties below 0.1 %, the application of directional response correction factors may be required even for high-performance radiometer standards. In some cases, the uncertainties of the directional response measurements are so high it is not possible to determine the directional response correction factors with the desired low uncertainty.

In summary, the introduced conical directional error, $f_d(\alpha)$, could be used to evaluate the effect of the CIE defined directional error, $f_2(\varepsilon,\phi)$, for transfer standard radiometers [76]. For a given incident beam geometry, $f_d(\alpha)$ can be determined as a weighted integral of the CIE $f_2(\varepsilon,\phi)$ directional error. A directional response correction factor, C_d, could be calculated. The uncertainty budget of detector response measurements could be decreased by applying this response correction. The CIE directional error can thus be replaced by the directional response correction factor determination, which has a smaller uncertainty. The suggested calculation]76] can be applied to all irradiance, illuminance, power, and directional luminance flux meters. For the most frequently used beam geometries at the NIST, the conical directional error $f_d(\alpha)$ ranged between +0.022 % and +0.175 % for irradiance meters, and from -0.003 % to +0.037 % for radiant power meters. In order to simplify the calculation of C_d, circularly symmetric radiometers should be designed for standardization. A high-accuracy measurement setup is required to determine the directional response correction factor with a small enough uncertainty for the needs of standards-quality detectors. The described response correction method [76] can be applied for medium-performance detector standards as well.

2.7. Spectral responsivity calibration of illuminance meters and tristimulus colorimeters

Photometry and tristimulus colorimetry are based on light measurement using radiometers with spectral responsivities matched to the CIE

$\bar{x}(\lambda)$, $\bar{y}(\lambda)$, and $\bar{z}(\lambda)$ functions [82]. To achieve low measurement uncertainty for a large variety of light sources, the spectral matches should be as close as possible to the CIE functions. The tristimulus-meter channels are usually realized with silicon photodiodes and attached filter packages. Often, the spectral mismatch between the realized and the CIE functions gives a dominant contribution toward the measurement uncertainties in the results of photometric and tristimulus color measurements of different source distributions.

A detector-based method, using spectrally resolved responsivities and numerical integration for the calibration factors of photometers and tristimulus colorimeters, can produce lower contributions of measurement uncertainty associated to the values of the calibration factors as compared to spectrally integrated calibrations with traditional lamp standards [83]. The broadband calibration factor values that can be calculated for all of the channels of a photometer/colorimeter are discussed in Volume 5 of this book series: Broadband UV-, VIS-, and IR-Radiometric, Photometric, Color, and Temperature Measurements. Typically, spectral responsivity measurements are performed for these meters as reference measurements to determine their channel calibration factors. The illuminance responsivity (luminous responsivity) can be determined from the measured spectral irradiance responsivity of the photometer and the incident irradiance from a CIE standard (such as A) illuminant source. The calibration factors of the channels of a tristimulus colorimeter are produced similarly to the illuminance responsivity calibration of a single photometer as discussed in Section 2.2.3 of Volume 5.

2.8 Spectral calibration issues of electronic imaging devices (cameras)

Electronic imaging systems include digital cameras, spectrographs, microscopes, etc. Radiometric calibrations usually include pixel-to-pixel uniformity of responsivity, linearity, and spectral radiance responsivity. In many applications, such as with CCD cameras, the photometric and colorimetric performances are important issues as well.

In many cases, digital imaging systems are calibrated against broad-band incandescent sources, such as Illuminant A, and subsequently measure sources with very different spectral power distributions. In

this case, the measurement uncertainties are not well known in general, and can be much larger than expected. If the spectral radiance responsivity of an imaging device is known, one can predict its performance under differing operating conditions.

In order to characterize and calibrate digital imaging systems, monochromatic uniform sources are needed that can overfill the detector array with a uniform field of radiation in radiance measurement mode. Possible uniform sources are laser illuminated integrating sphere sources. Sometimes monochromators are used too. If the source exit port has spatially uniform radiance, the pixel-to-pixel uniformity can be evaluated. If the exit port is not very uniform, the spatial distribution of the port radiance can be mapped out and spatial corrections can be applied. Before determining the spectral responsivity of a camera, it is necessary to measure and correct for any non-linearity in the response of that camera.

The non-linearity can be measured by changing the radiance of the sphere exit port. The radiance levels should be calibrated (referenced) against either an irradiance radiometer standard (measuring the irradiance from the exit port) or a previously calibrated monitor detector of the sphere source. A CCD camera should have the same exposure time for all radiance levels. Usually, the ratio of the camera signal (digital number, DN) to the sphere radiance versus the camera signal is plotted. If the camera response were linear, the ratio of the camera signal to the sphere radiance would remain constant as a function of count level. Usually, the ratio, for a CCD camera, increases sharply when the camera signal increases from 10 DN to 100 DN. Above 100 DN, the ratio usually continues to rise slightly. In determining the radiance responsivity of the CCD camera, individual data sets should be normalized to the high-count level, with the individual scaling factors determined by the results of the measured non-linear response curve (DN/sphere-radiance versus DN). After applying non-linearity corrections and changing the offset level in the non-linear response curve, a 1 % non-linearity could be achieved over the range from 25 DN to 230 DN [84].

In this example, after non-linearity correction [84], the CCD camera was positioned in front of the sphere exit port, and its spectral responsivity, in DN per second per unit radiance, was measured. During the calibration, the laser was tuned to the wavelength of

interest. The CCD camera measured the radiance from the sphere-port and the radiance responsivity (DN/s/(W/cm^2/sr)) was calculated by dividing the CCD output signal, corrected for the exposure time, by the sphere radiance. During the calibration, images were acquired with several different exposure times. The responsivity was measured for different exposure times at several wavelengths during the calibration. The CCD responsivity agreed to within 1 % for the different exposure times. The pixel-to-pixel responsivity of the camera was measured with and without a photopic filter. Without the filter in place, the total response variation over the central 90 % of the array was about 5 %. With the filter installed, the non-uniformity of responsivity increased to about 10 %. The data were not corrected for the non-uniformity of the sphere-radiance because it was negligible compared with the non-uniformity of the pixel-to-pixel responsivity of the CCD camera.

3. UNCERTAINTY OF DETECTOR SPECTRAL RESPONSIVITY MEASUREMENTS

General discussions of the contribution to the measurement uncertainty sources in radiometry are available elsewhere [85] [40]. General principles for the method of uncertainty analysis are given in the ISO "Guide to the Expression of Uncertainty in Measurement" (GUM) [39]. The mathematical methods based on the GUM are discussed in the CIE TC 2-43 document [86]. Uncertainties are always calculated as standard uncertainties, and in radiometry and photometry generally expressed as numbers in a relative presentation.

The standard uncertainty of spectral radiant power responsivity values can be derived from the principal measurement equation (for detector substitution method) described by Eq. 8 in 2.1.1 above [91]. It is common to use a monitor detector to account for fluctuations in the radiant power of the source, and the modified version of the measurement equation is then:

$$s_T = s_S \cdot \frac{I_T/I_{MT}}{I_S/I_{MS}} = s_S \cdot \frac{R_T}{R_S}$$

$$(45)$$

where R_T, R_S are ratios of the electrical output signals I_T, I_S to their simultaneously measured monitor output signals I_{MT}, I_{MS}. Hence the relative standard uncertainty in the spectral radiant power responsivity of the test detector, $u_{rel}(s_T)$, is given by

$$u_{rel}\left(s_T\right) = \left[u_{rel}^2\left(s_S\right) + u_{rel}^2\left(R_T\right) + u_{rel}^2\left(R_S\right)\right]^{1/2}$$

$$(46)$$

The first contribution, $u_{rel}^2\left(s_S\right)$, is the relative standard measurement uncertainty calculated from the certificate for the reference detector and its operational conditions during transfer. The two other contributions, $u_{rel}^2\left(R_T\right)$ and $u_{rel}^2\left(R_S\right)$, come from the

measurement transfer.

Note that at present, calibration certificates do not report correlation coefficients or uncorrelated and correlated components separately. While measurements at the one wavelength do not depend on these correlations, they become important when combining values at different wavelengths in spectrally integrated components; this is discussed in Volume 5 of this book series.

The effective radiant responsivity s_S of the reference detector requires correction for a possible temperature deviation ΔT, as difference to that during calibration at the NMI, for a relative non-uniformity β_S, and for a wavelength shift $\Delta\lambda$:

$$s_S = s_S' \cdot \left(1 + \alpha_S \cdot \Delta T + \beta_S + (\partial R_S / \partial \lambda) / R_S \cdot \Delta\lambda\right) \tag{47}$$

where s_S' is the radiant power responsivity of the reference detector, α_S is the relative temperature coefficient for the responsivity and $(\partial R_S / \partial \lambda) / R_S$ is the relative derivative of the ratio R_S with respect to the wavelength.

The relative standard measurement uncertainty $u_{rel}(s_S')$ of the radiant power responsivity s_S' of the reference detector is calculated from the expanded measurement uncertainty $U(s_S')$ divided by the coverage factor, usually $k = 2$, given in the calibration certificate when the responsivity s_S' was certified for operation at ambient temperature T_C, and is given by

$$u_{rel}(s_S') = U(s_S') / (2 s_S') \tag{48}$$

The temperature deviation $\Delta T = T_S - T_C$ is calculated from the temperature T_C in the certificate (nominal value, no uncertainty contribution) and the measured ambient temperature T_S during use. Often the standard deviation

$s\left(T_{\mathrm{S}}\right)$ of repeated readings of the thermometer is smaller than its resolution, which is an interval $\pm res\left(T_{\mathrm{S}}\right)$ with rectangular probability distribution. The temperature is measured with the thermometer certified with an (absolute) expanded measurement uncertainty $U\left(T_{\mathrm{S}}\right)=\delta T$ for a $k=2$ coverage interval and gives the standard variance $\left(\delta T/2\right)^{2}$. The three contributions are combined to the standard variance of the temperature deviation:

$$u^{2}\left(\Delta T\right)=\left(\frac{\delta T}{2}\right)^{2}+s^{2}\left(T_{\mathrm{S}}\right)+\frac{res^{2}\left(T_{\mathrm{S}}\right)}{3} \qquad (49)$$

The relative temperature coefficient α_{S} is measured separately and the value can be determined with an associated standard measurement uncertainty $u\left(\alpha_{\mathrm{S}}\right)$ or taken from the related literature.

The relative non-uniformity β_{S} has a zero value (it is included in the responsivity value) but its variation contributes to the measurement uncertainty of the responsivity within an interval $\pm\Delta s_{\mathrm{S}}$, having a rectangular probability distribution. Therefore, the standard variance is calculated as $u^{2}\left(\beta_{\mathrm{S}}\right)=\Delta s_{\mathrm{S}}^{2}/3$.

Finally, the correction for a wavelength shift is given. It is relevant for differently shaped relative spectral responsivity functions of the test detector and the reference detector. The wavelength correction $\Delta\lambda=\Delta\lambda_{1}+\Delta\lambda_{2}$ has two components, an offset $\Delta\lambda_{1}$ with rectangular probability distribution, constant for all wavelengths (correlated uncertainty contribution) and a correction $\Delta\lambda_{2}$ individual for each wavelength due to limited repeatability of the wavelength drive with associated uncertainty normally distributed (uncorrelated uncertainties).

After these preparations and two assumptions, (i) $1>>\left|\alpha_{\mathrm{S}}\cdot\Delta T\right|+\left|\beta_{\mathrm{S}}\right|+\left|\left(\partial R_{\mathrm{S}}/\partial\lambda\right)/R_{\mathrm{S}}\cdot\Delta\lambda\right|$ and (ii) no correlations between the uncertainties of the values of

quantities, the relative combined variance associated to the responsivity of the standard detector can be written:

$$
\begin{aligned}
u_{\text{rel}}^2\left(s_{\text{S}}\right) = {} & u_{\text{rel}}^2\left(s_{\text{S}}'\right) + u^2\left(\beta_{\text{S}}\right) + \alpha_{\text{S}}^2 \cdot u^2\left(\Delta T\right) + u^2\left(\alpha_{\text{S}}\right) \cdot \Delta T^2 + \\
& + \left(\left(\partial R_{\text{S}}/\partial\lambda\right)/R_{\text{S}}\right)^2 \cdot u^2\left(\Delta\lambda\right) + u^2\left(\left(\partial R_{\text{S}}/\partial\lambda\right)/R_{\text{S}}\right) \cdot \Delta\lambda^2 + \\
& + \left[u^2\left(\Delta T\right) \cdot u^2\left(\alpha_{\text{S}}\right)\right] + \left[u^2\left(\Delta\lambda\right) \cdot u^2\left(\left(\partial R_{\text{S}}/\partial\lambda\right)/R_{\text{S}}\right)\right]
\end{aligned}
$$
(50)

If the temperature at the time of measurement is just the same as the one at the time of calibration $\Delta T = 0$, then the second order term $\left[u^2\left(\Delta T\right) \cdot u^2\left(\alpha_{\text{S}}\right)\right]$ has to be considered. Similarly, if the wavelength shift $\Delta\lambda = 0$ is (nearly) zero, then the other second order term $\left[u^2\left(\Delta\lambda\right) \cdot u^2\left(\left(\partial R_{\text{S}}/\partial\lambda\right)/R_{\text{S}}\right)\right]$ becomes relevant. For the test detector, similar contributions have to be taken into consideration. The corrected value of the radiant power responsivity s_{T}' of the test detector can be calculated for the ambient temperature T_{C} and for zero contribution of its own homogeneity

$$
s_{\text{T}} = s_{\text{T}}' \cdot \left(1 + \alpha_{\text{T}} \cdot \Delta T + \beta_{\text{T}} + \left(\partial R_{\text{T}}/\partial\lambda\right)/R_{\text{T}} \cdot \Delta\lambda\right)
$$
(51)

Similarly to the considerations before, the associated relative standard uncertainty of s_{T} can be determined assuming small corrections $1 >> \left|\alpha_{\text{T}} \cdot \Delta T\right| + \left|\beta_{\text{T}}\right| + \left|\left(\partial R_{\text{T}}/\partial\lambda\right)/R_{\text{T}} \cdot \Delta\lambda\right|$ and no correlation. Then the relative variance can be written:

$$
\begin{aligned}
u_{\text{rel}}^2\left(s_{\text{T}}\right) = {} & u_{\text{rel}}^2\left(s_{\text{T}}'\right) + u^2\left(\beta_{\text{T}}\right) + \alpha_{\text{T}}^2 \cdot u^2\left(\Delta T\right) + u^2\left(\alpha_{\text{T}}\right) \cdot \Delta T^2 + \\
& + \left(\left(\partial R_{\text{T}}/\partial\lambda\right)/R_{\text{T}}\right)^2 \cdot u^2\left(\Delta\lambda\right) + u^2\left(\left(\partial R_{\text{T}}/\partial\lambda\right)/R_{\text{T}}\right) \cdot \Delta\lambda^2 + \\
& + \left[u^2\left(\Delta T\right) \cdot u^2\left(\alpha_{\text{T}}\right)\right] + \left[u^2\left(\Delta\lambda\right) \cdot u^2\left(\left(\partial R_{\text{T}}/\partial\lambda\right)/R_{\text{T}}\right)\right]
\end{aligned}
$$
(52)

The combination of Eq. (45) with the corrections in Eq. (47) and Eq. (51) give a new model for the radiant power responsivity evaluation:

$$s_T' = s_S' \cdot \left[\frac{1 + \alpha_S \cdot \Delta T + \beta_S + (\partial R_S / \partial \lambda) / R_S \cdot \Delta \lambda}{1 + \alpha_T \cdot \Delta T + \beta_T + (\partial R_T / \partial \lambda) / R_T \cdot \Delta \lambda} \right] \cdot \frac{I_T / I_{M,T}}{I_S / I_{M,S}}$$
(53)

and taking the earlier assumptions into account (first order approach), the bracket is simplified to

$$\left[1 + (\alpha_S - \alpha_T) \cdot \Delta T + \beta_S - \beta_T + ((\partial R_S / \partial \lambda) / R_S - (\partial R_T / \partial \lambda) / R_T) \cdot \Delta \lambda \right]$$
.

This approach directly shows that for very similar test and reference detectors the temperature and spatial uniformity errors will cancel out.

The four photocurrents, combined into a double-ratio in Eq. (53), also contribute to the measurement uncertainty:

a) For the test and reference detectors the same amplifier and DVM are used, assuming gain and range settings are valid for both photocurrents.

b) With the test detector in place, a series of $n \geq 20$ repeated readings are carried out simultaneously for both the test detector (I_T') and the monitor detector (I_{MT}').

c) Under the same conditions (especially for amplifier gain and DVMs range) but with the shutter closed "dark measurements" (I_{T0}', I_{MT0}') are carried out.

d) With the reference detector in place and "shutter open" n repeated readings are carried out simultaneously for both reference (I_S') and monitor detectors (I_{MS}').

e) Under the same conditions, but with the shutter closed, "dark measurements" (I_{S0}'), (I_{MS0}') are carried out.

Mean values like $\overline{I_T'}$ and related standard deviations $s(\overline{I_T'})$ are calculated for all the measured quantities and additionally for the two ratios: $R_T' = I_T' / I_{MT}'$; $R_S' = I_S' / I_{MS}'$. In principle, instead of these ratios, the dark current corrected ratios should be averaged. However, if the dark current is small and the measurement setup is fairly stable, then a modification is valid that will simplify the measurement uncertainty evaluation:

$$R_{\mathrm{T}} = \frac{1}{n} \sum \frac{I'_{\mathrm{T},i} - \overline{I}'_{\mathrm{T0},i}}{I'_{\mathrm{MT},i} - \overline{I}'_{\mathrm{MT0},i}} \approx \overline{R}'_{\mathrm{T}} \cdot \left(1 - \frac{\overline{I}'_{\mathrm{T0}}}{\overline{I}'_{\mathrm{T}}} + \frac{\overline{I}'_{\mathrm{MT0}}}{\overline{I}'_{\mathrm{MT}}} \right) \tag{54}$$

In the same way, the ratio for the reference detector readings can be calculated and finally for the double ratio in Eq. (45) we have:

$$\frac{R_{\mathrm{T}}}{R_{\mathrm{S}}} \approx \frac{\overline{R}'_{\mathrm{T}}}{\overline{R}'_{\mathrm{S}}} \cdot \left(1 + \frac{\overline{I}'_{\mathrm{S0}}}{\overline{I}'_{\mathrm{S}}} - \frac{\overline{I}'_{\mathrm{T0}}}{\overline{I}'_{\mathrm{T}}} + \frac{\overline{I}'_{\mathrm{MT0}}}{\overline{I}'_{\mathrm{MT}}} - \frac{\overline{I}'_{\mathrm{MS0}}}{\overline{I}'_{\mathrm{MS}}} \right) \tag{55}$$

Usually, there are four contributions to the measurement uncertainty of a series of repeated readings of a radiometer: the standard deviations of the two mean values for light and dark readings; the calibration factor, which cancels out in Eq.(55); and the resolution $\pm \Delta I$ of the DVM. The latter is significant only if the noise is very low. For all of the photocurrents the standard measurement uncertainties are calculated similarly to.

$$u\left(\overline{I}'_{\mathrm{S0}}\right) = \sqrt{s^2\left(\overline{I}'_{\mathrm{S0}}\right) + \left(\Delta I / \sqrt{3}\right)^2} \tag{56}$$

Provided one amplifier is used for both the standard detector and the test detector, then the currents $\overline{I}'_{\mathrm{S0}}, \overline{I}'_{\mathrm{T0}}$ for offset and dark measurement are typically the same, as are their measurement uncertainties. As they are determined in a series one after the other there is no statistical correlation, even if recorded by the same amplifier.

Finally, the model for the evaluation of the radiant power responsivity of the test detector is calculated from the combination of Eqs. (53) and (55) with the higher orders omitted:

$$s'_{\mathrm{T}} = s'_{\mathrm{S}} \cdot \frac{\overline{R}'_{\mathrm{T}}}{\overline{R}'_{\mathrm{S}}} \cdot corr$$

$$corr = \left[\begin{array}{l} 1 + \left(\alpha_{\mathrm{S}} - \alpha_{\mathrm{T}}\right) \cdot \Delta T + \beta_{\mathrm{S}} - \beta_{\mathrm{T}} + \left(\left(\partial R_{\mathrm{S}}/\partial\lambda\right)/R_{\mathrm{S}} - \left(\partial R_{\mathrm{T}}/\partial\lambda\right)/R_{\mathrm{T}}\right) \cdot \Delta\lambda \\ + \dfrac{\overline{I}'_{\mathrm{S0}}}{\overline{I}'_{\mathrm{S}}} - \dfrac{\overline{I}'_{\mathrm{T0}}}{\overline{I}'_{\mathrm{T}}} + \dfrac{\overline{I}'_{\mathrm{MT0}}}{\overline{I}'_{\mathrm{MT}}} - \dfrac{\overline{I}'_{\mathrm{MS0}}}{\overline{I}'_{\mathrm{MS}}} \end{array} \right] \tag{57}$$

All the contributions in the brackets are very small corrections and the associated relative standard measurement uncertainty is often negligible. In a reduced form, the relative standard measurement uncertainty associated to the radiation power responsivity is combined from four dominant contributions:

$$u_{rel}\left(s_T'\right) = \sqrt{u_{rel}^2\left(s_T'\right) + u_{rel}^2\left(\overline{R}_T'\right) + u_{rel}^2\left(\overline{R}_S'\right) + u_{rel}^2\left(corr\right)}$$

(58)

The principles in the measurement equation Eq. (57) are valid for each single wavelength λ. That means, all quantities have to be regarded as functions of wavelength.

$$s_T'\left(\lambda\right) = s_S'\left(\lambda\right) \cdot \frac{\overline{R}_T'\left(\lambda\right)}{\overline{R}_S'\left(\lambda\right)} \cdot corr\left(\lambda\right)$$

(59)

The correction factor $corr\left(\lambda\right)$ includes the quantities temperature deviation ΔT, relative temperature coefficients α_S, α_T, relative non-uniformities β_S, β_T, wavelength offsets $\Delta \lambda$, and the dark currents $\overline{I}_{S0}', \overline{I}_{T0}', \overline{I}_{MT0}', \overline{I}_{MS0}'$, all of which are independent of wavelength or with small changes in neighbouring wavelength regions. These factors are independent for measurements at one wavelength and hence added in quadrature as in Eq. (58), but are common or correlated for values measured at different wavelengths.

The ratios $\overline{R}_T'\left(\lambda\right), \overline{R}_S'\left(\lambda\right)$ are formed from output signals $I_T\left(\lambda\right), I_S\left(\lambda\right)$ with simultaneously measured monitor output signals $I_{MT}\left(\lambda\right), I_{MS}\left(\lambda\right)$ using the correlation between the related photocurrents to eliminate noise from possible fluctuations of the source. Usually this is totally independent of wavelength.

For the determination of any single responsivity value and the associated uncertainty, the contributions are typically uncorrelated (at the given wavelength where the measurement transfer is made). These significant independent uncertainty components are added in

quadrature. In case of independent variables, their covariances are zero. The quadrature sum can be applied to all random components at a given wavelength.

One component that may correlate the test and standard measurements is that of wavelength uncertainty. Random wavelength setting errors are correlated between test and standard measurements if the wavelength is set and the test and standard detectors measured; they are not correlated if the spectral range is swept independently for the test detector and standard detectors.

The correlations between the uncertainties of the responsivity at different wavelengths can be determined using the Monte-Carlo-Method [65]. The correlation matrix of the relative spectral responsivities of a photometer is shown in Figure 79.
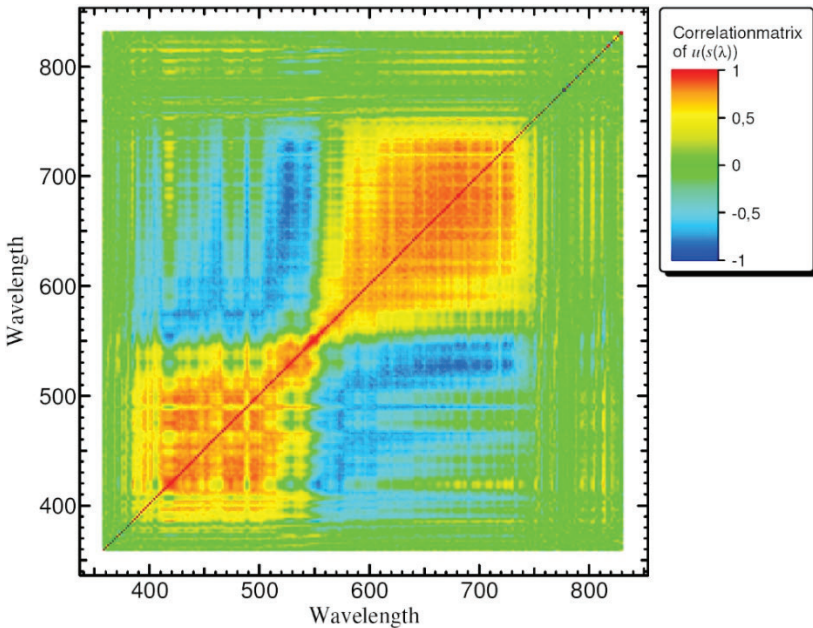

Figure 79. Correlation matrix of the relative spectral responsivities of a photometer.

Measurement uncertainties in certificates are generally quoted as expanded uncertainties, where the standard uncertainty is multiplied by the required coverage factor to give the level of confidence desired. A confidence level of about 95 % is usually quoted for routine measurements and calibrations. Provided sufficient measurements are taken for Type A components (statistical), and if particular distribution functions are assumed for Type B components (systematic), then the coverage factor is $k = 2$ to achieve this level of confidence. Typical expanded relative uncertainties (coverage factor $k = 2$) associated with values of detector spectral radiant power responsivity, performed by leading (well equipped) calibration laboratories, are:

- 0.2 % for the 405 nm to 920 nm wavelength range;
- 1 % to 2 % for the 250 nm to 405 nm and the 920 nm to 1700 nm wavelength range; and
- 2 % to 3 % for the 1700 nm to 2500 nm wavelength range.

3.1   Uncertainty associated to the Differential Spectral Responsivity

Usually, the spectral responsivity $s(\lambda) = s_0 \cdot s_{\mathrm{rel}}(\lambda)$ of a DUT is divided in a product with two factors, an absolute value $s_0 = s(\lambda = \lambda_0)$ and a relative function $s_{\mathrm{rel}}(\lambda) = s(\lambda)/s_0$ of wavelength. In case of a non-linear responsivity, additional factors are needed to fit the variation of the responsivity with the increasing level of irradiance E_{b} .

The two reasons for non-linearity are "ohmic resistance" and "deep traps". The ohmic resistance creates nonlinearity without spectral dependencies, which can be modelled as an additional factor $f(E_{\mathrm{b}})$. While the variation of the responsivity $s(\lambda, E_{\mathrm{b}})$ due to the deep traps is dependent on the material, the corresponding function $g(\lambda, E_{\mathrm{b}})$ will in general also depend on wavelength and irradiance. The DSR is measured as ratio $\tilde{s}(\lambda, E_{\mathrm{b}})$ of small variations and it is just the derivative of the model with respect to the irradiance as given in the second line.

$$s(\lambda, E_b) = s_0(\lambda_0, E_0) \cdot s_{rel}(\lambda) \cdot \left[1 + f(E_b) + g(\lambda, E_b)\right]$$

$$\widetilde{s}(\lambda, E_b) = s_0(\lambda_0, E_0) \cdot s_{rel}(\lambda) \cdot \frac{\partial}{\partial E_b}\left[f(E_b) + g(\lambda, E_b)\right]$$

(60)

The uncertainty of the responsivity values from Eq. (60) is determined just as explained in the chapters above, with a standard detector as reference and a monitor for a stabilisation of the irradiance for the AC signal. The additional effects of nonlinearity are functions $f(E_b) + g(\lambda, E_b)$ with coefficients which are correlated. The level of the irradiance is calculated from the DSR values and thus also correlated.

In practice the measurement of the AC-photocurrents is small enough not to affect the nonlinear behaviour. Therefore, it can be measured directly by substitution method and the so called systematic components are cancelled out for the AC-part and are mainly important for the values of the bias irradiance.

3.2 Uncertainties of the standard detector spectral responsivity values

As seen in Eqs. (8) and (45) above, determination of spectral responsivity is a transfer from a reference standard to the detector under test (DUT),

$$s_{T,n} = s_{S,n} \cdot t_n$$

(61)

where n denotes wavelength and t_n is the transfer ratio at the n-th wavelength. Uncertainties in spectral responsivity values of the test detector arise from those values of the standard detector and from the transfer process; these are treated independently and then added in quadrature.

$$u\left(s_{T,n}\right) = t_n \cdot u\left(s_{S,n}\right) = \frac{s_{T,n}}{s_{S,n}} u\left(s_{S,n}\right)$$

(62)

where the uncertainties in spectral responsivity of the reference detector are obtained from the calibration certificate. These may be complex, depending on the method of generating the primary

standard. In such cases, a full propagation using covariances between the reference values is required [39] [87] – these must be sought from the supplier of the reference standard.

Some certificates provide total random component uncertainties and total correlated uncertainties at each wavelength. Provided the coverage factor is the same for each and the ratio of their standard uncertainties is approximately constant through the spectral range of interest, the correlation coefficient r is also approximately constant and given by the square of the ratio. Then two uncertainties, one random and one fully-correlated between wavelengths are readily determined. The uncertainty in spectral responsivity from the combined random components is then given by

$$u_R\left(s_n\right) = \sqrt{1-r} \cdot u\left(s_n\right)$$

(63)

and the combined contribution of random effects to the uncertainty in the integrated spectral quantity is given by

$$u_R^2\left(R\right) = \left(1-r\right)\sum_n \left(P_n^2 \cdot u^2\left(s_n\right)\right)$$

(64)

The uncertainty in spectral responsivity of the combined components fully correlated between wavelengths is given by

$$u_S\left(s_n\right) = \sqrt{r} \cdot u\left(s_n\right)$$

(65)

The total contribution of the systematic effects is given by the linear sum:

$$u_S\left(R\right) = r\sum_n \left(P_n \cdot u\left(s_n\right)\right)$$

(66)

Where the correlation varies through the spectral range, the standard uncertainties of random components of the reference spectral responsivity with the same degrees of freedom can be combined in quadrature and propagated as a single item through to the standard uncertainty in the combination over wavelengths. However, individual systematic components of the reference spectral responsivity must be propagated separately (as linear sums).

The uncertainty contribution of the reference standard to the standard uncertainty of the combination is the quadrature sum of the independent systematic and random components of the reference.

A further complication is that spectral responsivity values for the reference standard may require interpolation to the wavelength values of the measurement. Interpolation introduces correlations and these must be taken into account when propagating the uncertainties of the standard detector. A simple process that avoids these complications is to interpolate the transfer ratio to the wavelengths at which the reference standard is calibrated and propagate random uncertainties in the integral sum (including the change in wavelength spacing) using only those values [88], as a relative uncertainty. Systematic components (fully correlated) are propagated individually again as linear sums.

3.3   Uncertainty contributions of quantities involved in the transfer process

Each effect contributing to uncertainty in the transfer can be classified as independent and either random between wavelengths or fully-correlated between wavelengths. These effects can also be separately determined for the numerator or denominator of the transfer ratio (as shown in Eq. (8) and Eq. (45)) and combined either linearly or in quadrature depending on whether the effects are correlated or random between test and reference signals at the one wavelength.

Once the uncertainty in the transfer ratio and hence its uncertainty in spectral responsivity:

$$u_e\left(s_{\mathsf{T},n}\right) = s_{\mathsf{S},n} \cdot u_e\left(t_n\right)$$
(67)

is determined for each effect at each wavelength, its contribution to the integral sum is calculated. For random components,

$$u_e^2\left(R\right) = \sum_n \left(P_n^2 \cdot u_e^2\left(s_n\right)\right)$$
(68)

For systematic components, uncertainties in the values of spectral responsivity at different wavelengths are generally positively correlated, and the contribution to the integral sum is given by

$$u_e\left(R\right) = \sum_n \left(P_n \cdot u\left(s_n\right)\right)$$
(69)

However some effects (e.g. wavelength offsets) can produce correlations that are positive or negative between wavelength pairs. These effects are properly handled by attaching a sign, that of the sensitivity coefficient for the effect, to the uncertainty in the transfer ratio. For example, consider the transfer ratio shown in Eq. (61). In the presence of a wavelength uncertainty fully correlated between test and reference, the signed uncertainty in the transfer ratio test: standard signals at the n-th wavelength is given by

$$u_{e,s}\left(t_n\right) = \left(\frac{1}{R_{S,n}}\frac{\partial R_{T,n}}{\partial \lambda} - \frac{R_{T,n}}{R_{S,n}^2}\frac{\partial R_{S,n}}{\partial \lambda}\right) \cdot u\left(\lambda\right)$$

(70)

The signed uncertainty in spectral responsivity for this effect at the n-th wavelength is then given by combining Eqs. (67) and (70):

$$u_{e,s}\left(s_{T,n}\right) = \frac{s_{R,n}}{R_{S,n}}\left(\frac{\partial R_{T,n}}{\partial \lambda} - t_n\frac{\partial R_{S,n}}{\partial \lambda}\right) \cdot u\left(\lambda\right)$$

(71)

This expression can be positive or negative depending on the slopes of the test and reference signals with respect to wavelength. The propagated uncertainty for a wavelength offset applicable at all wavelengths, including these mixed correlations, is found by the linear sum

$$u_e\left(R\right) = \sum_n \left(P_n \cdot u_{e,s}\left(s_{T,n}\right)\right)$$

(72)

Detailed discussions and examples for uncertainty contributions of different correlated combinations can be found in [87].

When reporting uncertainties associated to spectral responsivity values, the uncertainty contribution of effects systematic over wavelengths should be given at each wavelength, instead of the total uncertainty as is the usual practice.

4. REFERENCES

1. CIE, *International Lighting Vocabulary*, in http://eilv.cie.co.at, CIE, Editor. 2011.
2. B. ISO, IEC etc, *International Vocabulary of Basic and General Terms in Metrology.* 1993(ISO, 1993): p. 11-49.
3. J. Lehman, et al., *Domain-engineered pyroelectric radiometer.* Appl. Opt., 1999. **38**(34): p. 7047-7055.
4. G.P. Eppeldauer, M. Racz, and L.M. Hanssen, *Spectral responsivity determination of a transfer-standard pyroelectric radiometer.* SPIE Proceedings, 2002. **4818**: p. 118-126.
5. T.C. Larason, S.S. Bruce, and A.C. Parr, *Spectroradiometric detector measurements.* NIST Special Publication, 1998. **250-41**.
6. CIE, *The Basis of Physical Photometry.* Publication CIE, Central Bureau of the CIE, A-1033 Vienna, P. O. Box 169, Austria, 1983. **18.2**.
7. G.P. Eppeldauer, J. Zeng, and H.W. Yoon, *Low NEP pyroelectric radiometer standards.* SPIE Proc., 2008. **6940**: p. 694036-1 to 694036-8.
8. G.P. Eppeldauer, et al., *Low-NEP pyroelectric detectors for calibration of UV and IR sources and detectors.* SPIE Proc. 2017. **10378**: p. 1037809-1 to 1037809-13.
9. G.P. Eppeldauer, et al., *Broadband radiometric LED measurements.* SPIE Proc., 2016. **9954**: p. 99540J-1 to 99540J-15.
10. G.P. Eppeldauer and D.C. Lynch, *Opto-mechanical and electronic design of a tunnel-trap Si- radiometer.* J. Res. NIST, 2000. **105**(6): p. 813-828.
11. G.P. Eppeldauer, et al., *Radiometer standard for absolute responsivity calibrations from 950 nm to 1650 nm with 0.05 % (k=2) uncertainty.* Metrologia, 2009. **46**: p. S139-S145.
12. G.P. Eppeldauer, et al., *Extension of the NIST spectral power-responsivity calibration service to 2500 nm.* Metrologia, 2012. **49**: p. S112-S117.
13. Disclaimer, *The mention of certain commercial products in this publication is for information purposes only and does not constitute an endorsement of the product by the author.*

14. V.B. Podobedov, G.P. Eppeldauer, L.M. Hanssen, T.C. Larason, *Calibration of spectral responsivity of IR detectors in the range from 0.6 mm to 24 mm.* SPIE Proceedings, 2016. **9819**(Infrared Technology and Applications XLII, 98190P (May 20, 2016); doi:10.1117/12.2228384).

15. L. Werner, *Ultraviolet stability of silicon photodiodes.* Metrologia, 1998. **35**: p. 407-411.

16. CIE, *The spectroradiometric measurement of light sources.* Technical Report, 1984. **63**: p. 20-23.

17. D.S. Goodman, *Basic optical instruments, Chapter 4.* Geometrical and Instrumental Optics, Editor Malacara, D., Academic, 1988.

18. G.J. Zissis, *Dispersive Prisms and Gratings, Chapter 5.* Handbook of Optics, 2nd ed., Bass, M. editor, Vol. II, McGraw-Hill, 1995.

19. S.W. Brown, et al., *Stray-light correction algorithm for spectrographs.* Metrologia, 2003. **40**: p. S81-S84.

20. Y. Zong, et al., *Simple spectral stray light correction method for array spectroradiometers.* Appl. Opt., 2006. **45**: p. 1111-1119.

21. J.M. Palmer and M.G. Tomasko, *Broadband radiometry with spectrally selective detectors.* Opt. Lett., 1980. **5**: p. 208.

22. H.J. Kostkowski, *Reliable Spectroradiometry*. 1997: Spectroradiometry Consulting, La Plata, MD.

23. S.-Y. Ho, *New calibration method for prism infrared spetrometers.* Applied Optics, 1971. **10**: p. 1584.

24. J.L. Gardner, *Bandwidth correction for LED chromaticity.* Color Res. Application, 2006. **31**: p. 374-380.

25. V.B. Podobedov, G.P. Eppeldauer, and T.C. Larason, *Evaluation of optical radiation detectors in the range from 0.8 to 20 um at the NIST spectral calibration facility.* SPIE, 2012. **Vol. 8550,** 855029-1.

26. L.P. Boivin, *Study of bandwidth effects in monochromator-based spectral responsivity measurements.* Applied Optics, 2002. **41**: p. 1929-1935.

27. J. Campos, et al., *Spectral responsivity uncertainty of silicon photodiode due to calibration spectral bandwidth.* Meas. Sci. Technol., 2001. **12**: p. 1926-1931.

28. E.I. Stearns and R.E. Stearns, *An example of a method for correcting radiance data for bandpass error.* Color Res. Application, 1988. **13**: p. 257-259.

29.   Y. Ohno, *A flexible bandpass correction method for spectrometer.* Proc. of the Intern. Colour Assoc., 2005. **Part 1**: p. 697-700.

30.   T.R. Gentile and C.L. Cromer, *Mode-locked lasers for high-accuracy radiometry.* Metrologia, 1996. **32**: p. 585-587.

31.   S.W. Brown, et al., *Spectral Irradiance and Radiance responsivity Calibrations using Uniform Sources (SIRCUS) facility at NIST.* SPIE proceedings, 2004. **5542**: p. 363-374.

32.   J. Fowler and M. Litorja, *Geometric area measurements of circular apertures for radiometry at NIST.* Metrologia, 2003. **40**: p. S9-S12.

33.   V.E. Anderson, N.P. Fox, and D.H. Nettleton, *Highly stable, monochromatic and tunable optical radiation source and its application to high accuracy spectrophotometry.* Applied Optics, 1992. **31**(4): p. 536-545.

34.   S.W. Brown, G.P. Eppeldauer, and K.R. Lykke, *Facility for Spectral Irradiance and Radiance Responsivity Calibrations using Uniform Sources (SIRCUS).* Appl. Opt., 2006. **45**(32): p. 8218-8237.

35.   P.S. Shaw, et al., *Synchrotron radiation based irradiance calibration from 200 nm to 400 nm at the Synchrotron Ultraviolet Radiation Facility III.* Applied Optics, 2007. **46**(25).

36.   P.S. Shaw, et. al, *Ultraviolet characterization of integrating spheres.* Applied Optics, 2007. **46**: p. 5119.

37.   Y. Zong, et al.,*Correction of stray light in spectrographs: implications for remote sensing.* SPIE Proceedings, 2005. **5882**: p. 588201-1 to 588201-8.

38.   Y. Zong, et al.,*Correction of stray light in spectroradiometers and imaging instruments.* CIE Proceedings, 2007. **CIE 26th Session**.

39.   ISO, *Guide to the Expression of Uncertainty in Measurement.* 1993(Geneva).

40.   C.L. Wyatt, V. Privalsky, and R. Datla, *Recommended practice; symbols, terms, units, and uncertainty analysis for radiometric sensor calibration.* NIST Handbook, 1998. **152**.

41.   C.L. Cromer, et al., *The NIST detector-based luminous intensity scale.* J. Res. NIST, 1996. **101**(2): p. 109-132.

42.   *Burgthaler Electronik GmbH.*

43.   *KaleidaGraph, Synergy Software, Reading , PA.*

44.   *Mitutoyo Corp., Aurora, IL. Electronic ruler.*

45.   J.H. Walker, et al., *Spectral Irradiance Calibrations*. NBS Spec. Publ. 250-20. 1987, Washington, DC: U.S. Government Printing Office.

46.   J.L. Gardner, *Correlated color temperature-uncertainty and estimation.* Metrologia, 2000. **37**: p. 381-384.

47.   J.L. Gardner, *Correlations in primary spectral standards.* Metrologia, 2003. **40**(1): p. S167-S176.

48.   M. Noorma, et al., *Characterization of filter radiometers with a wavelength-tunable laser source.* Metrologia, 2003. **40**: p. S220-S223.

49.   C.E. Gibson, B.K. Tsai, and A.C. Parr, *Radiance Temperature Calibrations.* NIST Special Publication 250-43, 1998.

50.   S.W. Brown, et al., eds. *Advances in Radiometry for Ocean Color*. Volume VI: Special Topics in Ocean Optics Protocols and Appendices. 2004. 8-35.

51.   G.P. Eppeldauer, et al., *IR-enhanced Si reference detectors for one-step scale transfers from 300 nm to 1000 nm.* Metrologia, 2014. **51**: p. S252-S257.

52.   T.C. Larason and J.M. Houston, *Spectroradiometric detector measurements: ultraviolet, visible, and near-infrared detectors for spectral power.* NIST Special Publication, 2008. **250-41**.

53.   G.P. Eppeldauer and H.W. Yoon, *Short-wave infrared radiometers design and characterizations.* SPIE Proc., 2007. **6542**: p. 65420O-1 to 65420O-10.

54.   S.W. Brown, G.P. Eppeldauer, and K.R. Lykke, *NIST Facility for spectral irradiance and radiance responsivity calibrations with uniform sources.* Metrologia, 2000. **37**: p. 579-582.

55.   G.P. Eppeldauer, et al., *Extension of the NIST spectral responsivity scale to the infrared using improved-NEP pyroelectric detectors.* Metrologia, 2009. **46**: p. S155-S159.

56.   G.P. Eppeldauer, et al., *Extension of the NIST spectral power and irradiance responsivity calibrations to 2.5 micrometers.* Proceedings of the CIE Expert Symposium on spectral and imaging methods for photometry and radiometry, CIE Central Bureau, 9/9A Babenbergerstrasse, 1010 Vienna, Austria, 2010. **CIE x036:2010**(CIE Bern Proc.): p. 66-71.

57.   G.P. Eppeldauer, J. Zeng, and H.W. Yoon, *Low NEP pyroelectric radiometer standards.* SPIE proceedings, 2008. **6940**: p. 694036-1 to694036-8.

58.   G. Eppeldauer, L. Novak, Linear HgCdTe radiometer, SPIE Proc., 1989, **1110**, p. 267-273.

59.   G.P. Eppeldauer, J. Zeng, and L.M. Hanssen, *Development and calibration of pyroelectric radiometer standards at NIST.* SPIE Proc., 2006. **6201**: p. 620119-1 to 620119-12.

60.   P.Y. Barnes, E.A. Early, and A.C. Parr, *NIST Measurement Services: Spectral Reflectance.* NIST Special Publication, 1998. **250-48**.

61.   L.M. Hanssen, S.G. Kaplan, and R. Datla, *Infrared Optical Properties of Materials.* NIST Special Publication, 2015. **250-94**.

62.   G.P. Eppeldauer, A.L. Migdall, and L.M. Hanssen, *InSb Working Standard Radiometers.* Metrologia, 1998. **35**: p. 485-490.

63.   G. Eppeldauer and A.L. Migdall, *Realization of an Infrared Spectral Radiant Power Response Scale on a Cryogenic Bolometer.* Metrologia, 1998. **35**: p. 307-315.

64.   A. Migdall and G.P. Eppeldauer, *Realization of an IR spectral radiant power response scale on a cryogenic bolometer.* Metrologia, 1998. **35**: p. 307-315.

65.   J. Zeng, et al., *Spectral irradiance responsivity calibration of InSb radiometers with improved IR SIRCUS.* CALCON-2007 Conference, **Conference Proc.** 2007.

66.   G.P. Eppeldauer and H.W. Yoon, *Short-wave infrared radiometers design and characterizations.* SPIE Proceedings, 2007. **6542**: p. 65420O-1 65420O-10.

67.   G.P. Eppeldauer and M. Racz, *Spectral Power and irradiance responsivity calibration of InSb working standard radiometers.* Appl. Opt., 2000. **39**(31): p. 5739-5744.

68.   G.a.O.A.E.S. ASTM Committee E44 on Solar, Subcommittee E44.09, *Standard Test Method for Spectral Responsivity Measurements of Photovoltaic Devices.* Annual Book of ASTM Standards, 2006. **12.02**.

69.   S. Winter, T. Wittchen, and J. Metzdorf, *Primary Reference Cell Calibration at the PTB Based on an Improved DSR Facility.* Proc. of 16th European Photovoltaic Solar Energy Conference, Glasgow, 2000.

70.   A. Sperling, et al., *Silicon detector linearity at high UV irradiance levels.* NEWRAD 2008 Proc., 2008: p. 207-208.

71.   Fresnel, *PolyIR5 material.* Fresnel Technologies. http://www.fresneltech.com.

72.   G.P. Eppeldauer, *Optical Radiation Measurement with Selected Detectors and Matched Electronic Circuits Between 200 nm and 20 µm.* NIST Technical Note, **1438**, U.S. Government Printing Office, 2001.

73.   H.W. Yoon and G.P. Eppeldauer, *Measurement of thermal radiation using regular glass optics and short-wave infrared detectors.* Optics Express, 2008. **16**(2): p. 937-949.

74.   G.P. Eppeldauer and M. Racz, *Design and characterization of a photometer/colorimeter standard.* Applied Optics, 2004. **43**(13): p. 2621-2631.

75.   G.P. Eppeldauer, S.W. Brown, T.C. Larason, M. Racz, and K.R. Lykke., *Realization of a spectral radiance responsivity scale with a laser-based source and Si radiance meters.* Metrologia, 2000. **37**: p. 531-534.

76.   M. Racz and G.P. Eppeldauer, *Correction of directional errors for radiometric and photometric standard detectors.* Metrologia, 2000. **37**: p. 489-492.

77.   CIE, *Methods of characterizing the performance of radiometers and photometers.* CIE Publication, 1982. **53**.

78.   CIE, *Methods of characterizing illuminance meters and luminance meters.* Publication CIE, Central Bureau of the CIE, A-1033 Vienna, P. O. Box 169, Austria, 1987. **No. 69**.

79.   G.P. Eppeldauer, Editor, *Optical radiation measurements based on detector standards*, NIST Technical Note #1621, Printing and Duplicating, National Institute of Standards and Technology, March, 2009.

80.   G.P. Eppeldauer, M. Racz, and T.C. Larason, *Optical characterization of diffuser-input standard irradiance meters.* SPIE Proc., 1998. **3573**: p. 220-224.

81.   G. Eppeldauer, *Near Infrared Radiometer Standards.* SPIE proceedings, 1996. **2815**: p. 42-54.

82.   CIE, *Colorimetry.* Publication CIE, Central Bureau of the CIE, A-1033 Vienna, P. O. Box 169, Austria, 1986. **15.2**.

83.   G.P. Eppeldauer, *Spectral response based calibration method of tristimulus colorimeters.* J. Res. NIST, 1998. **103**(6): p. 615.

84.   S.W. Brown, T.C. Larason, C. Habazuit, G.P. Eppeldauer, Y. Ohno, and K.R. Lykke, *Absolute radiometric calibration of digital imaging systems.* SPIE proceedings, 2001. **4306**: p. 13-21.

85.   E.F. Zalewski, *Radiometry and Photometery, Chapter 24.*

      Handbook of Optics, 1995. **II**: p. 24.3-24.51.
86.   CIE, *Uncertainty.* TC2-43 Document, 2009.
87.   J.L. Gardner, *Chapter 6: Uncertainty estimates in radiometry.*
      Experimental Methods in the Physical Sciences, 2005. **41,**
      Editors: A.C. Parr, R.U. Datla, and J.L. Gardner, (Elsevier
      Inc.): p. 291-325.
88.   J.L. Gardner, *Uncertainties in interpolated spectral data.* J.
      Res. Natl. Inst. Stand. Technol., 2003. **108**: p. 69-78.
89.   H. W. Yoon, G. P. Eppeldauer, and J. Zeng, *Detector-based
      NIST-traceable calibration and validation of infrared
      collimators*, Applied Optics. 2010.
90.   Howard W. Yoon and George P. Eppeldauer, *The use of
      thermo-electric cooled short-wave infrared detectors in heat-
      seekig systems*, Proc. of MSS Conf. in Orlando, FL, Feb. 5-
      7, 2007.
91.   G.P. Eppeldauer, G. Sauter, and J.L. Gardner, *Uncertainties
      of Spectral Responsivity Measurements*, Proc. of the 2nd CIE
      Expert Symposium on Measurement Uncertainty, p. 133-
      138, CIE Central Bureau, 27 Kegelgasse, A-1030, Vienna,
      Austria, 2006.